Universidad de Alcalá

Facultad de Biología, Ciencias Ambientales y Química

Departamento de Química Analítica, Química Física e Ingeniería Química

SYNTHESIS AND CHARACTERIZATION OF NANOWIRES AND MICROMOTORS FOR ELECTROCHEMICAL SENSING AND BIOSENSING IN MICROFLUIDIC ANALYTICAL SYSTEMS

Tesis Doctoral

Miguel García García

Alcalá de Henares, Diciembre 2013

Universidad de Alcalá

DEPARTAMENTO DE QUÍMICA ANALITICA, QUIMICA FISICA E INGENIERIA QUIMICA
Edificio Polivalente
Carretera Madrid-Barcelona, Km. 33,600
28871 Alcalá de Henares (Madrid)
Telf: 91 885 4 941
FAX: 91 885 5 088
E-mail: dpto.quimanafising@uah.es

ALBERTO ESCARPA MIGUEL, Profesor Titular de Química Analítica del Departamento de Química Analítica, Química Física e Ingeniería Química de la Universidad de Alcalá,

CERTIFICA:

Que el trabajo descrito en la presente memoria, titulado "**SYNTHESIS AND CHARACTERIZATION OF NANOWIRES AND MICROMOTORS FOR ELECTROCHEMICAL SENSING AND BIOSENSING IN MICROFLUIDIC ANALYTICAL SYSTEMS"**, ha sido realizado bajo su dirección por D. Miguel García García en el Área de Química Analítica del Departamento de Química Analítica, Química Física e Ingeniería Química de esta Universidad excepto el trabajo descrito en el Capítulo III que ha sido llevado a cabo en el Departamento de Nanoingeniería de la Universidad de California, San Diego (UCSD) (EEUU). Asimismo, autoriza su presentación para que sea defendido como Tesis Doctoral.

Y para que conste y surta los efectos oportunos, firma el presente en Alcalá de Henares a 22 de octubre de 2013.

Universidad de Alcalá

DEPARTAMENTO DE QUÍMICA ANALITICA, QUIMICA FISICA E INGENIERIA QUIMICA
Edificio Polivalente
Carretera Madrid-Barcelona, Km. 33,600
28871 Alcalá de Henares (Madrid)
Telf: 91 885 4 941
FAX: 91 885 5 088
E-mail: dpto.quimanafising@uah.es

ALBERTO ESCARPA MIGUEL, Profesor Titular de Química Analítica y Director del Departamento de Química Analítica, Química Física e Ingeniería Química de la Universidad de Alcalá,

CERTIFICA:

Que el trabajo descrito en la presente memoria, titulado "**SYNTHESIS AND CHARACTERIZATION OF NANOWIRES AND MICROMOTORS FOR ELECTROCHEMICAL SENSING AND BIOSENSING IN MICROFLUIDIC ANALYTICAL SYSTEMS"**, ha sido realizado en este departamento por D. Miguel García García bajo la dirección del Dr. Alberto Escarpa Miguel, Profesor Titular de dicho departamento. El trabajo experimental recogido en el Capítulo III ha sido llevado a cabo en el Departamento de Nanoingeniería de la Universidad de California, San Diego (UCSD) (EEUU).

Y para que conste y surta los efectos oportunos, firma el presente en Alcalá de Henares a 22 de octubre de 2013.

Llegado este momento, echar la vista atrás da un poco de vértigo, vértigo por qué ha pasado mucho tiempo y en ese tiempo infinidad de cosas que serán difíciles de olvidar, las buenas las recordare con cariño y las malas… recordaré que han pasado por algo y que me han enseñado.

Aún me acuerdo cuando el que ha sido mi director de Tesis, el Dr. Alberto Escarpa me preguntó ¿tú has pensado en hacer investigación? Y no lo había hecho, pero finalmente lo hice y me alegro por ello. Quiero agradecerle aquí su apoyo sin el cual no pudiera haber realizado esta Tesis, por ser capaz de contagiar ese entusiasmo e ilusión por la ciencia y por exigir siempre lo máximo para sacar lo mejor de uno mismo y conseguir (o por lo menos intentarlo) todo lo que nos propusimos hace mucho tiempo ya.

No puedo olvidarme de Cristina González, que aunque sabes cómo ponerme nervioso has sabido ganarte mi cariño y amistad a base de esas charlas en el laboratorio, de ciencia y de la vida, y por estar ahí siempre para lo que necesitara.

Miguel Ángel, como no ibas a estar aquí, si por ti he aprendido que uno se puede divertir mucho trabajando en este mundo, gracias por tu apoyo, amistad y supongo que también por tus bromas.

A Jose y a Antonio del servicio de microscopía de la universidad de Alcalá por su ayuda para ver el nanomundo.

Me gustaría agradecer también a Joseph Wang, del "nanobioelectronics group" de la Universidad de California en San Diego (Estados Unidos) por brindarme la oportunidad de trabajar en su grupo y enseñarme ese gran mundo de los micromotores. Sin olvidar a mis compañeros de laboratorio durante mi aventura Americana, Aoife, Amay,

Josh, Alexandra, Filiz, Gabriela, Jonathan, Vinci, Wenzhao, Younge, Aysegul, Allen, Serguey y especialmente al equipo de nanomotors, Wei, Sirilak, Victor, Allan, Ashley The Spanish Team: Jahir and María y el resto de gente de la que me llevo un buen recuerdo de allí, Cawas, Jordi, Azu, Raj y Laura.

I would like to thank Joseph Wang from "nanobioelectronics group" of the University of California San Diego, for giving me the opportunity of work in his group and show me the fantastic world of micromotors. Without forgetting my lab mates during my American adventure, Aoife, Amay, Josh, Alexandra, Filiz, Gabriela, Jonathan, Vinci, Wenzhao, Younge, Aysegul, Allen, Serguey and specially nanomotors team, Wei, Sirilak, Victor, Allan, Ashley The Spanish Team: Jahir and María and the rest of people from whose I have great memories, Cawas, Jordi, Azu, Raj and Laura.

A mis compañeros de laboratorio porque sin ellos esta experiencia no habría sido ni parecida, me llevo de ellos en estos años innumerables recuerdos, se podría escribir otro libro con ellos. Entre ellos a los que estaban cuando llegué y me acogieron y enseñaron, Agus, Miri, Ana, Elena, Lauri, Cris, Clari, Vir y a todos los que fueron llegando poco a poco, Diana, Paty, Miguelito, Luci, Aída, Adrián, Pilar, Estefania, Elena, Rommy, Patricia y a los chicos explosivos, Jorge, María, M.A., Charlie, André, Matías y Lucía. De manera más especial a la gente con la que más he compartido y que más se ha ganado mi cariño, Cristi por ser una gran amiga siempre con una palabra de apoyo, Clari por la alegría que dejas por donde pasas, Vir por tu risa fácil y contagiosa que hacía de las comidas el gran momento del día, Paty por ser esa Polaca divertida, Jorge por los crucis, Aída por esos momentazos con los Simpsons, Adrián, pequeño, por lo bien que me lo he pasado en el poco tiempo que he compartido contigo, que me gustaría que hubiese sido mucho más, Pilar por que personas como tu hacen este mundo mejor y como no Miri, por los buenos ratos echando pan a los patos, por

esas conversaciones de todo y de nada con las mandarinas en el pasillo y por estar ahí siempre ayudándome, gracias Trompi.

También me gustaría acordarme aquí de toda la gente que nos visitó desde lejos y que compartieron una parte de su tiempo conmigo, Tereza, Fanny, Conrado, Raquel, Olga, Pauline y Flavio.

A mis compañeros de la carrera, sobre todo a Sara, Jorge, Alfonso, Antonio y Vero por todo lo vivido juntos durante aquellos maravillosos años, con sus tardes metidos en laboratorios de prácticas y alguna que otra al sol en el césped.

A mis amigos de siempre, por estar ahí para cualquier cosa y por aguantar conversaciones sobre nanohilos y microchips. A mis amigos de Trillo, por ayudarme a cambiar de aires de vez en cuando y despejarme cuando lo he necesitado.

A Alba, por estar a mi lado y ayudarme y animarme siempre, pese a la locura que genera a veces hacer una Tesis.

No podía terminar sin agradecer a mi familia, por su apoyo incondicional y por interesarse en cada momento por lo que he hecho en estos años, no estaría aquí si no hubieseis creído en mí.

Finalmente, quisiera dar las gracias a la Universidad de Alcalá por la beca FPI concedida que ha permitido la realización de esta Tesis.

"Un científico en su laboratorio no es sólo un técnico: es también un niño colocado ante fenómenos naturales que le impresionan como un cuento de hadas"

(Marie Curie)

A mis padres

Acronyms

MCH	6-mercapto-1-hexanol
1-D	1- Dimensional
AAO	Anodic alumina oxide
AA	Ascorbic acid
CNT	Carbon nanotube
CSPE	Carbon screen printed electrode
CVD	Chemical vapor deposition
CE	Cholesterol esterase
COx	Cholesterol oxidase
CV	Cyclic voltammetry
DASA	Double antibody sandwich assays
DPV	Differential pulse voltammetry
ED	Electrochemical detection
EIS	electrochemical impedance spectroscopy
EDS	Energy dispersive X-ray spectrometry
ESEM	Environmental SEM
EG	Ethylene glycol
FESEM	Field emission scanning electron microscopy
FIA	Flow injection analysis
GCE	Glassy Carbon Electrode
GOx	Glucose oxidase
GlutOx	Glutamate oxidase
GLA	Glutaraldehyde
GNP	Gold nanoparticles
HRP	Horseradish peroxidase
MFA	Mefenamic acid
MNW	Metallic nanowire
MB	Methylene blue
MC	Microfluidic chip
MWNT	Multi-wall carbon nanotube
NW	Nanowire
LOC	Lab on a chip
OAP	*o*-aminophenol
PPy-COOH	Poly(1-(2-carboxyethyl)pyrrole
PEDOT	Poly(3,4-ethylenedioxythiophene)
PVP	Poly(vinylpyrrolidone)
PANI	Polyaniline

PC	Polycarbonate
PolyNW	Polymeric nanowire
PPy	Polypyrrole
PVB	Polyvinyl butyral
PAD	Pulsed amperometric detection
SEM	Scanning electron microscopy
SPE	Screen printed electrode
SWV	Square Wave voltammetry
TBO	Toluidine blue O
TEM	Transmission electron microscopy
UA	Uric acid
XPS	X-ray photoelectron spectroscopy

SUMMARY

On the one hand, microfluidic systems and *lab-on-a-chip* (LOC) technologies seek to improve analytical performance by reducing the analysis time, decreasing the consumption of sample and reagents, diminishing the risk of contamination, integrating multiplexing analysis, and especially portability to provide the possibility of point-of-care and in field applications. In addition, one of the most powerful analytical applications of microfluidic-LOC systems relies on their inherent potency as screening tools for rapid diagnosis.

On the other hand, one-dimensional nanomaterials (1-D) as structures with only one dimension extend, are very unique not only because they offer a high surface to volume, but also because they can easily be designed and fabricated with different segments which add tunable electronic properties and controlled functionality. Indeed, one important characteristic of these structures is related to its tunable surface through different functionalization which can be used in many applications involving different kind of biomolecules, such as, enzymes or antibodies.

Relevant examples of 1-D nanostructures are metallic nanowires (MNWs), both, elemental and bimetallic and also micromotors, sophisticated structures with autonomous movement being constituted both kinds of structures as new and innovative alternatives for detection in microfluidic-LOC devices.

Firstly, metallic nanowires (MNWs) are metallic or semiconducting nanostructures with cylindrical shape, without any hollow in the structure. They are one-dimensional anisotropic structures, with high specific surface and high aspect ratio (nanometers in diameter, micrometers in length).

MNWs are very valuable tools for electrochemical sensing. They offer high currents because of their large surface area, thereby enabling large scale redox conversion, which increases the analytical sensitivity, and resistance passivation, yielding very good reproducibility. In addition, electrocatalysis can be strategically exploited and well-conducted toward the selective detection of target analytes. Since it is well-known that the electrochemical oxidation of carbohydrates is favored by the electrocatalytic effect of copper and nickel; an improved analytical performance by the use of these catalytic nickel (NiNWs) and copper nanowires (CuNWs), is highly expected for detection of these important analytes.

In addition, in microfluidic-LOC systems, electrochemistry is a valuable detection mode that provides inherent sensitivity, permits miniaturization, and is highly compatible with micro- and nanotechnologies. Because of the extremely low sample volumes introduced into microfluidic-LOC systems, the chip sensitivity is often low and presents a drawback of these systems; however the sensitivity can be enhanced and the problem overcome by exploiting the surface characteristics of nanomaterials, become as consequence the microfluidic-LOC systems coupling very pertinent.

Secondly, micromotors are devices in the micro and nano scales capable of converting energy into movement and forces. The energy source is closely related to the microstructure shape, actually both shape and propulsion systems are connected. We can expect from micromotors new and enhanced features related to their special characteristics. A remarkable one is its autonomous movement which can improve different steps of the analytical process, such as sample enrichment and detection. The employment of these micromotors in confined microfluidic-LOC systems offers extraordinary promises such as the development of future free-fluidic

pumping LOCs and avoids their derived instrumentation (i.e. pumps or high voltage suppliers) supporting the new (bio) sensing in the micromotors autonomous guided movement.

All the characteristics mentioned above, convert these 1-D structures into unique tools in the current analytical nanoscience and nanotechnology field, and their exploration for improving detection of microfluidic-LOC systems has constituted the main motivation of this Doctoral Thesis accordingly to the following two well-defined objectives.

The first objective has been the synthesis and characterization of nickel and copper NWs for electrochemical carbohydrate sensing using miniaturized flow-based and microfluidic-LOC systems

The second objective has been the synthesis and characterization of micromotors for optical immunoassay of proteins in microfluidic-LOC systems.

The main identified milestones were:

1- Optimization of the electro synthesis of nickel, copper and bimetallic nickel-copper nanowires using anodized alumina membranes as templates

2- Analytical characterization of the nickel, copper and bimetallic nickel-copper nanowires using optical and electron microscopy, spectroscopy and electrochemical techniques

3- Design and construction of screen printed detectors based on nickel, copper and bimetallic copper-nickel nanowires coupled to miniaturized flow injection devices for carbohydrate sensing

4- Design and construction of electrochemical detectors based on nickel and copper nanowires coupled to microfluidic-LOC systems for carbohydrate sensing

5- Optimization of the electro synthesis of micromotors using polycarbonate double conical membranes as templates

6- Analytical characterization of the micromotors using optical and electron microscopy.

7- Design of micromotors for immunoassay in microfluidic-LOC systems

Accordingly to the target objectives, the results of this Doctoral Thesis are grouped in chapters **II and III**. In **chapter II**, synthesis and characterization of nanowires for carbohydrate electrochemical sensing using flow and microfluidic-LOC systems are discussed. Further, the works involving flow injection analysis and microfluidic-LOC systems will be presented in two well-separated sections, respectively. In **chapter III**, the

synthesis and characterization of micromotors for optical immunoassay in microfluidic-LOC systems are further presented.

Next, a brief summary of each related works will be presented.

Regarding **chapter II**, electro synthesis and characterization of nanowires were firstly approached in deep. In these works, elemental nickel (NiNWs) and bimetallic nickel-copper nanowires (Ni-CuNWs) were synthesized by the electroplating method using alumina template and characterized by scanning electron microscopy (SEM), transmission electron microscopy (TEM) and energy-dispersive X-ray spectrometry (EDS). Using a alumina templates (200 nm) and under controlled deposition of 45C of charge, both NWs exhibited a high structural perfection with a length of about 7 μm and a width of about 300 nm. EDS analysis confirmed their chemical composition with a percentage of Ni of 97% along the whole NiNWs and with a percentage of Ni of 50.6% and copper of 49.4% in the Ni-CuNWs. Both electro-synthesized NWs exhibited a marked electrocatalysis towards detection of the target carbohydrates studied (glucose, fructose, galactose, sucrose, lactose and inulin).

After synthesis and characterization, NiNWs and CuNWs were studied as electrochemical detectors in both miniaturized flow injection analysis (FIA) and microfluidic-LOC systems.

Firstly, disposable screen-printed electrochemical detectors based on nickel nanowires for carbohydrate sensing were constructed for its employment in FIA. XPS revealed that NiNWs based electrodes contained just a 0.9% of Ni with an enhancement of current density of about 65 times in comparison with Ni-bulk electrode. Interestingly, Ni magnetism was essential to keep them over the electrode surface under flow conditions and

reached an excellent analytical performance. Electrochemically activated NiNWs (at -1.5V, 600s) under magnetic field (2x4200 Gauss) gave the best signal-to-noise performance exhibiting fast response time, very good mechanical stability, and an extreme resistance to fouling under hydrodynamics conditions allowing an excellent analytical performance on the board of just one disposable single-electrode (RSDs≤7%, n=50). Analytical performance of NiNWs was also excellent in the analysis of selected samples exhibiting very good precision (RSDs≤2%) and recovery (95-115%).

These nano-scaled disposable detectors were also employed for determination of total sugars (glucose+fructose) in honey samples using a simplified calibration protocol. The total sugar content obtained by the electrochemical approach was compared with those obtained by a high-performance liquid chromatography-refractive index (HPLC-RI) method. Low systematic errors were yielded (Er<10%) revealing a very good accuracy of the method. Also, a sample high-throughput with a processing of 2 samples min^{-1} was obtained on the board of just one electrode without loss of performance. The term "Electrochemical monosaccharide index" to describe the total sugars was proposed.

In a second separated well-defined section in **chapter II**, analytical applications of metallic nanowires (MNWs) for electrochemical sensing of carbohydrates using microfluidic systems was successful achieved. In these works, screen-printed electrochemical detectors (10x1 mm) suitably designed to be coupled to microfluidic-LOC systems, displayed well-defined nickel and copper nanowires (6 μm lengths, 300 nm widths) randomly distributed over the electrode surface as it was observed by field emission scanning electron microscopy (FESEM). Chronoculombimetry revealed

that the modified electrodes exhibited an enhanced electro active surface area higher than the non-modified ones.

Then, these electrodes were suitably coupled to microfluidic systems-LOC (into microchip format) developing three well-defined analytical applications in the agro-food and clinical fields. In all of these contributions, conceptually speaking, we hypothesize that the inherent selectivity and sensitivity of CuNWs, towards carbohydrates detection in connection with microfluidic-LOC systems selectivity, could allow the fast and simultaneous detection of the these target analytes with low analysis times and extremely low sample consumption become an attractive alternative to well-established reported approaches in the literature (mostly based on the use of enzymes or high-consuming HPLC protocols)

In the first application, an enzymeless electrochemical microfluidic-LOC sensor coupled with electro synthesized NiNWs and CuNWs for inulin detection was developed. Inulin is a fructo-oligosaccharide containing up to 35 fructose units linked via β-1,2-glycosidic bonds with a high significance in the agro-food and clinical fields becoming an important carbohydrate with several benefits in human health. Inulin sensing was selectively performed in presence of free fructose in less than 300s. Although both Ni and CuNWs exhibited electro catalysis towards inulin detection, 3-folds higher sensitivity was obtained using CuNWs in comparison with NiNWs. Very good *intra*-electrode repeatability with RSDs<8% (n=5) and *inter*-electrode reproducibility with RSDs<9% (n=4) were obtained, indicating an excellent stability of the copper nano-scaled electrochemical detectors. Interestingly, inulin detection exhibited impress sensitivity despite its complex structure with a sensitivity 40 times higher than found for its fructose monomer. Combining the high sensitivity of the CuNWs with its low noise level resulted in LODs of 3 μM for inulin. Inulin

determination in a selected samples was also carried out with good quantitative and reproducible recoveries (97-103%, RSDs<4%) indicating an excellent method´s reliability.

Microfluidic chips used as microchip electrophoresis (ME) with electrochemical detection (ED) have demonstrated to be a powerful tool in food analysis. However, the coupling between ME-ED with nano-technologies is still in its infancy, even knowing that nanomaterials can significantly improve the ME analytical performance. This second work, reports the coupling between ME with copper nanowires (CuNWs) for the selective analysis of monosaccharides in honey samples. To this end, a representative group of nine honey samples were analyzed and the results were compared with those previously obtained by HPLC-RI. ME-CuNWs approach allowed the separation of glucose and fructose in less than 250 s under optimized separation (20 mM NaOH + 10 mM H_3BO_3, pH=12; separation voltage +1000 V) and detection (E= +0.70 V in 20 mM NaOH + 10 mM H_3BO_3, pH=12) conditions. An excellent stability of electro-osmotic flow (EOF) during sample analysis was achieved (RSDs<2% for migration times).The quantitative contents for individual glucose and fructose obtained using ME-CuNWs in comparison with those obtained by HPLC-RI were highly in agreement with errors below 10% indicating the reliability of the approach.

In this last work, we are describing the coupling of microfluidic-LOC systems to CuNWs as electrochemical detectors for the fast diagnosis of galactosemia in precious newborn urine samples. Galactosemia is a rare disease which is diagnosed towards the identification of different metabolite profiles. Therefore, the specific detection of galactose 1-phosphate (Gal 1-P), galactose (Gal) and uridyl diphosphate galactose (UDP-Gal) confirms types I, II and III galactosemia diseases. Due to the low prevalence of

galactosemia, sample availability is very scarce and screening methods to diagnose the illness are not commonly employed around the world. Again, a very good *intra*-electrode repeatability with RSDs<8% (n=10) and *inter*-electrode reproducibility with RSDs<12% (n=5) were obtained, indicating an excellent stability of the nano-scaled electrochemical detector. Under optimum chemical (NaOH 3 mM, pH=11.5), electrokinetic (separation voltage +750 V, injection +1500 V for 5 s) and electrochemical (E=+0.70 V in NaOH 3 mM pH=11.5) conditions, galactosemia diseases were unequivocally identified differentiating between type I, II, III using selected precious ill diagnosed newborn urine samples. Detection proceeded in less than 350 s, required negligible urine sample consumption, and displayed impressive signal-to-noise characteristics (ranging from 14 to 80) and micro-molar LODs much lower than the cut-off levels (Gal 1-P > 0.4 mM and Gal > 1.4 mM). Excellent reproducible recoveries (93-107%, RSDs <6%) were also achieved revealing the reliability of the approach. The significance of the newborn urine samples studied confirms the analytical potency of microfluidic-CuNWs approach, enhancing the maturity of the microchip technology and opening new avenues for future implementation of screening applications in the field.

On the other hand, **chapter III** deals with the results obtained in the synthesis and characterization of micromotors for the optical detection of proteins using microfluidic-LOC devices, in this case fabricated in polydimethil-siloxane (PDMS). In this work, self-propelled catalytic micromotors functionalized with antibodies were designed and developed for capture, interact and transport of target proteins between the different reservoirs of a microfluidic-LOC device. These catalytic micromotors were constituted by the architecture polymer/Ni/Pt. The polymer contains carboxy moieties on its outermost layer of the mixed poly (3,4-

ethylenedioxythiophene) (PEDOT)/COOH–PEDOT polymer and was further functionalized with the antibody receptor to selectively recognize and capture the target protein and be able to carry out in this way and successfully all the immunoassay steps. Pt allowed the oxygen bubble generation by the catalysis decomposition of hydrogen peroxide on its surface, and nickel allowed the correct guidance of the self-propelled micromotor. In these works all the immunoassay operations were carried out without any bulk fluid flow, replacing the common washing steps in antibody-based protein bioassays thanks to the active transport of the captured protein throughout the different reservoirs of the microfluidic system.

Finally, from the main conclusions obtained from this Doctoral Thesis it can be established that the studied one dimensional materials – catalytic nickel and copper nanowires and micromotors– have demonstrated to be very powerful analytical tools to improve the (bio-) detection of target molecules in both, agro-food and clinical fields, using miniaturized flow injection analysis and microfluidic systems based in *lab-on-a-chip* (LOC) technology. The inherent advantages of microfluidic systems such as, fast analysis and very low sample and reagents consumption and in addition those derived from the high specific surface of the studied 1-D materials, have been creative and synergicly exploited. Due to all the premises stated above, the results presented in this Doctoral Thesis reveal the pertinence and convenience of the coupling between microtechnologies and nanotechnologies for the detection of target molecules in complex analytical systems in agro-food and clinical fields broadening new horizons in current Analytical Chemistry.

RESUMEN

Por una parte, los sistemas microfluídicos y las tecnologías *lab-on-a-chip* (LOC) persiguen dismunir los tiempos de análisis, el consumo de muestras y reactivos y la generación de residuos así como integrar las etapas analíticas en un sólo dispositivo y mejorar la portabilidad de los sistemas analíticos favoreciendo el análisis *in situ*. Estas características hacen que una de las aplicaciones más importantes de los sistemas microfluídicos-LOC sea su inherente potencial como herramientas analíticas de cribado para diagnósticos rápidos.

Por otra parte, los nanomateriales unidimensionales (1-D) son estructuras en las que sólo una de sus dimensiones se corresponde con la escala nanométrica revelándose como estructuras que nos ofrecen no sólo una elevada relación superficie-volumen, sino también nos permiten la posibilidad de diseñar segmentos unidimensionales constituidos por diferentes materiales con propiedades electrónicas y funcionalidad controladas. En efecto, una característica importante de estas estructuras está relacionada con su química superficial a través de funcionalizaciones que se pueden diseñar para diferentes aplicaciones involucrando a diferentes tipos de biomoléculas, como por ejemplo, enzimas o anticuerpos.

Ejemplos reveladores, de estas nanoestructuras 1-D, son los nanohilos metálicos (MNWs), tanto elementales como bimetálicos y los micromotores, sofisticadas estructuras que poseen movimiento autónomo; constituyéndose ambas estructuras como nuevas e innovadoras alternativas para la detección en sistemas microfluídicos-LOC.

En primer lugar, los MNWs son nanoestructuras metálicas o semiconductoras con forma cilíndrica, sin ningún hueco en la estructura. Son estructuras anisotrópicas unidimensionales, con una alta superficie

específica y con dimensiones del orden de los nanómetros de diámetro y micrómetros de longitud.

Los MNWs son herramientas muy valiosas para la detección electroquímica. En efecto, debido a su gran área superficial, estas nanoestructuras ofrecen no sólo elevadas corrientes amperométricas lo que implica un aumento de la sensibilidad analítica, sino que también exhiben una elevada resistencia a la pasivación, implicando una muy buena reproducibilidad. Además, la electrocatálisis puede ser estratégicamente aprovechada y dirigida hacia la detección selectiva de analitos diana. Un ejemplo revelador lo constituyen los carbohidratos cuya oxidación electroquímica se ve favorecida por el efecto electrocatalítico del níquel y el cobre y, como consecuencia, cabría esperar una mejora en la eficacia de dicha electrocatálisis a través del empleo de nanohilos catalíticos de níquel (NiNWs) y cobre (CuNWs) para su detección.

Además, en los sistemas microfluídicos-LOC, la detección electroquímica es una herramienta muy valiosa debido a su inherente miniaturización, elevada sensibilidad y su compatibilidad con las micro y las nanotecnologías. Debido a los volúmenes extremadamente pequeños de muestra introducidos en los sistemas microfluídicos-LOC, la sensibilidad se convierte en uno de los inconvenientes más importantes de estos sistemas. Sin embargo, la sensibilidad puede ser mejorada mediante la explotación de las características superficiales de los nanomateriales, por lo que la incorporación de los mismos en la detección electroquímica en sistemas microfluídicos-LOC resulta pertinente.

En segundo lugar, los micromotores son dispositivos en la micro y nano escala, capaces de convertir la energía en movimiento autónomo. La fuente de energía de estos micromotores está estrechamente relacionada

con su forma, encontrándose el sistema de propulsión vinculado con la forma del micromotor. El movimiento autónomo de estas estructuras permite realizar diferentes etapas y funciones del proceso analítico de forma creativa y novedosa. El movimiento autónomo de estos micromotores funcionalizados y adecuadamente dirigido mediante la aplicación de fuerzas externas, ofrece extraordinarias oportunidades, tales como el desarrollo de futuros LOC sin necesidad de ningún movimiento de fluidos, evitando así su instrumentación derivada para producirlos.

Todas estas características mencionadas anteriormente, convierten a estas estructuras 1-D en herramientas únicas en el campo de la nanociencia y nanotecnología analíticas, y su exploración para la mejora de la detección en los sistemas microfluídicos-LOC ha constituido la principal motivación de esta Tesis Doctoral, articulada en dos objetivos claramente diferenciados.

El primer objetivo ha sido la síntesis y caracterización de los NiNWs y CuNWs para la detección electroquímica de carbohidratos empleando sistemas de flujo miniaturizados y sistemas microfluídicos-LOC

El segundo objetivo ha sido la síntesis y caracterización de micromotores para el desarrollo de un inmunoensayo con visualización óptica para la detección de proteínas en sistemas microfluídicos-LOC.

Los principales hitos a alcanzar fueron:

1. Optimizar la electrosíntesis de nanohilos de níquel, cobre y bimetálicos de níquel-cobre, empleando membranas de alúmina anodizada como moldes.

2. Caracterizar los nanohilos de níquel, cobre y bimetálicos de níquel-cobre empleando técnicas de microscopía electrónica, técnicas espectroscópicas y técnicas electroquímicas.

3. Diseñar y construir electrodos serigrafiados basados en nanohilos níquel, cobre y bimetálicos de níquel-cobre acoplados a sistemas de flujo miniaturizados para la detección de carbohidratos.

4. Diseñar y construir electrodos serigrafiados basados en nanohilos de níquel y cobre acoplados a sistemas microfluídicos-LOC para la detección de carbohidratos.

5. Optimizar la electrosíntesis de micromotores empleando membranas de policarbonato con forma de doble cono como moldes.

6. Caracterizar los micromotores empleando técnicas de microscopía óptica y electrónica.

7. Diseñar y funcionalizar los micromotores para el desarrollo de inmunoensayos en sistemas microfluídicos-LOC.

De acuerdo con los objetivos definidos, los resultados obtenidos en esta Tesis Doctoral se han agrupado en dos grandes **capítulos (II y III).** En el primero de ellos, se presentan la síntesis y caracterización de los NWs para la detección electroquímica de carbohidratos utilizando sistemas miniaturizados de flujo y sistemas microfluídicos-LOC. Los resultados

correspondientes a los sistemas de análisis por inyección en flujo por una parte y aquellos que emplean sistemas microfluídicos-LOC por otra, se han agrupado en dos partes claramente diferenciadas. Por su parte, en el **capítulo III**, se presentan los resultados obtenidos en la síntesis y caracterización de micromotores para el inmunoensayo óptico en sistemas microfluídicos-LOC.

A continuación se expondrán los resultados más relevantes obtenidos.

En el **capítulo II**, y en primer lugar, se ha estudiado con detalle la electrosíntesis y caracterización de los NWs. En estos trabajos, los nanohilos de níquel (NiNWs) y los bimetálicos de níquel-cobre (Ni-CuNWs) fueron sintetizados mediante electrodeposición utilizando moldes de alúmina y fueron caracterizados mediante microscopía electrónica de barrido (SEM), microscopía electrónica de transmisión (TEM) y espectrometría de dispersión energía de rayos X (EDS). Se emplearon para ello moldes de alúmina (200 nm) y condiciones de electrodeposición controlada de carga (45 C). Los MNWs exhibieron una alta perfección estructural con una longitud aproximada de 7 μm y un diámetro aproximado de 300 nm. El análisis por EDS confirmó su composición química con un porcentaje de Ni del 97% a lo largo de todo el NiNWs y con un porcentaje de níquel del 50,6% y de cobre del 49,4% en los Ni-CuNWs. Ambos NWs electrosintetizados exhibieron electrocatálisis hacia la detección de los carbohidratos estudiados (glucosa, fructosa, galactosa, sacarosa, lactosa e inulina).

A continuación, los NiNWs y los CuNWs fueron empleados para la construcción de los detectores electroquímicos, tanto en sistemas

miniaturizados de inyección en flujo (FIA) como en sistemas microfluídicos-LOC.

En primer lugar, se construyeron detectores electroquímicos serigrafiados desechables basados en NiNWs para la detección de carbohidratos en flujo hidrodinámico. Los estudios de XPS revelaron que los electrodos basados en NiNWs contenían sólo un 0.9 % de Ni y mostraron una mejora de la densidad de corriente de alrededor de 65 veces en comparación con el electrodo de disco de níquel. El magnetismo del níquel fue esencial para mantener la superficie nanoestructurada sobre la superficie del electrodo bajo las condiciones hidrodinámicas de trabajo. Los NiNWs activados electroquímicamente (-1.5 V, 600 s) bajo la acción de un campo magnético (2x4200 Gauss) exhibieron las mejores características analíticas en términos de excelentes relaciones S/N, tiempo de respuesta rápido y una elevada resistencia al ensuciamiento (RSD≤7 %, n=50). El comportamiento analítico de los NiNWs también resultó ser excelente durante el análisis de las muestras estudiadas, exhibiendo recuperaciones cuantitativas (95-115%) y reproducibles (RSD≤2%).

Estos eletrodos nanoestructurados, fueron también empleados para llevar a cabo la determinación de carbohidratos totales (glucosa+fructosa) en muestras de mieles empleando a su vez una estrategia de calibración simplificada (calibración con un punto y empleando una mezcla de glucosa-fructosa como patrón). El contenido total de azúcares obtenido por el método electroquímico se comparó con el obtenido por el método de cromatografía líquida con índice de refracción (HPLC-RI). Se obtuvieron errores sistemáticos bajos (Er<10%) revelando una buena exactitud del método. Asimismo, se obtuvo un elevado rendimiento de análisis de muestras (2 muestras/min.) sin pérdida aparente de las prestaciones analíticas del método. Debido a los resultados obtenidos, se ha propuesto el

término "Índice electroquímico de monosacáridos" para evaluar el contenido total de azúcares en estas muestras.

En una segunda parte claramente diferenciada, en el **capítulo II** se han recogido también los resultados correspondientes a las aplicaciones analíticas desarrolladas empleando sistemas microfluídicos-LOC con detección electroquímica basada en MNWs para el sensado de carbohidratos. En estas trabajos, los detectores electroquímicos serigrafiados (10x1 mm) adecuadamente diseñados para acoplarse a los sistemas microfluídicos-LOC, fueron caracterizados por microscopia electrónica de barrido con emisión de campo (FESEM); revelándose unas superficies constituidas por NiNWs y CuNWs bien definidos (6 μm de longitud, y 300 nm de diámetro). Asimismo, estos electrodos modificados mostraron una superficie específica aumentada (un factor de 2) en comparación con aquellos sin modicar, tal y como se dedujo de los estudios de cronocoulombimetría.

A continuación, estos electrodos se acoplaron de manera adecuada a los sistemas microfluídicos-LOC (en formato de microchip) para el desarrollo de tres aplicaciones analíticas bien definidas dentro de los ámbitos agroalimentario y clínico. En estas contribuciones, conceptualmente hablando, se partió de la hipótesis de que la selectividad y la sensibilidad inherentes de los CuNWs hacia la detección de los carbohidratos, en conjunción con la selectividad de los sistemas microfluídicos-LOC, permitiría la detección rápida y simultánea de estos analitos-diana con la ventajas adicionales que nos ofrecen los LOC de tiempos de análisis cortos y bajo consumo de muestras; constituyendo una alternativa atractiva a las aproximaciones analíticas bien establecidas en la literatura (basadas en su mayoría en el uso de enzimas o protocolos de HPLC).

En primer lugar, se desarrolló un sensor microfluídico-LOC con detección electroquímica empleando NiNWs y CuNWs electrosintetizados para la detección de inulina. La inulina es un fructo-oligosacárido que contiene hasta 35 unidades de fructosa unidas a través de enlaces β-1,2-glicosídicos y que posee una alta importancia en los ámbitos agroalimentario y clínico llegando a ser un carbohidrato importante con diversos beneficios para la salud. La detección de inulina se realizó de forma selectiva, en presencia de fructosa libre, en menos de 300 s. Aunque tanto los NiNWs y los CuNWs mostraron electrocatálisis hacia la detección de inulina, se obtuvo 3 veces mayor sensibilidad usando los CuNWs en comparación con los NiNWs; por lo que estos nanohilos fueron los elegidos como más adecuados. Asimismo, se obtuvo una muy buena repetibilidad *intra*-electrodo (RSD<8%; n=5) y una también muy buena reproducibilidad *inter*-electrodos (RSD<9%; n=4), lo que indicó una excelente estabilidad del cobre nano-escalado. Un resultado muy interesante resultó ser la elevada sensibilidad que exhibió la inulina, a pesar de su estructura compleja, en comparación con la encontrada para su monómero, fructosa, resultando ser 40 veces superior. La combinación de la elevada sensibilidad y del bajo nivel de ruido permitió obtener LODs de 3 μM para este carbohidrato. Durante el análisis de muestras reales, se obtuvieron, asimismo, recuperaciones cuantitativas y reproducibles (97-103%, RSD<4%) indicando un comportamiento analítico del método excelente en dichos términos.

La detección electroquímica acoplada a los sistemas microfluídicos cuando éstos son utilizados como microchips de electroforesis (ME), ha demostrado ser una herramienta poderosa en el análisis de alimentos. Sin embargo, el empleo de nanomateriales en estos sistemas microfluídicos no se ha estudiado con profundidad, aun sabiendo que los nanomateriales pueden mejorar significativamente el rendimiento analítico de los mismos,

tal y como se ha indicado anteriormente. En este sentido y seguidamente, se estudió el acoplamiento entre el ME con nanohilos de cobre (CuNWs) para el análisis individual de monosacáridos (glucosa y fructosa) en muestras de mieles. La estrategia empleando los ME-CuNWs permitió la separación de glucosa y fructosa en tiempos inferiores a 250 s bajo condiciones optimizadas de separación (NaOH 20 mM + 10 mM H_3BO_3, pH=12; voltage de separación de 1000 V) y detección (E=+0,70 V en NaOH 20 mM + H_3BO_3 10 mM, pH=12). Asimismo se obtuvo una excelente estabilidad en el flujo electro-osmótico (EOF) durante el análisis de las muestras (RSDs<2% en tiempos de migración). Los contenidos cuantitativos de glucosa y fructosa obtenidos individualmente empleando ME-CuNWs fueron comparados con los obtenidos mediante HPLC-RI encontrándose una elevada concordancia entre ellos y mostrando errores por debajo de 10% indicando una buena exactitud del método.

Por último, se estudió el acoplamiento de los sistemas microfluídicos-LOC con CuNWs como detectores electroquímicos para el diagnóstico rápido de galactosemia en muestras de orina de neonatos. La galactosemia es una enfermedad rara que se diagnostica mediante la detección específica de galactosa 1-fosfato (Gal 1-P), galactosa (Gal) y galactosa uridil difosfato (UDP-Gal), según se corresponda con los diferentes tipos de galactosemia, I , II y III; respectivamente. Debido a la baja prevalencia de esta enfermedad, la disponibilidad de muestra es muy escasa y los métodos de cribado para el diagnóstico de la misma no son comúnmente empleados. En estos trabajos, de nuevo el detector electroquímico nanoescalado mostró una excelente estabilidad tal y como lo indicaron la repetibilidad *intra*-electrodo (RSD<8%; n=10) y la reproducibilidad *inter*-electrodos (RSD <12%; n=5) obtenidas. Bajo condiciones óptimas de separación (NaOH 3 mM, pH=11,5; voltaje de

separación de +750 V) y de detección (E=+0,70 V en NaOH 3 mM, pH=11,5), se identificaron los diferentes tipos de galactosemias de manera inequívoca, diferenciando entre los tipos I, II, III usando muestras de orina de neonatos enfermos previamente diagnosticados. La detección se llevó a cabo en menos de 350 s, requiriéndose un bajísimo consumo de muestra de orina, con una relación S/N excelente (comprendida entre 14 y 80), LODs en el rango micro-molar, mucho más bajos que los niveles de corte (Gal 1-P>0,4 mM y Gal>1,4 mM) y recuperaciones cuantitativas y reproducibles (93-107%, RSD<6%). La importancia de las muestras de orina de neonatos estudiadas confirmó el potencial analítico del acoplamiento LOC-CuNWs revelando la madurez de la tecnología y abriendo nuevas vías para la futura implementación de aplicaciones de cribado en el campo.

Por otra parte, el **capítulo III** agrupa los resultados obtenidos en la síntesis y caracterización de micromotores para la detección óptica de proteínas usando sistemas microfluídicos-LOC, en este caso de polydimetil-siloxano (PDMS). En este trabajo, se diseñaron y desarrollaron micromotores catalíticos auto-propulsados y funcionalizados con anticuerpos para el reconocimiento, interacción y transporte de proteínas diana entre los diferentes reservorios de un dispositivo microfluídico-LOC. Estos micromotores catalíticos estuvieron constituidos por la arquitectura polímero/Ni/Pt. El polímero contiene restos carboxi en la capa polimérica más externa del polimero mixto (3,4-etilendioxitiofeno) (PEDOT)/COOH-PEDOT y fue funcionalizado posteriormente con el receptor de anticuerpo para reconocer selectivamente y capturar la proteína diana y poder llevar a cabo de esta forma y con éxito todas las etapas que constituyen un inmunoanálisis. El Pt permitió la generación de burbujas de oxígeno producidas por la catálisis del peróxido de hidrógeno sobre su superficie y el níquel permitió guiar adecuadamene el movimiento autónomo de dicho

micromotor generado por la propulsión ejercida por las mencionadas burbujas de oxígeno. En estos trabajos, todas las etapas del inmunoensayo se llevaron a cabo sin el empleo de ningún flujo y evitando todas las etapas de lavado comunes en bioensayos de proteínas empleando anticuerpos, gracias el transporte autónomo de la proteína capturada a través de los diferentes reservorios del sistema microfluídico.

Finalmente, del conjunto de los resultados obtenidos en esta Tesis Doctoral, se puede concluir que los materiales unidimensionales estudiados -nanohilos catalíticos de níquel y cobre y los micromotores- han demostrado ser herramientas de análisis muy poderosas para mejorar la (bio)detección de moléculas diana en los campos tanto agroalimentario como clínico, empleando sistemas miniaturizados de análisis por inyección en flujo y sistemas microfluídicos basados en la tecnología *lab-on-a-chip* (LOC). Las ventajas inherentes de los sistemas de microfluídicos, tales como, la rapidez de análisis y bajo consumo de muestra y reactivos, además de las derivadas de la alta superficie específica y altamente funcionalizada de los nanomateriales estudiados, han sido creativa y sinérgicamente explotadas.

Asimismo, el conjunto de los resultados presentados revelan la pertinencia y conveniencia del acoplamiento entre las microtecnologías y las nanotecnologías para la detección de moléculas diana en sistemas analíticos complejos dentro de los ámbitos agroalimentario y clínico, ampliándose nuevos horizontes en la Química Analítica contemporánea.

.

LIST OF FIGURES

Figures in the main text

Figures in supporting information

LIST OF TABLES

Tables in the main text

Tables in supporting information

I. Hypothesis, motivation and milestones

On the one hand, microfluidic systems and lab-on-a-chip (LOC) technologies seek to improve analytical performance by reducing the analysis time, decreasing the consumption of sample and reagents, diminishing the risk of contamination, integrating multiplexing analysis, and especially portability to provide the possibility of point-of-care and in field applications. In addition, one of the most powerful analytical applications of microfluidic-LOC systems relies on their inherent potency as screening tools for rapid diagnosis.

On the other hand, the discovery of new materials, at the micro and nanoscale has opened new opportunities for the development of creative research. The inherent versatility of nanomaterials produces different shapes and sizes reaching the different dimensions of the material. As important blocks of nanotechnology, 1-D nanomaterials as structures with only one dimension extend, are very unique not only because they offer a high surface to volume, but also because they can easily be designed and fabricated with different segments which add tunable electronic properties and controlled functionality. This functionality includes from bimetallic nanowires that implies two materials and shows two functions (i.e. nickel and gold for magnetic guidance and chemistry functionalization, respectively) to sophisticated structures that possess autonomous movement (micromotors) as new and innovative alternatives for sensing and biosensing.

Therefore, the development of new (bio)-sensing methods on boards of microfluidic-LOC systems based on the use of smart 1-D nanostructures such as metallic nanowires and micromotors comprise a new spectacular horizon.

Firstly, metallic nanowires (MNWs) are metallic or semiconducting nanostructures with cylindrical shape, without any hollow in the structure. They are one-dimensional anisotropic structures, with high specific surface and high aspect ratio (nanometers in diameter, micrometers in length).

MNWs are very valuable tools for electrochemical sensing. They offer high currents because of their large surface area, thereby enabling large scale redox conversion, which increases the analytical sensitivity, and resistance passivation, and it yields very good reproducibility. In addition, electrocatalysis can be strategically exploited and well-conducted toward the selective detection of target analytes. Since it is well-known that the electrochemical oxidation of carbohydrates is favored by the electrocatalytic effect of copper and nickel; an improved analytical performance by the use of these catalytic nickel and copper nanowires, is highly expected for detection of these important analytes.

In addition, in microfluidic-LOC systems, electrochemistry is a valuable detection mode that provides inherent sensitivity, permits miniaturization, and is highly compatible with micro- and nanotechnologies. Because of the extremely low sample volumes introduced into microfluidic-LOC systems, the chip sensitivity is often low and presents a drawback of these systems; however the sensitivity can be enhanced and the problem overcome by exploiting the surface characteristics of nanomaterials, become as consequence the microfluidic-LOC systems coupling very pertinent.

Secondly, micromotors are devices in the micro and nano scales capable of converting energy into movement and forces. The energy source is closely related to the microstructure shape, actually both shape and propulsion systems are connected. We can expect from micromotors new

and enhanced features related to their special characteristics. A remarkable one is its autonomous movement which can improve different steps of the analytical process, such as sample enrichment or detection. Another important characteristic of these micromotors is related to its tunable surface through different functionalization which can be used in many applications involving different kind of biomolecules, such as, enzymes or antibodies. The employment of these micromotors in confined microfluidic-LOC systems offers extraordinary promises such as the development of future free-fluidic pumping LOCs and avoids their derived instrumentation (i.e. pumps or high voltage suppliers) supporting the new (bio) sensing in the micromotors autonomous guided movement.

All the characteristics mentioned above, convert these 1-D structures into unique tools in the current analytical nanoscience and nanotechnology field, and their exploration for improving detection of microfluidic-LOC systems has constituted the main motivation of this Doctoral Thesis.

Accordingly, this Doctoral Thesis has two well-defined objectives.

The first objective has been the synthesis and characterization of nickel and copper NWs for electrochemical carbohydrate sensing using flow-based miniaturized systems and microfluidic-LOC systems

The second objective has been the synthesis and characterization of micromotors for optical immunoassay of proteins in microfluidic-LOC systems. IgG protein was chosen as model analyte.

The main identified milestones were:

1- Optimization of the electro synthesis of nickel, copper and bimetallic nickel-copper nanowires using anodized alumina membranes as templates

2- Analytical characterization of the nickel, copper and bimetallic nickel-copper nanowires using optical and electron microscopy, spectroscopy and electrochemical techniques

3- Design and construction of screen printed detectors based on nickel, copper and bimetallic copper-nickel nanowires coupled to miniaturized flow injection devices for carbohydrate sensing

4- Design and construction of electrochemical detectors based on nickel and copper nanowires coupled to microfluidic-LOC systems for carbohydrate sensing

5- Optimization of the electro synthesis of micromotors using polycarbonate double conical membranes as templates

6- Analytical characterization of the micromotors using optical and electron microscopy.

7- Design of micromotors for immunoassay in microfluidic-LOC systems

Accordingly to the target objectives, this thesis is divided in two main chapters. In the first chapter, synthesis and characterization of nanowires for carbohydrate electrochemical sensing using flow and microfluidic-LOC systems are presented. Further, the works involving flow injection analysis and microfluidic-LOC systems will be presented in two well-separated sections, respectively. In the second chapter, the synthesis

and characterization of micromotors for optical immunoassay in microfluidic-LOC systems are further presented. Finally, a general conclusion is briefly stated and future works are outlined.

II. Synthesis and characterization of nickel and copper nanowires for carbohydrate electrochemical sensing in miniaturized and microfluidic systems

II.1. Nanowires for electrochemical sensing and biosensing. *State of the art*

II.1.1. Why nanowires for electrochemical (bio-)-sensing?

Nanotechnology refers to any technology built in the nanoscale metrics that has applications on the real world[1]. For this reason, it covers the production and application of physical, chemical and biological systems at different scales: it goes from individual atoms or molecules to the integration of the resulting nanostructures into larger systems. Nanotechnology presents applications in a variety of fields, so research in nanotechnology encourages breakthroughs in many different areas such as materials, nanoelectronics, healthcare, energy or biotechnology. For the construction of the necessary elements two approaches are employed: top-down and bottom-up. The top-down approach is based on the modification of an original piece of material that is modeled, removing the unnecessary parts until the desired shape is achieved; comparatively is like a sculptor building a statue from a raw piece of stone. It is commonly employed in electronics for chips construction, it is required the use of a mask to protect certain parts of the material and then chemically (i.e. acids) or physically (i.e. UV light) etched to get the desired design. The bottom-up approach can be understood as the opposite way; the fabrication of nano or micro structures made by linking small pieces as is done with the bricks for building houses. Atoms and small molecules are linked to fabricate the desired object; some examples of bottom-up approaches are the chemical synthesis or the electrochemistry, because atoms in a solution react to form a specific compound with a specific shape.

The nature inspires the design of new processes to create micro and nano devices, being the bottom-up processes an alternative to overcome the inherent difficulties of the top-down approach related to the complex processes and instrumentation needed. Micro and nanosystems were usually at the beginning fabricated using top-down techniques, but the continuous

improvement for the construction of smaller devices provides nowadays a wide variety of approaches.

Mimicking the nature, we are able to chemically control the assembly of nanomaterials as building blocks to construct new devices with innovative properties derived from its nano constituents[2, 3]. The discovery of new materials, shapes, processes and unexpected characteristics at the nanoscale have opened new opportunities for the development of imaginative and creative research[1, 4, 5].

The inherent versatility of nanomaterials produces different nano-shapes and sizes reaching the different dimensions of the material. Depending on the shape and the nanomaterial distribution they can be considered as 0-D materials when are single dots (quantum dots, nanoparticles); 1-D material, structures with only one dimension extend (nanotubes, nanowires, nanorods, or narrow sheets); 2-D materials with a planar structure forming a sheet or a network (graphene), and 3-D nanomaterials when they possess a similar size in all dimensions but always being under 100 nm to fit the nano definition. These 3-D nanomaterials are usually formed by a combination of other nanostructures. **Figure II.1** illustrates each of the examples.

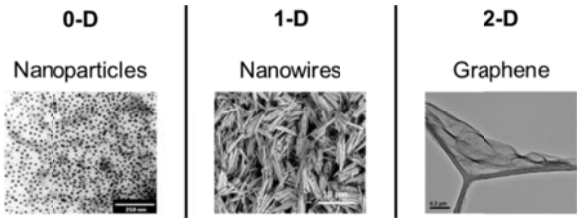

Figure II.1. The nanomaterials and their dimensional distribution

Among these nanomaterials, nanowires (NWs) are 1-D important blocks of nanotechnology and they can be formed by a variety of materials.

The most relevant are the metallic (MNWs) and polymeric (PolyNWs) ones; being the metallic ones from elements or oxides. MNWs are metallic or semiconducting nanostructures with cylindrical shape, completely filled without any hollows in the structure, because if the structure were hollow it would be a nanotube. They are one-dimensional anisotropic structures, small in diameter and large in surface to volume ratio. They can be found in different sizes from a few nanometers to the limit of the nano scale (100 nm). The length of NWs is bigger, involving from a few micrometers (2-3) up to tens of micrometers. Because of their geometry, one of the most relevant features making them unique with respect other nanostructures is that they can be easily designed and fabricated with different segments which add controlled functionality. An extremely simple and relevant example is illustrated in **Figure II.2** where a bimetallic MNW constituted by gold and nickel segments would be applied for functionalization chemistry and magnetic guidance control respectively.

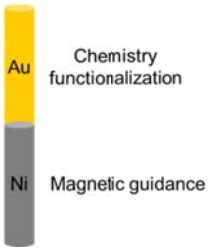

Figure II.2. Bimetallic nickel-gold nanowires

NWs are capturing the scientific community attention due to their improved functionalities when comparing them to the bulk material. We can tailor their properties by controlling certain parameters and exploiting singular aspects of the one-dimensional electronic density states. As electroanalysis is a surface dependent technique, the introduction of NWs opens the door to larger areas and we can expect from them an improved analytical performance. Among these characteristics, stand out the

enhanced conductivity and high specific surface area due to this new material configuration. Herein, we are conceptually describing the advantages derived from the use of NWs in the electrochemical sensing and biosensing field:

(i) *Lower detection potentials*. The greater surface area of NWs-based electrodes leads to lower current densities and therefore to lower "overpotentials" and a high efficiency in the electrocatalysis. It might have a strong effect on the electrocatalysis of analytes, therefore on lowering the detection potentials and in consequence, improving the overall selectivity of the analysis.

(ii) *Higher currents* because the greater surface area of NWs-detectors enable larger scale redox conversion, consequently increasing the analytical sensitivity.

(iii) *Higher resistance to passivation* originated from the greater surface area of the NWs-based detectors. This characteristic implies better reproducibility because the resulting signal is prone to fouling.

(iv) *High compatibility and functionality with bio-molecules*. Biological systems can be very complex and sometimes, in order to work properly, they need several biomolecules in intimate proximity. As NWs can be made with fragments of different metals, a differentiated and oriented biofunctionalization of the NWs can be performed, developing a selective functionalization strategy for each NWs' metal-fragment.

NWs made from different materials (metal, metal oxides or polymers) have appeared in relevant literature during the last years, not only dealing with the fabrication but also for its application in electrochemical

sensing and biosensing[6-10], however no reviews covering NWs in electrochemical sensing and biosensing have been reported in the field with the exception of a specific short review of adaptative nanowires for microsystems[10]. Accordingly with the scope of this Thesis, this introduction pretends to give an overview and rational approach about the synthesis, characterization and applications of NWs in the field of electrochemical sensing and biosensing.

In the following sections, after a brief outline about synthesis and characterization of NWs, we will critically discuss along selected examples the use of NWs in the electroanalysis field. Firstly, electrochemical sensing and biosensing based NWs approaches will be discussed in two well-separated sections and then we will mention the approaches involving NWs in microfluidic systems.

II.1.2. Synthesis of nanowires

NWs are the perfect candidates for the bottom-up fabrication approach, permitting the design of nanostructures and its consequent assembly to reach nanotechnology-based applications. Over the last years, MNW have been fabricated using a variety of techniques, such as template assisted electrodeposition, chemical methods or chemical vapor deposition (CVD). Recently, the template assisted electrodeposition of NWs has attracted considerable attention; mainly owing to the possibility of controlling the length, diameter, and density of the fabricated NWs by varying the deposition parameters or the template in a simple protocol without the necessity of complex instrumentation. In the following sections, we are going to describe briefly the different approaches.

II.1.2.1 Template assisted approaches

The template assisted synthesis of NWs is an easy and intuitive manner to fabricate these nanostructures. These templates present small pores with cylindrical shape, which are the hollows that will be filled with the desired material adapting the shape of the pore to form the NWs. **Figure II.3** shows a synthesis template assisted scheme.

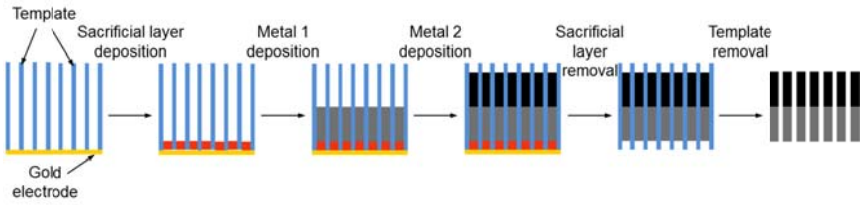

Figure II.3. Scheme of NWs synthesis by template assisted method.

Firstly, a suitable template must be selected. It is necessary to consider the mechanical and chemical stability of the template as well as other properties such as the pore size, shape or template material. The most

common employed materials for NW fabrication are anodic alumina oxide (Al_2O_3) (AAO) and ion track-etched polycarbonate (PC) templates. Both materials, AAO and PC, are widely employed for fabrication of filtration membranes, existing a broad variety of them with the adequate characteristics for its employment as template for NW synthesis. Other sort of membranes has also been used as templates, such as porous materials like porous silicon[11], zeolites[12], CNTs[13, 14] and even biomolecules like DNA[15].

Alumina templates are produced by anodization of pure aluminum films utilizing acids, obtaining at the end of the process quasi cylindrical and parallel channels. They are very appreciated due to the uniformity of the pores and the high pore density achieved during the fabrication (10^9-10^{11} pores/cm^2). Furthermore, different pore diameters can be obtained by varying the anodization conditions, ranging from diameters of a few nanometers (<10) to 200 nm. PC templates are fabricated by ion bombardment of PC foils, followed by chemically etching of the ion tracks, obtaining a pore density up to 10^9 pores/cm^2. Pores in this kind of templates are randomly distributed due to the fabrication process. Pore size and geometry can be tuned by varying the ion bombardment conditions.

In order to simplify the process of NW synthesis these commercial membranes are commonly employed[16, 17], avoiding the template fabrication step and focusing the efforts on the NW fabrication parameters. As the principal aim of this review is NWs fabrication and its applications for sensing and biosensing, we will focus on those works employing the commercial available membranes as templates and we will not go into details about the templates synthesis.

II.1.2.1.1 Electrochemical deposition

The electrochemical synthesis of NWs by electrochemical deposition involves the reduction of a metal salt in the case of metals, following the reaction:

$$M^{n+}_{(solution)} + ne^- \longrightarrow M_{(metallic)}$$

The necessary electrons to carry out the process are provided by an external power supply (potentiostat)[18, 19]. The electrodeposition combined with membranes for the synthesis of NWs creates a low-cost technique that contributed to increase the interest in NWs.

Direct template electrodeposition is a wet chemical synthesis technique based on the NW growth by reduction of metal ions within the pores of a membrane. When the potential is applied, cations diffuse through the channels and are deposited on the cathode, growing the NWs inside the template. The process usually takes place at room temperature and at ambient pressure, avoiding complex and high cost equipment and making this approach extremely attractive for a low cost and easy production of NWs[20].

Three electrodes compose the system, as in a regular electrochemical cell. An Ag/AgCl electrode and a platinum wire act as reference and counter electrodes, respectively. The NWs will grow on a surface that will act as the working electrode. The working electrode is the most special one in these devices. Indeed, to get the metal ions reduced inside the membrane pores, the membrane is transformed into a working electrode by sputtering a gold or platinum thin layer in one side of the membrane. The membrane sputtering introduces a thin working electrode at the membrane bottom, and over this new electrode the electrochemical

process of NWs growth happens. NWs grow in the unique free space, this is the membrane pores. Consequently, the NWs will adopt the shape of the pores whereas the length of the NWs can be easily controlled by monitoring the deposited charge.

As already mentioned, among the membranes, AAO membranes have been considered an ideal template as they have many desirable characteristics, including a variety of pore dimensions, good mechanical strength, thermal stability and ordered nanotubes. For all these reasons they have also been widely used for electrochemical deposition. Moreover, AAO membranes present a high pore density (10^9–10^{11} cm^2) which makes possible an elevated number of nanostructures.

The electrochemical approach offers considerable advantages over other methods due to the wide variety of materials that can be electrolyzed to form the desired nanostructures, like metals (Ni, Cu, Au, Zn, Ag, Fe)[21-24]; conducting polymers (polypirrole, polyaniline, 3,4-ethylenedioxythiophene)[25, 26]; and semiconductors (CdSe, ZnO)[27]. This wide variety provides the possibility to synthesize NWs with sequentially deposited materials just by changing the electroplating solution or by changing the deposition conditions [24]; opening the possibility to customize the nanostructures on demand for specific applications. As already mentioned, and as representative example, NWs with gold and nickel segments would be useful for thiol chemistry and magnetic control respectively, as it was already shown in **Figure II.2**.

Electrochemical techniques can also be employed for growing polymeric NWs; this is, NWs synthesized by oxidative polymerization of the corresponding monomer. In this case, the monomer also polymerize inside the pores of the template adapting to its cylindrical shape[25].

II.1.2.1.2 Electroless deposition

Another NWs synthesis approach is the electroless deposition process. It is a chemical deposition process involving the use of a chemical agent to coat a material onto the template surface. There are two differences with the previous described technique. Firstly, electroless deposition is not limited to electrically conductive reagents. Secondly, the deposition starts from the pore wall and proceeds inwardly in contrast to electrodeposition where the growth starts at the bottom of the pores and from there the NWs grow. This particular way of growing allows the formation of hollow structures, like nanotubes, instead of solid NWs[28, 29]. The length of the nanotubes depends on several factors; mainly in the length of the deposition channels because the deposition time would affect nanotubes' wall thickness. An increase in deposition time leads to thicker walls but not affects NWs' thickness.

II.1.2.1.3 Template filling

With this technique, the template pores are filled with a liquid precursor or a colloidal suspension. Afterwards, a solidification process takes place. This is a very simple route but it is very important to ensure that the pores are completely filled with the liquid[30, 31]. If a solution has a good wettability for the template, the solution is able to diffuse through the membrane producing an enrichment of the solid component in the interior of the pores. When the pores are completely filled, the template is removed from the solution and dried. Later on, the membrane was burnt to remove the template and obtain the free NWs. Another alternative way for filling the pores with metallic materials is the use of molten metals. In this case, the template is immersed in the liquid metal and high gas pressure is applied to allow the pore filling. Polymeric NWs have also been synthesized by this

method, with a solution that contains not only the monomer but also a polymerization agent able to trigger the reaction.

II.1.2.2 Template free approaches

In order to avoid the employment of templates to simplify the synthesis of NWs or elude the hard conditions employed for the template removal, some template free methods have been developed[32].

II.1.2.2.1 Chemical approach

Chemical approach is a strategy employed for NWs fabrication that does not need any template. The NWs grow over a metal wire or an electrodic surface that act like a support for the growth. The wire is dipped briefly into a solution which contains the reagents that will form the NW, being afterwards dried. This process can be repeated to obtain the desired structure or to get higher yields in the process. A similar approach is the polymerization of a monomer over an electrode, creating a new surface able to load biological material, such as enzymes, and also increasing the surface improving the electrochemical characteristics of the resulting composite electrode.

One relevant example of this approach is the polyol synthesis method which is based on the addition of reagents drop by drop at a constant solution temperature in which ethylene glycol (EG) act as both, solvent and reducing agent. The polyol synthesis was originally introduced by Fievet et al.[33] as an excellent method for the synthesis of submicrometer-sized metallic nanoparticles. Nowadays, is a common approach for the synthesis of metallic nanostructures.

The chemical approach is a highly versatile method, with many possible variations, such as temperature, additives, or stirring speed. As an

example, Sun et al.[34] developed a protocol for the synthesis of silver NWs, introducing poly(vinylpyrrolidone) (PVP) as a coordination reagent able to control the size and shape of the formed nanostructures.

II.1.2.2.2 Nanowires built from nanoparticles

This templateless approach is based on the growing of NWs using nanoparticles as construction material. A mixture solution of an aqueous colloidal metal nanoparticle suspension and an organic solvent (i.e. toluene) is agitated. The vigorous movement facilitates the drain of the nanoparticles to the organic phase. The interaction between the organic phase and the nanoparticles decreases the mutual electrostatic repulsion allowing the nanoparticle coalescence and subsequently the NWs formation. With this methodology, the fabricated NWs are like a chain linked by the nanoparticles[35]. The main advantage of this method remains in avoiding the step of the template removal, often difficult or aggressive, to the already synthesized nanostructure.

Sun et al.[36], have developed a synthetic method for growing silver NWs from platinum nanoparticles seeds. In a first step, platinum nanoparticles are formed by reduction of $PtCl_2$ with EG that acts as both solvent and reducing agent. Once Pt nanoparticles are formed, $AgNO_3$ is added to the solution forming silver nanoparticles. The reaction mixture is refluxed at 160 °C, to induce the smaller silver nanoparticles to dissolve and grow over the bigger ones, producing as a result silver NWs. Modification of the experimental conditions, such as, temperature or the seed solution concentration, directly influence in the characteristics of the NWs.

Caswell et al.[32] followed a different approach modifying the methodology for nanoparticles' synthesis: metal ions are reduced by citrate or another reducing agent in a boiling solution to form nanoparticles. The

novelty of this work consists in obtaining NWs by varying the experimental conditions. Hence, it is possible to promote the growth of these nanoparticles in a certain direction, influenced by the reducing agent, and as a result NWs are finally synthesized. This method offers a simple route for NWs fabrication being a very clean alternative because it avoids the template removal and the presence of interferences due to this step.

II.1.2.2.3 Chemical vapor deposition

Chemical vapor deposition (CVD) is a common technique for CNT synthesis without using any template which has also been explored for NWs. In short, CVD is based in the deposition of a solid material from a gaseous phase, on a solid substrate. This solid support is usually silicon wafers but also other materials as metal sheets can be employed.

During the process, the precursor gases pass through a reaction chamber and come into contact with the heated substrate, then it reacts or decomposes forming a solid phase.

This technique is able to produce large-scale amounts of nanomaterials, so it is very promising for future applications involving nanomaterials such as energy storage or new materials with a nanostructure coating[37, 38]. In contrast, this technique involves the use of complex instrumentation and usually high temperatures and longtime processes are required.

II.1.2.3. Carbothermal reduction

This method is based in the mixture of a compound, containing the desired element that will form the NW, with the carbon reduction agent (i.e. graphite powder). The mixture is placed in the furnace at several hundreds of Celsius degrees. This process permit to achieve the elemental form of

many metals but is not suitable for the metal oxides due to the drastic conditions employed[39].

II.1.2.4. Chemical etching

Chemical etching is not strictly a metal NW synthesis technique as it is employed to decorate previously synthesized NWs. Metals are deposited by electroless plating on the NWs, typically silicon NWs. Silicon NWs are usually fabricated by lithography or by CVD processes[40, 41] because the characteristics of the silicon NWs obtained by these methods are well-known.

In summary, the methods described above have different characteristics, with well-defined advantages and disadvantages. The fabrication process is commonly related to the later application. For example, NWs are grown directly over an electrode to avoid its fixation over the surface, electrochemical deposition assisted by templates is used in order to obtain free NWs ready for different processes (modifications, functionalization) using simple instrumentation while chemical protocols are needed when the reagents are not electroactive, because harder conditions are required.

II.1.3. Characterization of nanowires

The characterization of the NWs is an essential step to check the correct fabrication of the nanostructures. Commonly, NWs are defined by their shape, i.e. their length and their diameter and also by its chemical composition, so we need to ensure all these characteristics by using different techniques.

NWs characterization is commonly carried out using electron microscopy, both transmission electron microscopy (TEM) and scanning electron microscopy (SEM).

SEM is more extensively employed for NWs study because it covers the wide size range of NWs (from a few nanometers to hundreds of nanometers in diameter, as well as microns in length) allowing not only a complete visualization of the nanostructure but also a detailed study of their surfaces. The employment of SEM for NWs characterization also enables the study of bulk materials. Additionally, it allows the observation of larger areas, studying the distribution of these nanomaterials over the surface and getting more information about the size distribution.

TEM is used when NWs size is in the resolution limits of SEM (a few nanometers) or when higher magnification is desired although it is not frequently employed for NWs study. This technique is more convenient for other kind of nanostructures observation such as nanoparticles.

Field-emission scanning electron microscopy (FESEM) has also been employed when the electrodes are modified with the NWs to study its distribution over the electrode. FESEM is employed to obtain higher resolution images in less aggressive conditions enabling the sample conservation, since no metal coating of the sample is needed. FESEM also

offers the advantage of a non-destructive technique and can work in the presence of humidity in the chamber.

Energy dispersive X-ray spectrometry (EDS) is an analytical technique used for elemental analysis of a sample that supports the study of NWs composition or its purity. For a more complete elemental composition, X-ray photoelectron spectroscopy (XPS) is done. XPS gives quantitative information about the surface chemistry including the empirical formula or the chemical state of the compounds in the surface.

When the NWs are functionalized with a biomolecule, several electrochemical techniques can be applied in order to characterize the binding of the biomolecule to the NWs' surface. Among these techniques cyclic voltammetry (CV) and electrochemical impedance spectroscopy (EIS) are the most used ones, because they compare the behavior of the electrodes depending on their modification and study the interface properties of modified electrodes.

II.1.4. Nanowires in electrochemical sensing

A variety of inorganic and organic target molecules have been electrochemically detected using both MNWs and PolyNWs. In this section, firstly the application of NWs in sensing of hydrogen peroxide (excluding when this molecule comes from an enzymatic reaction) and inorganic analytes will be presented. Then, the critical discussion of organic molecules will be stated involving a wide range such as ascorbic acid (AA), hydrazines, carbohydrates, alcohols, drugs and dyes.

Several examples for free-enzyme electrochemical sensing-based NWs for H_2O_2 have appeared in the literature. H_2O_2 is widely extended in nature as human metabolite indicating the existence of an illness as well as a product metabolite in food decomposition, being indicative of the product quality as well. X. Gao et al.[42] employed a chitosan film to hold the synthesized silver NWs over the surface of a glassy carbon electrode (GCE) and in that way enhancing not only the sensor sensitivity due to the NWs but also the architecture stability through the chitosan polymer film. In another strategy[43], a modified GCE with ultra-long MnOOH NWs achieved an amperometric detector with enhanced sensitivity and selectivity. Y. Zhou et al.[44] synthesized gold-platinum alloy NWs for hydrogen peroxide detection in microelectrode devices. The obtained synergies are derived from the combination of the metals present in the alloy; as a result of the enhanced sensitivity of the alloy versus individual metals, a wider linear range and selectivity in the presence of common interference species was achieved easily. Taking advantage of the great background existing on silicon structures synthesis techniques, Q. Yan et al.[41] synthesized silicon NWs via chemical etching and afterwards these silicon NWs were decorated with nickel via an electroless deposition. CV and amperometry were employed to investigate the suitability of the Ni/Si NWs electrodes. As

happens with other transition metals, the presence of nickel oxides in the surface of the electrode is related with the observed electrocatalysis. It is hypothesized that the H_2O_2 reacts with the nickel oxides reducing its form Ni^{3+} to Ni^{2+} and the subsequent electrochemical re-oxidation to Ni^{3+} produce the analytical current.

Polypyrrole (PPy) conducting polymers have also been nanoscaled to build NWs for detection of important molecules such as ammonia and hydrazines. M.P. Massafera et al.[45], presented a sensor based on PPy-NWs grown by a template free approach on the surface of a gold electrode for ammonia sensing in solution. An increment in the amount of PPy produced a current increase. In contrast, longer NWs led to a reduction in the conductivity and therefore in the sensor sensitivity, then a compromise between the PPy amount deposited and the length of the NWs was required. The length of the NWs influences the electrochemical response, but there is not a general conclusion about it. Longer NWs often result in a loss of performance but it depends on each specific case.

J. Lin et al.[46] built a sensitive and selective sensor for sensing hydrazine and hydroxylamine by a two steps modification process. Firstly PPy-NWs were deposited on the surface of a GCE, then, gold nanoparticles (GNPs) were electrochemically deposited over the PPy-NWs modified electrode. PPy-NWs network is an efficient electron transporter between the GNPs and the GCE surface, and also provides a 3D structure to support the GNPs increasing the active surface area and the mass transport rate, and as a result it reduces the accumulation of oxidation products preventing the electrode fouling. This antifouling effect gives the system the necessary reproducibility. It is also remarkable the electrocatalytic effect of the composite electrode that lowered the potential peak for both compounds from +0.600 V to +0.181 and +0.218 in the CV studies for

hydrazine and hydroxylamine respectively. It provides the necessary selectivity towards other electroactive nitrogen containing compounds converting the developed sensor in a suitable platform for monitoring industrial processes regarding these important and extensively used compounds.

Detection of AA and formaldehyde has been explored using palladium NWs. D. Wen et al.[47] employed a GCE as a supporting electrode for the modification with ultrathin Pd NWs for the detection of AA. **Figure II.4** shows different TEM images of the ultrathin Pd NWs employed for the AA determination in this work. The presence of the Pd NWs enhances the electron transfer between the analyte and the electrode, reduces the oxidation over-potential and improves analytical features like linear range or reproducibility. Another work based on the employment of Pd NWs was done by Y. Zhang et al.[48], where the Pd NWs grew directly on the surface of a GCE using an AAO template. The amperometric detection of formaldehyde was carried out with negligible interferences from acetaldehyde, ethanol or 1-propanol. The bare GCE does not present activity towards the formaldehyde oxidation; therefore, the NWs are responsible of the analytical signal. Furthermore the authors assure an antifouling effect related to a different oxidation pathway introduced by the Pd NWs that bypass the formation of the poisonous intermediate CO.

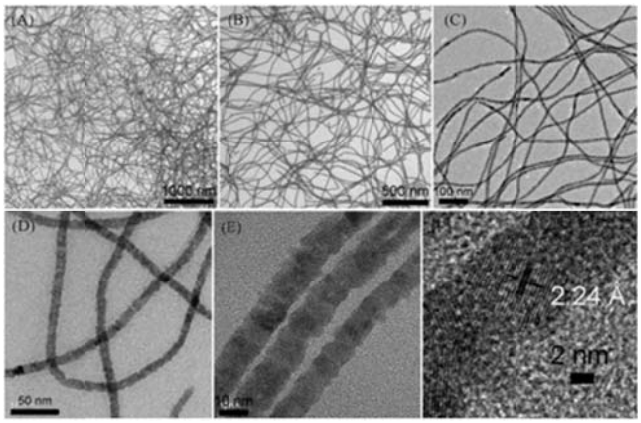

Figure II.4. TEM **(A-E)** and HRTEM **(F)** images of PdNWs at different magnifications. Reprinted with permission from reference 47.

The electrochemical detection (ED) of carbohydrates is very useful, because it avoids some difficulties that arise from their lack of chromophores for photometric detection. Moreover, electrochemical techniques for carbohydrate analysis do not need a derivatization step, and they offer other technical advantages, such as high compatibility with nanomaterials and their inherent miniaturization. Pulsed amperometric detection (PAD) has been employed to overcome the electrode fouling[49, 50] using a platinum electrode. Both Ni and Cu display electrocatalytic activity towards carbohydrates, and alcohols. This activity involves redox reactions between different oxides in alkaline media that have been extensively studied[51] and could potentially be exploited in nanoscale environments, making them excellent candidates for carbohydrate detection[51-54].

Electrochemical sensing of glucose is one of the hottest topics in the literature due to the devices used for glucose monitoring by diabetic patients. Different non enzymatic NW-based approaches have been published. In this way, copper NWs have been used in different approaches to detect glucose. Y. Zhang et al.[55] proposed a non-enzymatic sensor based on copper NWs for sensitive and selective detection of glucose in human

serum. Once synthesized the NWs are entrapped in the surface of a GCE using a Nafion film. The suitability of the composite Nafion/CuNWs/GCE was studied amperometrically and by CV. The Nafion film offers the necessary stability to the system, holding up the NWs over the electrode surface for a proper contact and avoiding the NWs leakage, and also introducing new features such as selectivity due to the nanoarchitecture of the formed film. Similarly P. Zhang et al.[56] developed another glucose sensor also based on CuO NWs. In both cases, excellent precision and no interference of common analytes (i.e. uric acid, AA) were achieved indicating the convenience of the CuNWs for non-enzymatic glucose sensors. **Figure II.5** shows the NWs effect demonstrated upon de observation of the cyclic voltammograms where the signal is greatly enhanced when NWs are present.

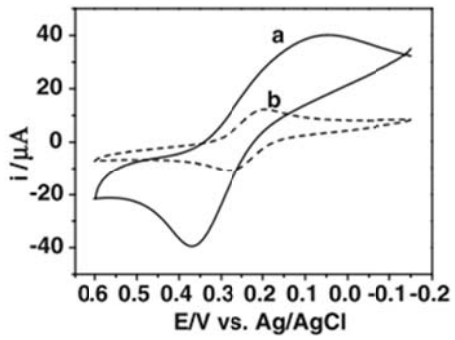

Figure II.5. CVs of **(a)** the CuO NWs-Nf/GCE and **(b)** the bare GCE in 0.20 M KCl solution containing 5 mM $K_3Fe(CN)_6$ solution with scan rate of 100 $mV \cdot s^{-1}$. Reprinted with permission from reference 56.

Also, Pt/Ni NWs arrays were used by S.S. Mahshid et al.[57] to perform the detection of glucose. The combination of the nickel catalytic effect and the great conductivity of platinum introduce a synergic effect creating an ingenious detector with excellent results in terms of sensitivity and selectivity towards common interference species in glucose determination such as ascorbic or uric acid (UA).

With the aim of producing cheaper but sensitive enough sensors, iron has been studied as a novel material for the synthesis of nanostructures able to introduce new features on common detectors for glucose detection. C. Xia et al.[58] synthesized FeOOH NWs using a simple solution phase route. The NWs were immobilized in the surface of a GCE using QPVP-Os (quaternized poly (4-vinylpyridine)) partially complexed with osmium bis (2, 2'-bipyridine). The study of the electrode behavior revealed an enzyme mimetic electrocatalytic effect of the FeOOH NWs similar to peroxidases. Differential pulse voltammetry (DPV) was used for the determination of glucose concentration without interference from common species like dopamine or AA.

Since ED of alcohols is also favored by the use of Ni and Pt materials, their electrochemistry based MNWs have also been reported. B. Tao et al. constructed different sensors based on Pd-Ni/SiNWs[59, 40]. SiNWs were fabricated following a wet chemical etching and then nickel and palladium were co-plated by an electroless deposition onto the silicon NWs surface in a decorated approach. In both cases the detection is performed using amperometry and CV with good results in terms of sensitivity and limit of detection (LOD) in the micro molar range, indicating the suitability of the developed electrodes for alcohol determination.

Literature offers also elegant NWs approaches for electrochemical sensing of other important target molecules such as morphine and cysteine. G. Yang et al.[60] constructed a morphine sensor based on gold nanotubes attached onto the surface of a GCE. The gold nanotubes were fabricated following an electrodeposition protocol on an AAO membrane and later on attaching the synthesized NWs array on the surface of the electrode.

Morphine was determined successfully in serum samples by DPV with the necessary selectivity towards potential interferents such as glucose, ascorbic or uric acids or others narcotics like cocaine. The determination of cysteine has also been carried out using gallium nitride NWs synthesized via vapor–liquid–solid mechanism, on silicon substrate with Au as catalyst[61]. The synthesized NWs were directly employed as working electrode for the CV studies showing electrocatalytic effect towards cysteine under physiological conditions. Another cysteine sensor based on manganese dioxide NWs modified GCE is reported by Y. Bai et al.[62]. The authors used an electrochemical templateless approach for the NWs synthesis and the β-MnO_2 NWs were then trapped in the surface of a GCE using a chitosan hydrogel. The β-MnO_2 NWs are the responsible of the cysteine oxidation through a specific reaction with the –SH group of the amino acid.

Other important biological molecules such as NADH have also been electrochemically explored using a non-enzymatic NWs approaches. Following with the advantages provided by the combination of various nanostructures, an electrode formed by poly (toluidine blue O)/CNT composite NWs for the detection of NADH at a lower potential was fabricated by A. Zeng et al.[63]. Briefly, first of all an adduct formed by the CNTs and toluidine blue O (TBO) was prepared and then a drop of the mixture was cast in the surface of a GCE, dried at room temperature, and finally electropolymerized by CV. The composite electrode was applied to oxidize NADH obtaining a broad linear range from 2.0 μM to 4.5 mM and a LOD of 0.5 μM. The amperometric response of the composite electrode was much higher than the other approaches tested demonstrating the suitability of the bottom-up approach for constructing composite electrodes for sensitive and reproducible determinations. In addition, the detection

was performed at 0.0 V increasing the selectivity due to the low potential employed.

L. Liu et al.[64] have employed lanthanum hydroxide NWs to modify a carbon paste electrode for the detection of the non-steroidal anti-inflammatory drug mefenamic acid (MFA). The NWs were fabricated following a chemical method and were mixed with graphite powder and paraffin oil to construct the paste electrode. The results showed a high sensitivity of 6 pM for MFA and the necessary selectivity versus potential interferents like amino acids or ascorbic and uric acids, being suitable for the determination of MFA in biological samples.

Finally, S.S. Mandal et al.[65], proposed a sensor based on TiO_2 NWs for the detection of cationic industrial dyes, using methylene blue (MB) as a representative cationic dye. The detection was performed via CV on a GCE modified with the TiO_2 NWs. Interestingly, the authors found out that the sensing capabilities were enhanced in bigger NWs indicating a surface dependent effect. The authors also proposed these NWs for photocatalytic degradation of cationic dyes in aqueous solution.

Accordingly to the target analytes studied, **Table II.1** condenses the main analytical information of the studied works in this section. Firstly, table shows the analytes studied in each work and its application regarding to the analysis of real samples; secondly, the material of which the NWs are built, the synthesis method and the dimensions of them and finally how these NWs are incorporated to the electrochemical system, the detection principle itself and the LODs achieved by these works.

In most of the works, NWs are built using template assisted or wet chemical methods as they are the more versatile and easier approaches. In many cases, NWs are used to modify GCE in order to improve the

characteristics of a well-established electrode, but some new ways are being opened, or using the NWs as electrodic substrate itself. CV and AD are commonly used as they are useful simple techniques to achieve the development of sensors. NWs are usually characterized employing techniques such as SEM, TEM or XPS to study its morphological features and the modified electrodes are extensively explored by CV to determine the experimental conditions for the later experiments and to check every step and its influence to the system during the modifications.

II.1.5. Nanowires in electrochemical biosensing

When the potential of the NWs is combined with the selectivity and sensitivity of biomolecules, the power of these hybrid structures becomes enhanced. These biosensors are increasing their relevance in the last years and different MNWs have been employed as immobilization surface for biomolecules. Conceptually speaking, and as we have already stated in the introduction, in biosensing, NWs present not only all the electronic advantages previously mentioned, moreover they permit an oriented functionalization of its surface. Biological systems can be very complex and sometimes, to work properly, they need several biomolecules in intimate proximity. As NWs can be made with fragments of different metals, a differentiated and oriented biofunctionalization of the NWs can be performed, developing a selective functionalization strategy for each NW's metal-fragment. This characteristic permits to co-immobilizate on the same NWs different biomolecules, mimicking nature's pattern. Not only MNWs are applied in biosensing. PPy is a conducting polymer with excellent characteristics for biosensing due to its high conductivity and electrochemical activity; moreover PPy shows biocompatibility being a perfect candidate for developing this kind of biosensors.

A variety of biomolecules have been utilized in combination with NWs. In this section, firstly the application of enzymes in biosensing is presented, then the integration between antibodies and NWs creates interesting immunosensors, and finally the most new sensors being the ones based in aptamers and DNA sensors, are explained.

Glucose oxidase (GOx) is one of the most studied enzymes using different NWs, (Au, Ag, PPy, PANI, ZnO, MnO_2…) for glucose biosensing. NWs in these systems can be doped with another nanostructure

as PtNPs[66] or with a material that facilitates the immobilization as chitosan, glutaraldehyde (GLA) or Nafion[67-70].

In these glucose sensors, in most of the cases, the deposition of NWs on the electrode follows a drop casting method[68, 70], drying a drop of a NWs suspension onto the electrode. Another strategy consists in the direct electrodeposition of the NWs on the electrode, where the measurements will take place[71, 72]. There are methodologies where NWs and biomolecules are previously mixed and then with this mixture the working electrode is drop cast[73].

Considering the functionalization of the NWs with the GOx, several casting protocols have been evaluated by EIS, and have proved that GOx is steadily absorbed onto the MnO_2NWs film, maintaining high bioactivity[68]. Another functionalization methodology implies electrochemical processes that allows the reaction between the NWs and the enzymes[74]: an oxidation potential is applied in order to force the electrostatic interaction between the enzyme and the NWs. Irreversibly, the enzyme can be attached to the NWs via covalent interactions[71] utilizing the NHS/EDC chemistry for activating the carboxyl terminal groups of PPyCOOH/PPy composite NWs. In the case of GOx biosensors, in some cases, the immobilization via electrostatic interaction is combined with a cross-linking of the biomolecule with GLA, Nafion or both reagents[68, 72]. Cross-linkers are also used in GOx biosensors based in AgNWs, where chitosan is mixed with the enzyme and then the electrode modified with AgNWs is cast with the mixture solution[70, 75].

J. Li et al.[76] developed a composite glucose sensor through consecutive steps; firstly the authors synthesized amperometrically the PPyNWs directly on the surface of a GCE, secondly the platinum

nanoclusters were deposited by CV over the PPy-GCE and finally the GOx was immobilized together with the polymerization by CV in neutral media of *o*-aminophenol (OAP). It is hypothesized that the 3D structure generated on the electrode increases the amount of loaded enzyme and therefore the production of H_2O_2. The H_2O_2 is electrochemically oxidized at the highly sensitive PPy-Pt nanocomposite obtaining good linearity and a LOD of 0.45 μM and also good selectivity through common interferents (AA, UA and acetaminophen) was also achieved. GOx can be also attached to gold NWs[77]. With these NWs, a redox mediator ferrocene monocarboxylic acid (FcCOOH) has been employed in order to reduce problems related to oxygen consumption and interference effects, increasing the intensity of the signal[77]. In this case, the enzyme is not immobilized, it is mixed with the buffer and added under soluble conditions to the system where the measurements will take place. Gold NWs are also able to work properly with the enzyme immobilized on the electrode, without needing any mediator[73].

Although GOx has been the most widely used enzyme, more enzyme-based biosensors with different NWs have also been reported. In most of the cases, the enzymatic reaction generates H_2O_2 which is the final molecule that the electrode measures.

A cholesterol biosensor based in gold NWs activated with thioctic acid and two different enzymes (cholesterol oxidase and cholesterol esterase) immobilized on the NWs, showed good linearity and low interferences[78]. Glutamate oxidase (GlutOx) has been immobilized onto gold NWs arrays modified with Pt nanoparticles, binding the enzyme to this nanoarchitecture with a solution of GLA and Nafion[79]. In this glutamate detection system, the electrode shows an excellent performance towards the oxidation of H_2O_2 being a perfect candidate for the immobilization of an

enzyme and detects the H_2O_2 produced in the biological reaction as it is illustrated in **Figure II.6**. In another example, an enzymatic galactose sensor was developed with ZnO nanorods[53]. In this work, the galactose oxidase has been bond to the nanorods via GLA cross-linking, being the electrode able to detect the H_2O_2 generated by the enzyme. Biosensors that detect UA have been constructed using the enzyme uricase onto ZnONWs, with the presence of Nafion to prevent enzyme leakage[80], also measuring the H_2O_2 generated in the enzymatic reaction.

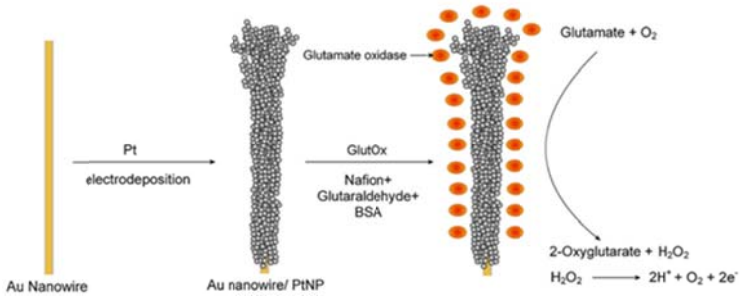

Figure II.6. Schematic illustration of stepwise fabrication of the GlutOx/PtNP/NAEs electrodes. Reprinted with permission from reference 79.

Also, other enzymatic-based H_2O_2 sensors have also been developed. This is the case of a mediator-free horseradish peroxidase (HRP) based H_2O_2 biosensor onto Sb-doped SnO_2 NWs. The immobilized enzyme retained bioactivity onto this surface and, the Sb doping helped the direct electron transfer of the enzymes through NWs[81]. In a similar manner, a biosensing platform using poly neutral NWs and entrapping HRP during the NWs growth has been previously reported[82]. The composite formed by the NWs and the enzyme was used to cast a GCE to carry out the H_2O_2 detection.

Following the previously mentioned order, apart from enzymes, other biomolecules have been employed to develop biosensors based in

NWs. It can be found in the literature immunosensors with polyaniline (PANI) NWs functionalized with EDC/NHS which binds the primary antibody[83]. These structures are able to detect proteins such as IgG or myoglobin, depending on which mAb is immobilized, by the measurement of the conductance changes of the NWs. Gold NWs combined with polyvinyl butyral (PVB) membranes are applied for detecting testosterone where antibodies have been immobilized onto the gold NWs combined with PVB[84].

Aptasensors are another kind of sensors that can be built onto NWs[85-87]. Aptamers, artificial oligonucleotides isolated from combinatorial nucleic acid libraries, present many advantages compared to antibodies, such as higher stability, higher affinity and reproducible chemical production. The detection of avian influenza virus H5N1 gene sequence has been performed with a DNA aptamer immobilized onto a hybrid nanomaterial electrode. The modified electrode presented multi-wall carbon nanotubes (MWCNT), PPy-NWs and GNPs[88]. Thrombin has been detected with aptamer conjugated $Mo_6S_{9-x}I_x$ NWs. A gold electrode is modified with the NWs and the aptamer conjugated electrode was prepared by placing the modified electrode into a thiolated aptamer solution[86].

Sophisticated composite electrodes have also been applied for the detection of DNA molecules[39]. In this work the authors constructed a nanoarchitecture over a GCE combining different nanomaterials. Firstly, ZnONW were prepared via a carbothermal reduction process, NWs aliquot was then dropped on the GCE surface; secondly a MWCNT suspension was cast over the ZnONW-GCE. Then GNPs were deposited on the modified electrode and finally the DNA probe was dropped on the GNP/MWCNT/ZnONW/GCE modified electrode. After modification the non-attached DNA probe was removed using SDS. The concentration

of the DNA complementary sequence was related to obtain a DPV signal of the reduction of RuHex, as the reduction peak currents of RuHex increased when complementary DNA increased. A logarithmic relation was found between both parameters with a broad linear range ($1.0 \cdot 10^{-13}$-$1.0 \cdot 10^{-7}$ M) and a LOD of 3.5×10^{-14} M.

However, other simpler DNA biosensors' configurations can be found in the literature. This is the example of the work presented by Ramulu et al.[89], where AuNWs were synthesized following a two-step electrodeposition technique, and GCE was modified with these AuNWs. A thiolated DNA probe is conjugated to the AuNWs via gold-thiol chemistry. The hybridization to the probe DNA was accomplished, following the reaction with DPV measurements. In another work, a mixed electrode configuration only with PANI-NWs and graphene was presented[90]. In this work, the oligonucleotide probe was immobilized through the formation of phosphoramidate bonds between the amino group of PANI and phosphate group of the oligonucleotides. The authors demonstrated the advantages of the application of nanomaterials in biosensors' performance: the larger electrode effective surface area of the PANI-NWs modified electrode provoques larger DPV current response compared to the PANI modified electrode; achieving detection limits of 3.25×10^{-13} M.

Regarding these works, the main analytical information is summarized in **Table II.2**. As previously discussed in the text, the information has been classified following enzymatic, immunosensor and genosensor approach accordingly to the biomolecule and the detected analyte. In each case, from left to right, it is specified the material, the synthesis process, the dimensions of the NWs when provided, and their characterization methods. The characterization has been applied to the NWs and also to the electrode modified with them. Usually, despite the

possibility of coimmobilizing several biomolecules in the NWs surface, only one enzyme or protein is immobilized on them. From top to down, the enzymatic sensors based in GOx are detailed, being organized the different articles depending on the NWs' nature. When the biosensor is an enzymatic one, an amperometry is the most employed analytical technique. Nevertheless, with aptasensors and DNA sensors, the measurements are recorded by DPV. Remarkably with this kind of sensors, extremely low LODs are obtained. It is also important to highlight that not many of the works are tested in real samples, probably due to the inherent complexity of the matrix.

II.1.6. Nanowires in microfluidic electrochemical sensing

The next natural step is the application of NWs as coupled detectors to flow and separation techniques. While no coupling of NWs neither flow injection analysis (FIA) nor to conventional separation techniques has been reported, there are some examples of NWs coupled to microfluidic devices.

Microfluidic and lab-on-a-chip technologies seek to improve analytical performance by reducing the analysis time, decreasing the consumption of sample and reagents, diminishing the risk of contamination, consuming less power, and increasing reliability, functionality and sensitivity through automation, integrating multiplexing analysis, and especially portability to provide the possibility of point-of-care applications[91-94]. Therefore, microfluidic platforms are especially suitable for sensing and biosensing as novel generation of sensors and biosensor[95]. Indeed, miniaturization dramatically reduces the consumption of expensive reagents and special samples (i.e. neonatal urine and spinal fluid) and procedures can be automated, since the different steps and fluid movement can be easily controlled, especially with electrokinetic fluidic motion, through the control of applied electric fields.

ED has been proven as an ideal and valuable technique to be incorporated in miniaturized devices, due to its inherent facility for miniaturization without loss of performance, high sensitivity and compatibility with the micro-and nano-technologies[96, 97]. When used in the electrochemical detectors of microfluidic systems, nanomaterials can significantly improve their analytical performance[91, 96, 98]. The scale of a typical nanomaterial is compatible with the scale of a typical microfluidic system. In addition, as it was stated in the introduction, the nanomaterials can offer high currents because of their large surface areas, thereby enabling

large-scale redox conversion, which increases the analytical sensitivity, resists passivation, and yields very good reproducibility. Because of the extremely low sample volumes introduced into microfluidic systems, the chip sensitivity is often low being this feature a drawback of these systems. This problem can be overcome by exploiting the surface characteristics of nanomaterials, turning the microfluidic systems-NWs coupling into a very pertinent application for a novel generation of microfluidic systems.

Although in the field of detection in microfluidics the most used nanomaterials have been CNTs[99-102]; some works using MNWs involving both electrochemical sensing and biosensing have also been reported. S. Aravamudhan et al.[103] developed a microfluidic platform for nitrate sensing based on doped PPy-NWs. The PPy NWs were synthesized using a chemical template assisted approach, where the nitrate was used during the synthesis as doping agent for further selective chemical recognition towards nitrate. The NWs were employed inside a flow through cell with the aim of developing field sensors for monitoring nitrate in the environment. The PPy NWs based electrode exhibited high sensitivity and selectivity even during the analysis of seawater samples.

The first example of the introduction of NWs as detectors in microfluidic separation system is constituted by the work realized by E. Piccin et al.[104] using nickel NWs for carbohydrate and amino acid sensing. The detector was constructed by sputtering a gold layer around the separation channel outlet that served as electrical contact for the NWs. This work showed the influence of the NWs and also its orientation towards the detection, concluding that the alignment of the NWs is critical for a better resolution and an enhanced sensitivity, where any signal is obtained when NWs are not positioned over the sputtered contact.

Finally, some examples integrating biosensing on microfluidic platform using NWs have also been reported. The detection of cholesterol in serum in a microfluidic platform using AuNW immobilized with cholesterol oxidase and cholesterol esterase has been reported[78]. The estimation of cholesterol is based on the H_2O_2 amperometrically detected as a result of the enzymatic reaction. Also, an aptamer-functionalized single PANI NW for the detection of IgE, an allergic biomarker, has been developed, immobilizing the aptamer to the NW in presence of EDC/NHS[87]. PPy NWs can also be synthesized with the aptamer present in the same solution. This protocol has been tested with an IgE aptamer and with another aptamer for Mucin 1, a protein over expressed in almost all human epithelial cells[85]. This kind of NWs has been applied in microfluidic applications, for rapid and label-free detection of proteins.

II.1.7. Outlook and perspectives

During the last years, the high potential of MNWs and PolyNWs in electrochemical sensing and biosensing applications has been demonstrated, leading to an important piece of work and advances.

NWs from different materials such as metals, metal oxides, alloys, polymers or hybrid materials have been employed in a wide variety of applications, ranging from surface enhanced electrodes to platform for biomaterials immobilization. Its outstanding characteristics related to its size and, as a consequence, to its high surface to volume ratio make these nanostructures excellent candidates to lead a new sensors generation with the doubtless advantage of their possible incorporation to portable and disposable devices.

NWs have been used as an electrochemical transducer in an effort to increase the electrode's surface area with the final objective of improved sensitivities and LODs. MNWs and PolyNWs have also been employed as a substrate for further modification with biomaterials serving as an excellent platform to connect the biomolecules, making possibly a faster electronic transfer rate even avoiding the use of mediators. The coupling between microfluidics with NWs is not very extended, but is a promising approach for further improvement of them achieving the necessary requirements for its implementation in the labs.

Although the developments in the field are really impressive, the works using NWs in the analysis of real samples remains very scarce, showing that this approach needs maturity for its implementation as a common tool. Therefore, the fabrication of new platforms of miniaturized devices involving NWs for analysis and bioanalysis is a great challenge and holds great promise for a huge range of applications such as clinical

diagnosis, food analysis, process control, and environmental monitoring. This growing background predicts an exciting horizon plenty of creativity and possibilities.

Table II.1. Electrochemical sensing based nanowires

Analyte	Sample	NWs (Electrode)	Synthesis	Size	Arrangement	Characterization	Detection	LOD (μM)	REF
H_2O_2	Milk	Ag (GC)	Wet Chemical	Ø= 100 nm L= Tens of μm	Chitosan entrapment	SEM, EDS, XRD, CV	Amperometry (E= -0.2 V)	2.0	42
H_2O_2	NR	MnOOH (GC)	Wet Chemical	Ø= 20 nm L= Tens of μm	Coimmobilized with QPVP-Os Film	SEM,HRTEM, XRD, CV	CV (From -0.9 to 0.0 V) Amperometry (E= -0.3 V)	0.115	43
H_2O_2	NR	Au/Pt alloy (Au micro-electrode)	Wet Chemical	Ø= 200 nm	Direct growing over the microelectrode	SEM, EDS, XRD, CV	CV (From -0.4 to 0.2 V) Amperometry (E= 0.0 V)	1.5×10^{-3}	44
H_2O_2	NR	Si (SiNWs)	Electroless plating of $Ni(OH)_2$ over SiNWs	Ø= 100 nm L= 80 μm	Electroless deposition	SEM, XRD, CV	CV (From -0.6 to 0.6 V) Amperometry (E= +0.2 V)	3.2	41
Ammonia	NR	Poly-pirrole (Au)	Templateless electrodeposition	L= 500-800 nm	Electro-polymerization over the Au electrode	SEM, FESEM, CV	Amperometry (E= +0.35 V)	5	45
Hydrazine hydroxyl-amine	NR	Poly-pirrole (GC)	Templateless electrodeposition	Ø= 60 nm	Electro-polymerization over the GCE modified with NWs decorated with Au NPs	FESEM, XPS, XRD	CV (From -0.2 to 0.8 V) Amperometry (E= +0.2 V)	0.20	46

Analyte	Sample	NWs (Electrode)	Synthesis	Size	Arrangement	Characterization	Detection	LOD (μM)	REF
Ascorbic acid	Serum Beverages	Pd (GC)	Wet Chemical	Ø= 10 nm L= Several μm	Casting	TEM, HRTEM, CV	Amperometry (E= 0.0 V)	0.2	47
Formal-dehyde	NR	Pd (GC)	Electrodeposition on a GCE within the pores of a synthesized AAO template	Ø=50 nm	Grow over the GCE	SEM, EDX, EIS, CV	Amperometry (E= +0.05 V)	0.5	48
Glucose	Serum	Cu (GC)	Wet Chemical	Ø= 50 nm L= Several μm	Casting	SEM, XRD, CV	CV (From -1 to 0.8 V) Amperometry (E= +0.55 V)	0.26	52
Glucose	Serum	Cu (GC)	Wet Chemical	Ø=150 nm L= 30 μm	Casting	SEM, EDX, CV	Amperometry (E= +0.6 V)	0.035	55
Glucose	NR	CuO (GC)	Wet Chemical	Ø= 10-20 nm L= 2-3 μm	Casting GCE modified with CuO NW and nafion film.	SEM, XRD, CV	Amperometry (E= +0.6 V)	0.045	56
Glucose	NR	Pt/Ni (GC)	Template assisted electrodeposition	Ø= 200 nm L= 4 μm	Grow over the GCE	SEM, TEM, CV	Amperometry (E= +0.45 V)	1.5	57
Glucose	NR	FeOOH (GC)	Wet Chemical	Ø= 30 nm L= 3-5 μm	Composite NWs entrapment using a QVP film	SEM, TEM, HRTEM, XRD, CV	DPV (From -0.2 to 0.7 V)	7.8	58

Analyte	Sample	NWs (Electrode)	Synthesis	Size	Arrangement	Characterization	Detection	LOD (μM)	REF
Methanol	NR	Pd/Ni (SiNWs)	Electroless plating of Pd/Ni over Si NWs	Ø= 100-300 nm L= 50 μm	Electroless deposition	SEM, TEM,EDS, CV	CV (From -0.6 to 0.1 V) Amperometry (E= -0.3 V)	25	59
Ethanol	NR	Pd/Ni (SiNWs)	Electroless plating of Pd/Ni over Si NWs	Ø= 100-300 nm L= 50 μm	Electroless deposition	SEM, TEM,EDS, CV	CV (From -1 to +0.1 V) Amperometry (E= -0.25 V)	10	40
Morphine	Serum	Au (GC)	Template assisted electrodeposition	Ø= 180 nm	Grow over the GCE	SEM, CV	DPV (From +0.2 to +0.75 V)	0.041	60
L-Cysteine	NR	GaN (GaNWs)	CVD mechanism on silicon substrate	Ø= 25-100 nm L= Several μm	NWs form the electrode	SEM, CV	CV (From -0.2 to +1.0 V)	0.5	61
Cysteine	Urine	β-MnO_2 (GC)	Wet Chemical	Ø= 30 nm L= 1 μm	Grow over the GCE modified with β-MnO2 NW and chitosan film.	TEM, XRD, IR, CV	CV (From 0.0 to +1.0 V) Amperometry (E= +0.5 V)	0.07	62
NADH	NR	Toluidine blue O (GC)	Electro-polymerization	NR	Electro-polymerization over the GCE	SEM, CV	Amperometry (E= 0.0 V)	0.5	63
Mefenamic acid	Drugs	$La(OH)_3$ (CP)	Wet Chemical	Ø= 15-20 nm	Mixing the NWs in the paste	TEM, CV	CV (From +0.6 to +1.3 V)	6 $x10^{-6}$	64
Methylene Blue	Textile industry effluents	TiO_2 (GC)	Wet Chemical	Ø= 800 nm L= 3 μm	Casting	XRD, FTIR, TEM, TGA, SEM	CV (From -0.6 to -0.1 V)	NR	65

Table II.2. Electrochemical biosensing based nanowires

Analyte (A) Biomolecule (B)	Sample	NWs (Electrode)	Synthesis	Size	Biological architecture	Characterization	Detection	LOD	REF
A: Glucose B: GOx	NR	ZnO (Au)	Wet chemical	NR	Aminosilanized ZnONWs immersed in GLA. GOx cast on the surface, 0.5% Nafion solution added.	XPS, EIS CV (from -0.2 V to +0.7 V)	Amperometry (+0.7 V)	NR	69
A: Glucose B: GOx	NR	ZnO (Au/PET)	Template assisted electrochemical deposition	NR	Dipping the modified electrode in a solution of GOx + Nafion (5%)	SEM, TEM	Amperometry (+0.8 V)	50μM	72
A: Glucose B: GOx	Human blood serum	Ag (GC)	Wet chemical	NR	GOx + chitosan (0.25%) cast onto the modified electrode	SEM, EIS CV (from -0.6 V to 0 V)	Amperometry (-0.15 V)	2.83 μM	70
A: Glucose B: GOx	NR	Au (GC)	Template assisted electrodeposition	NR	AuNWs+GLA+GOx in solution. Drop-casting the electrode 24h, 4ºC	SEM, TEM, XRD	Amperometry (+0.8 V)	5 μM	73
A: Glucose B: GOx	Urine	β-MnO_2 (GC)	Wet chemical	NR	Electrode modified with Nafion and NWs. Enzyme drop-casted, then GLA added.	SEM, XRD, EIS CV (from +1.0 V to 0 V)	Amperometry (+0.7 V)	25.56 μM	68
A: Glucose B: GOx	NR	PPyNWs + PtNPs (Au)	Template assisted electrochemical polymerization	NR	PtNPs deposited on PPyNW by CV. Adsorption of enzyme by immersing the electrode in GOx solution.	CV (from -0.2 to +0.2 V)	Amperometry (+0.7 V) Potentiometry	27.7 μM (AD) 5.6 μM (Pot.)	66
A: Glucose B: GOx	Human blood	PVP-Ag (GC)	Wet chemical	NR	GCE cast with NWs, then cast with GOx solution. After drying, chitosan 0.2 % was dropped.	TEM, SEM, AFM CV (from -0.8 to +0.25 V)	Amperometry (-0.63 V)	2.3 μM	76

Analyte (A) Biomolecule (B)	**Sample**	**NWs (Electrode)**	**Synthesis**	**Size**	**Biological architecture**	**Characterization**	**Detection**	**LOD**	**REF**
A: Glucose B: GOx	NR	PPyCOOH/ PPy (Au)	Template assisted electrochemical deposition	Ø= 90-100 nm L= 10 μm	Covalent interaction between carboxyl terminal groups of PPyCOOH/PPy activated and EDC/NHS	SEM, TEM, FTIR, XPS CV (from -0.9 to +0.5 V)	Amperometry (+0.4 V)	0.63 μM	71
A: Glucose B: GOx	NR	PANI (Carbon Cloth)	Template assisted electrochemical deposition	Ø= 60-80 nm Several μm length	PANI NWs + GOx: binding through electrochemical oxidation. Immobilization via electrostatic interaction between NWs and GOx.	SEM, TEM, FT-IR spectra CV (from -0.75 to + 1.25 V)	Amperometry (+0.5 V)	50 μM	74
A: Glutamate B: GlutOx	NR	AuNWs + PtNPs (PtNP/ AuNWArray)	Template assisted electrodeposition	ND	Casting of GlutOx + BSA + GLA + Nafion	SEM CV (from -0.2 to +1.6 V)	Amperometry (+0.65 V)	14 μM	79
A: Uric Acid B: Uricase	NR	ZnO	Wet chemical	Ø= 80-150 nm L= 0.9-1.5 μm	(i) Uricase electrostatically immobilized by dipping NWs into the enzyme. (ii) Electrode dipped in the enzyme solution. Then, Nafion added.	AFM, SEM	Potentiometry	ND	80
A: H_2O_2 B: HRP	NR	SnO_2 + Sb doped (GC)	Thermal evaporation	Ø= 100 nm	NWs + HRP suspension casted on GCE	XRD, SEM, TEM CV (from 0 to -0.6 V)	Amperometry (-0.3 V)	0.8 μM	81
A:IgG; Myo B: mAbs	NR	PANI	Template assisted electro-polymerization	NR	PANI NWs + mAbs + EDC/NHS incubated, then mAbs covalently coupled to NWs.	SEM, Raman Fluorescence microscopy	Conductometry	3 ng/mL (IgG) 1.4 ng/mL (Myo)	83
A: Testosterone B: IgG	NR	Au (Pt wire)	Template assisted electrodeposition	NR	Casting of Ab + NWs + PVB ethanol	SEM CV (from -0.3 to +0.7 V)	Potentiometry	0.1 ng/mL	84

Analyte (A) Biomolecule (B)	Sample	NWs (Electrode)	Synthesis	Size	Biological architecture	Characterization	Detection	LOD	REF
A: Thrombin B: Aptamer	NR	Mo_6S_9-I_x (Au)	Wet chemical	NR	Covalent association of thiolated thrombin binding aptamer to NWs through sulfur-sulfur bonding	XPS, HRTEM CV (from -0.6 to +0.2 V)	DPV(from -0.45 to 0.0 V)	~10^{-11} M	86
A: IgE B: Aptamer	NR	PANI	Template assisted electrochemical deposition	NR	Covalent bonds: Aptamer immobilization through their 5' ends to PANI NW via EDC/NHS chemistry	Fluorescence microscopy	Conductometry	~10^{-15} M	87
A: Avian influenza virus gene sequence B: Aptamer	NR	PPy-NW (Au)	Templateless electrochemical deposition	NR	DNA aptamer (HS-DNA) placed on Au electrode. Then treated with MCH.	CV (from -0.7 to +0.2 V) EIS	DPV (from 0.0 V to +0.40 V)	~10^{-13} M	88
A:DNA probe B: DNA probe	NR	ZnOWs (GC)	Carbothermal reduction process	NR	Electrodeposition of ZnONWs on GCE+ MWNT+AuNPs. A thiolated ssDNA (HS-ssDNA) covalently bound to the surface of AuNPs via Au-S bond.	XRD, SEM	DPV (from -0.4 V to +0.1 V)	~10^{-14} M	39
A:DNA probe B: DNA probe	NR	AuNWs	Template assisted electrodeposition	Ø= 200 nm L= 1.5 μm	DNA thiolated- probe bound to AuNWs modified electrode.	SEM, FESEM, EIS CV (from +0.6 to -0.4 V)	DPV (from -0.4 to +0.1 V)	~10^{-9} M	89
A:DNA probe B: DNA probe	NR	PANI NWs + graphene	Electrochemical deposition	NR	Oligonucleotide probe immobilized through phosphoramidate bonds.	FE-SEM, EIS CV (from -1.0 to +1.0 V)	DPV (from +1.2 to -0.3 V)	~10^{-13} M	90

II.1.8. References

[1] B. Bhushan, Springer handbook of nanotechnology, second ed., Springer, Berlin Heidelberg, 2007.

[2] Y. Zhang, Q. Xiang, J. Xu, P. Xu, Q. Pan, F. Li, Self-assemblies of Pd nanoparticles on the surfaces of single crystal ZnO nanowires for chemical sensors with enhanced performances, J. Mater. Chem. 19 (2009) 4701-4706.

[3] E.C.Walter, R.M. Penner, H. Liu, K.H. Ng, M.P. Zach, F. Favier, Sensors from electrodeposited metal nanowires, Surf. Interface Anal. 34 (2002) 409-412.

[4] M. Di ventra, S. Evoy, J.R. Heflin Jr., Introduction to nanoscale science and nanotechnology, Springer, USA, 2004.

[5] C.P. Poole Jr, F.J. Owens, Introduction to nanotechnology, second ed., Wiley, New Jersey, 2003.

[6] D. Vilela, M.C. González, A. Escarpa, Sensing colorimetric approaches based on gold and silver nanoparticles aggregation: Chemical creativity behind the assay. A review, Anal. Chim. Acta 751 (2012) 24-43.

[7] C.R. Martin, D.T. Mitchell, Peer Reviewed: Nanomaterials in analytical chemistry, Anal. Chem., 70 (1998) 322A–327A.

[8] X. Chen, G. Wu, Y. Jiang, Y. Wang, X. Chen, Graphene and graphene-based nanomaterials: the promising materials for bright future of electroanalytical chemistry, Analyst 136 (2011) 4631-4640.

[9] B. Pérez-López, A. Merkoçi, Carbon nanotubes and graphene in analytical sciences, Microchim. Acta 179 (2012) 1-16.

[10] J. Wang, Adaptive nanowires for on demand control of electrochemical microsystems, Electroanalysis 20 (2008) 611-615.

[11] L. Zhao, M. Yosef, M. Steinhart, P. Göring, H. Hofmeister, U. Gösele, S. Schlecht, Porous silicon and alumina as chemically reactive templates for the synthesis of tubes and wires of SnSe, Sn and SnO2, Angew. Chemie 45 (2005) 311-315.

[12] P. Enzel, J.J. Zoller, T.Bein, Intrazeolite assembly and pyrolysis of polyacrylonitrile, J. Chem. Soc., Chem. Commun. (1992) 633-635.

[13] Y. Zhang, J. Liu, R. He, Q. Zhang, X. Zhang, J. Zhu, Synthesis of alumina nanotubes using carbon nanotubes as templates, Chem. Phys. Lett. 360 (2002) 360, 579–584.

[14] W. Han, P. Redlich, F. Ernst, M. Ruhle, Synthesizing boron nitride nanotubes filled with SiC nanowires by using carbon nanotubes as templates, Appl. Phys. Lett. 75 (1999) 1875-1877.

[15] J. Richter, M. Mertig, W. Pompe, I. Monch, H.K. Schackert, Construction of highly conductive nanowires on a DNA template, Appl. Phys. Lett. 78 (2001) 536-538.

[16] C.R. Sides, C.R. Martin, Deposition into Templates, in P. Schmuki, S. Virtanen (Eds.), Electrochemistry at the Nanoscale Nanostructure Science and Technology, Springer, New York, 2009, pp. 279-320.

[17] T.R. Kline, M. Tian, J. Wang, A. Sen, W.H.M. Chan, T.E. Mallouk, Template-grown metal nanowires, Inorg. Chem. 45 (2006) 7555-7565.

[18] C. Guozhong, L. Dawei, Template-based synthesis of nanorod, nanowire, and nanotube arrays, Adv. Colloid Interf. 136 (2008) 45– 64.

[19] C. Schönenberger, B.M.I. van der Zande, L.G.J. Fokkink, M. Henny, C. Schmid, M. Krüger, A. Bachtold, R. Huber, H. Birk, U. Staufer, Template Synthesis of Nanowires in Porous Polycarbonate Membranes: Electrochemistry and Morphology, J. Phys. Chem. B 101 (1997) 5497-5505.

[20] C.R. Martin, Membrane-Based Synthesis of Nanomaterials, Chem. Mater. 8 (1996) 1739-1746.

[21] T. Gao, G.W. Meng, J. Zhang, Y.W. Wang, C.H. Liang, J.C. Fan, L.D. Zhang, Template synthesis of single-crystal Cu nanowire arrays by electrodeposition, Appl. Phys. A 73 (2001) 251–254.

[22] S. Kumar, D. Saini, G. Singh Lotey, N.K. Verma, Electrochemical synthesis of copper nanowires in anodic alumina membrane and their impedance analysis, Superlatt. Microstr. 50 (2011) 698–702.

[23] Q. Wang, G. Wang, X. Han, X. Wang, J.G. Hou, Controllable Template Synthesis of Ni/Cu Nanocable and Ni Nanotube Arrays: A One-Step Coelectrodeposition and Electrochemical Etching Method, J. Phys. Chem. B 109 (2005) 23326-23329.

[24] A. Bulbarello, S. Sattayasamitsathit, A.G. Crevillen, J. Burdick, S. Mannino, P. Kanatharana, P. Thavarungkul, A. Escarpa, J. Wang, Striped alloy nanowire optical reflectance barcodes prepared from a single plating solution, Small 4 (2008) 597-600.

[25] M. Delvaux, J. Duchet, P.Y. Stavaux, R. Legras, S. Demoustier-Champagne, Chemical and electrochemical synthesis of polyaniline micro and nano-tubules, Synthetic Met. 113 (2000) 275–280.

[26] K. Jackowska, A.T. Bieguński, M. Tagowska, Hard template synthesis of conducting polymers: a route to achieve nanostructures, J Solid State Electrochem 12 (2008) 437–443.

[27] M.J. Zheng, L.D. Zhang, G.H. Li, W.Z. Shen, Fabrication and optical properties of large-scale uniform zinc oxide nanowire arrays by one-step electrochemical deposition technique, Chem. Phys. Lett. 363 (2002) 123–128.

[28] M. Delvaux, S. Demoustier-Champagne, Immobilisation of glucose oxidase within metallic nanotubes arrays for application to enzyme biosensors, Biosens. Bioelectron. 18 (2003) 943-951.

[29] M. Wirtz, C.R. Martin, Template-Fabricated Gold Nanowires and Nanotubes, Adv. Mater. 15 (2003) 455-458.

[30] Q.Lu, F. Gao, S. Komarneni, T.E. Mallouk, Ordered SBA-15 Nanorod Arrays Inside a Porous Alumina Membrane, J. Am. Chem. Soc. 126 (2004) 8650-8651.

[31] B. Polyakov, B. Daly, J. Prikulis, V. Lisauskas, B. Vengalis, M.A. Morris, J.D. Holmes, D. Erts, High-Density Arrays of Germanium Nanowire Photoresistors, Adv. Mater. 18 (2006) 1812-1816.

[32] K.K. Caswell, C.M. Bender, C.J. Murphy, Seedless, Surfactantless Wet Chemical Synthesis of Silver Nanowires, Nano Lett. 3 (2003) 667-669.

[33] F. Fievet, J.P. Lagier, B. Blin, B. Beaudoin, M. Figlarz, Homogeneous and heterogeneous nucleations in the polyol process for the preparation of micron and sub-micron size metal particles, Solid State Ionics 32 (1989) 198-205.

[34] Y.G. Sun, Y.N. Xia, Large-scale synthesis of uniform silver nanowires through a soft, self-seeding, polyol process, Adv. Mat. 14 (2002) 833-837.

[35] T. Maddanimath, A. Kumar, J. D'Arcy-Gall, P.G. Ganesan, K. Vijayamohanan, G. Ramanath, Wet-chemical templateless assembly of metal nanowires from nanoparticles, Chem. Commun. (2005) 1435–1437.

[36] Y.G. Sun, B. Gates, B. Mayers, Y.N. Xia, Crystalline Silver Nanowires by Soft Solution Processing, Nano Lett. 2 (2002) 165-168.

[37] J.Benson, S. Boukhalfa, A. Magasinski, A. Kvit, G. Yushin, Chemical vapor deposition of aluminum nanowires on metal substrates for electrical energy storage applications, ACS Nano 6 (2012) 118-125.

[38] M.L. Zhong, D.C. Zeng, Z.W. Liu, H.Y. Yu, X.C. Zhong, W.Q. Qiu, Synthesis, growth mechanism and gas-sensing properties of large-scale CuO nanowires, Acta Mate. 58 (2010) 5926-5932.

[39] J. Wang, S. Li, Y. Zhang, A sensitive DNA biosensor fabricated from gold nanoparticles, carbon nanotubes, and zinc oxide nanowires on a glassy carbon electrode, Electrochim. Acta 55 (2010) 4436-4440.

[40] B. Tao, J. Zhang, S. Hui, L. Wan, An amperometric ethanol sensor based on a Pd-Ni/SiNWs electrode, Sens. Actuat. B 142 (2009) 298-303.

[41] Q. Yan, Z. Wang, J. Zhang, H. Peng, X. Chen, H. Hou, C. Liu, Nickel hydroxide modified silicon nanowires electrode for hydrogen peroxide sensor applications, Electrochim. Acta 61 (2012) 148-153.

[42] X. Gao, L. Jin, Q. Wu, Z. Chen, X. Lin, A Nonenzymatic hydrogen peroxide sensor based on silver nanowires and chitosan film, Electroanal. 24 (2012) 1771–1777.

[43] X. Cao, N. Wang, L. Wang, C. Mo, Y. Xu, X. Cai, G. Lin, A novel non-enzymatic hydrogen peroxide biosensor based on ultralong manganite MnOOH nanowires, Sens. Actuat. B 147 (2010) 730–734.

[44] Y .Zhou, G. Yu, F. Chang, B. Hub, C. Zhong, Gold–platinum alloy nanowires as highly sensitive materials for electrochemical detection of hydrogen peroxide, Anal. Chim. Acta 757 (2012) 56–62.

[45] M. Massafera, S. Córdoba de Torresi, Evaluating the performance of polypyrrole nanowires on the electrochemical sensing of ammonia in solution, J. Electroanal. Chem. 669 (2012) 90–94.

[46] J. Li, X. Lin, Electrocatalytic oxidation of hydrazine and hydroxylamine at gold nanoparticle-polypyrrole nanowire modified glassy carbon electrode, Sensor Actuat. B 126 (2007) 527–535.

[47] D. Wen, S. Guo, S. Dong, E. Wang, Ultrathin Pd nanowire as a highly active electrode material for sensitive and selective detection of ascorbic acid, Biosens. Bioelectron. 26 (2010) 1056–1061.

[48] Y. Zhang, M. Zhang, Z. Cai, M. Chen, F. Cheng, A novel electrochemical sensor for formaldehyde based on palladium nanowire arrays electrode in alkaline media, Electrochim. Acta 68 (2012) 172-177.

[49] P.L. Weber, S.M. Lunte, Capillary electrophoresis with pulsed amperometric detection of carbohydrates and glycopeptides, Electrophoresis 17 (1996) 302-309.

[50] J.C. Fanguy, C.S. Henry, Pulsed amperometric detection of carbohydrates on an electrophoretic microchip, Analyst 127 (2002) 1021-1023.

[51] J.M. Marioli, T. Kuwana, Electrochemical characterization of carbohydrate oxidation at copper electrodes, Electrochim. Acta 37 (1992) 1187-1197.

[52] J. Huang, Z. Dong, Y. Li, J. Li, J. Wang, H. Yang, S. Li , S. Guo, J. Jin, R. Li, High performance non-enzymatic glucose biosensor based on copper nanowires-carbon nanotubes hybrid for intracellular glucose study, Sensor Actuat B 182 (2013) 618- 624.

[53] K. Khun, Z.H. Ibupoto, O. Nur, M. Willander, Development of galactose biosensor based on functionalized ZnO nanorods with galactose oxidase, J. Sens. (2012) 696247-696253.

[54] M. García, A. Escarpa, Disposable electrochemical detectors based on nickel nanowires for carbohydrate sensing, Biosens. Bioelectron. 26 (2011) 2527–2533.

[55] Y. Zhang, L. Su, D. Manuzzi, H. Valdés Espinosa de los Monteros, W. Jia, , D. Huo, C. Hou, Y. Lei, Ultrasensitive and selective non-enzymatic glucose detection using copper nanowires, Biosens. Bioelectron. 31 (2012) 426– 432.

[56] P. Zhang, L. Zhang, G. Zhao, F. Feng, A highly sensitive nonenzymatic glucose sensor based on CuO nanowires, Microchim. Acta 176 (2012) 411–417.

[57] S.S. Mahshid, S. Mahshid, A. Dolati, M. Ghorbani, L.Yang, S. Luo, Q. Cai, Template-based electrodeposition of Pt/Ni nanowires and its catalytic activity towards glucose oxidation, Electrochim. Acta 58 (2011) 551– 555.

[58] C. Xia, W. Ning, A novel non-enzymatic electrochemical glucose sensor modified with FeOOH nanowire, Electrochem. Commun. 12 (2010) 1581–1584.

[59] Tao, B., Zhang, J., Hui, S., Chena, X., Wan, L. "An electrochemical methanol sensor based on a Pd–Ni/SiNWs catalytic electrode" Electrochimica Acta 55 (2010) 5019–5023.

[60] G. Yang, Y. Chen, L. Li, Y. Yang, Direct electrochemical determination of morphine on a novel gold nanotube arrays electrode, Clin. Chim. Acta 412 (2011) 1544–1549.

[61] Y. Lai, A. Ganguly, L. Chen, K. Chen, Direct voltammetric sensing of l-Cysteine at pristine GaN nanowires electrode, Biosens. Bioelectron. 26 (2010) 1688–1691.

[62] Y. Bai, J. Xu, H. Chen, Selective sensing of cysteine on manganese dioxide nanowires and chitosan modified glassy carbon electrodes, Biosens. Bioelectron. 24 (2009) 2985–2990.

[63] J. Zeng, W. Wei, L. Wu, X. Liu, K. Liu, Y. Li, Fabrication of poly(toluidine blue O)/carbon nanotube composite nanowires and its stable low-potential detection of NADH, J. Electroanal. Chem. 595 (2006) 152–160.

[64] L. Liu, J. Song, Voltammetric determination of mefenamic acid at lanthanum hydroxide nanowires modified carbon paste electrodes, Anal. Biochem. 354 (2006) 22–27.

[65] S. Mandal, A. Bhattacharyya, Titania nanowires as substrates for sensing and photocatalysis of common textile industry effluents, Talanta 82 (2010) 876–884.

[66] G. Xu, S.B. Adeloju, Y. Wu, X. Zhang, Modification of polypyrrole nanowires array with platinum nanoparticles and glucose oxidase for fabrication of a novel glucose biosensor, Anal. Chim. Acta 755 (2012) 100-107.

[67] S.M.U. Ali, O. Nur, M. Willander, B. Danielsson, A fast and sensitive potentiometric glucose microsensor based on glucose oxidase coated ZnO nanowires grown on a thin silver wire, Sens. Actuat. B 145 (2010) 869-874.

[68] L. Zhang, S.-M. Yuan, L.-M. Yan, Z. Fang, G.-C. Zhao, An enzymatic glucose biosensor based on a glassy carbon electrode modified with manganese dioxide nanowires. Microchim. Acta 180 (2013) 627-633.

[69] J. Jung, S. Lim, ZnO nanowire-based glucose biosensors with different coupling agents, Appl. Surf. Sci. 265 (2013) 24-29.

[70] L. Wang, X. Gao, L. Jin, Q. Wu, Z. Chen, X. Lin, Amperometric glucose biosensor based on silver nanowires and glucose oxidase. Sensor Actuat. B 176 (2013) 9-14.

[71] H. Jiang, A. Zhang, Y. Sun, X. Ru, D. Ge, W. Shi, Poly(1-(2-carboxyethyl)pyrrole)/polypyrrole composite nanowires for glucose biosensor, Electrochim. Acta 70 (2012) 278-285.

[72] D. Pradhan, F. Niroui, K.T. Leung, High-performance, flexible enzymatic glucose biosensor based on ZnO nanowires supported on a gold-coated polyester substrate, ACS Appl. Mater. Interfaces 2 (2010) 2409-2412.

[73] Q. Wang, F. Min, J. Zhu, Preparation of gold nanowires and its application in glucose biosensing, Mater Lett 91 (2013) 9-11.

[74] Y.-Y.Horng, Y.-K.Hsu, A. Ganguly, C.-C. Chen, L.-C. Chen, K.-H. Chen, Direct-growth of polyaniline nanowires for enzyme-immobilization and glucose detection, Electrochem. Commun. 11 (2009) 850-853

[75] X. Yang, J. Bai, Y. Wang, X. Jiang, X. He, Hydrogen peroxide and glucose biosensor based on silver nanowires synthesized by polyol process, Analyst 137 (2012) 4362-4367.

[76] J. Li, X. Lin, Glucose biosensor based on immobilization of glucose oxidase in poly(o-aminophenol) film on polypyrrole-Pt nanocomposite modified glassy carbon electrode, Biosens Bioelectron 22 (2007) 2898–2905.

[77] K. Dawson, M. Baudequin, A. O'Riordan, Single on chip gold nanowires for electrochemical biosensing of glucose, Analyst 136 (2011) 4507-4513.

[78] S. Aravamudhan, N.S. Ramgir, S. Bhansali, Electrochemical biosensor for targeted detection in blood using aligned Au nanowires, Sensor Actuat B 127 (2007) 29-35.

[79] M .Jamal, J. Xu, K.M. Razeeb, Disposable biosensor based on immobilisation of glutamate oxidase on Pt nanoparticles modified Au nanowire array electrode, Biosens. Bioelectron. 26 (2010) 1420-1424.

[80] S.M.U. Ali, N.H. Alvi, Z. Ibupoto, O. Nur, M. Willander, B. Danielsson, Selective potentiometric determination of uric acid with uricase immobilized on ZnO nanowires, Sensor actuat B 152 (2011) 241-247.

[81] L. Li, J. Huang, T. Wang, H. Zhang, Y. Liu, J. Li, An excellent enzyme biosensor based on Sd-doped SnO2 nanowires, Biosens. Bioelectron. 25 (2010) 2436-2441.

[82] F. Qu, M. Yang, J. Jiang, K. Feng, G. Shen, R. Yu, Novel poly (neutral red) nanowires as a sensitive electrochemical biosensing platform for hydrogen peroxide determination, Electrochem. Commun. 9 (2007) 2596–2600.

[83] I. Lee, X. Luo, X.T. Cui, M. Yun, Highly sensitive single polyaniline nanowire biosensor for the detection of immunoglobulin G and myoglobin, Biosens Bioelectron 26 (2011) 3297-3302.

[84] K.-Z. Liang, J.-S. Qi, W.-J. Mu, Z.-C. Chen, Biomolecules/gold nanowires-doped sol-gel fim for label-free electrochemical immunoassay of testosterone, J Biochem Biophys Methods 70 (2008) 1156-1162.

[85] J. Huang, X. Luo, I. Lee, Y. Hu, X.T. Cui, M. Yun, Rapid real-time electrical detection of proteins using single conducting polymer nanowire-based microfluidic aptasensor, Biosens. Bioelectron. 30 (2011) 306-309.

[86] M. McMullan, N. Sun, P. Papakonstantinou, M. Li, W. Zhou, D. Mihailovic, Aptamer conjugated Mo6S9-xIx nanowires for direct and highly sensitive electrochemical sensing of thrombin, Biosens. Bioelectron. 26 (2011) 1853-1859.

[87] X. Luo, I. Lee, J. Huan, M. Yun, X.T. Cui, Ultrasensitive protein detection using an aptamer-functionalized single polyaniline nanowire, Chem. Commun. 47 (2011) 6368-6370.

[88] X. Liu, Z. Cheng, H. Fan, S. Ai, R. Han, Electrochemical detection of avian influenza virus H5N1 gene sequence using DNA aptamer immobilized onto a hybrid nanomaterial-modified electrode, Electrochim. Acta 56 (2011) 6266-6270.

[89] T.S. Ramulu, R.Venu, B. Sinha, B. Lim, S.J. Jeon, S.S. Yoon, C.G. Kim, Nanowires array modified electrode for enhanced electrochemical detection of nucleic acid, Biosens. Bioelectron. 40 (2013) 258-264.

[90] Y. Bo, H. Yang, T. Yao, S. Huang, A novel electrochemical DNA biosensor based graphene and polyaniline nanowires, Electrochim. Acta 56 (2011) 2676-2681.

[91] M. Pumera, A. Escarpa, Nanomaterials as electrochemical detectors in microfluidics and CE: Fundamentals, designs, and applications, Electrophoresis 30 (2009) 3315-3323.

[92] A. Arora, G. Simone, G.B. Salieb-Beugelaar, J.T. Kim, A. Manz, Latest developments in micro total analysis systems, Anal. Chem. 82 (2010) 4830-4847.

[93] D. Mark, S. Haeberle, G. Roth, F. Von Stettenzab, R. Zengerle, Microfluidic lab-on-a-chip platforms: requirements, characteristics and applications, Chem. Soc. Rev. 39 (2010) 1153-1182.

[94] M. Lee, K.Y. Baik, M. Noah, Y. Kwon, J. Lee, S. Hong, Nanowire and nanotube transistors for lab-on-a-chip applications, Lab Chip 9 (2009) 2267–2280.

[95] M. Hervás, M.A. López, A. Escarpa, Electrochemical immunosensing on board microfluidic chip platforms, TrAC-Trend Anal. Chem. 31 (2012) 109-128.

[96] A. Escarpa, Food electroanalysis: sense and simplicity, The Chem. Rec. 12 (2012) 72-91.

[97] C.E. Banks, R.G. Compton, New electrodes for old: from carbon nanotubes to edge plane pyrolytic graphite, Analyst 131 (2006) 15-21.

[98] M. Pumera, Nanomaterials meet microfluidics, Chem. Commun. 47 (2011) 5671–5680.

[99] D. Vilela, A. Ansón-Casaos, M.T. Martínez, M.C. González, A. Escarpa, High NIR-purity index single-walled carbon nanotubes for electrochemical sensing in microfluidic chips, Lab Chip 12 (2012) 2006-2014.

[100] D. Vilela, J. Garoz, A. Colina, M.C. González, A. Escarpa, Carbon Nanotubes Press-Transferred on PMMA Substrates as Exclusive Transducers for Electrochemical Microfluidic Sensing, Anal. Chem., 84 (2012) 10838–10844.

[101] J.M. González-Domínguez, A.M. Díez-Pascual, A. Ansón-Casaos, M.A. Gómez-Fatou, M.T. Martínez, Epoxy composites with covalently anchored amino-functionalized SWNTs: towards the tailoring of physical properties through targeted functionalization, J. Mater. Chem. 21 (2011) 14948-14958.

[102] A. Ferrreira, J.G. Rocha, A. Ansón-Casaos, M.T. Martínez, F. Vaz, S. Lanceros-Mendez, Electromechanical performance of poly(vinylidene fluoride)/carbon nanotube composites for strain sensor applications, Sensor Actuat. A 178 (2012) 10–16.

[103] S. Aravamudhan, S. Bhansali, Development of micro-fluidic nitrate-selective sensor based on doped-polypyrrole nanowires, Sensor Actuat. B 132 (2008) 623–630.

[104] E. Piccin, R. Laocharoensuk, J. Burdick, E. Carrilho, J. Wang, Adaptive nanowires for switchable microchip devices, Anal. Chem. 79 (2007) 79, 4720-4723.

II.2. Miniaturized flow injection analysis with electrochemical detection based on elemental nickel and bimetallic nickel-copper nanowires for carbohydrate sensing

II.2.1. Introduction and objectives

Manipulation and assembly of metallic nanowires (MNWs) to develop highly ordered nanowire arrays could offer new possibilities since enhancements of sensitivity can be achieved through active surface increasing[1-4]. Normally, these ordered nanowire array sensors are built directly on the electrode surface[3-9] but this approach is stiff and it does not permit easy replacement of these nanowires. The incorporation of magnetic segments (e.g., nickel) in these NWs allows additionally magnetic manipulations through the application of an external magnetic field and opens the door for a wide range of exciting bioelectronic operations[6,10-12]. An impressive "proof-of-the-concept" has been published taking advantage of magnetic manipulation such as adaptive magnetic nanowires for controlling on-demand the operation of electrochemical sensors[13], for protecting on-demand electrochemical sensors against fouling[14] or for switching between active and passive detection states[9,15]. In addition, the use of magnetic NiNWs as amperometric sensors for detection of carbohydrates[9,13], alcohols[13,15-17] and hydrogen gas[18] have also been reported. Other metals such as copper, palladium, platinum and cobalt are often used to fabricate multi-segments of NiNWs with different lengths (6–60μm) and widths (20–300 nm) by template electrosynthesis, and then, they are included on the electrode surfaces.

However, from our point of view, in order to avoid complex and stiff configurations, a disposable approach is needed. In this way, NiNWs offer one of the most interesting alternatives for the easy construction of novel disposable electrochemical detectors using small quantities magnetically manipulated on screen-printed electronic transducers. Also, as it is has been stated in the previous section, NWs remains to be exploited in the analytical field and some developments should be

addressed such as: to propose a simple route for disposable electrode construction to perform the analysis in the field, to evaluate their stability under commonly used hydrodynamic flows, and to explore their analytical performance using real samples, which is negligible from the literature. Moreover, screen-printing technology is a well-established technology for the fabrication of both chemical sensors and biosensors[19]. Decentralized sensing is increasingly required in real world applications, so traditional techniques utilizing highly expensive, immovable analytical equipment are not feasible for sensing purposes outside the realms of standard laboratories[20]. Screen-printed electrodes address the issue of cost effectiveness, but they also satisfy the previously much sought after need for highly reproducible and sensitive methods of detection of target analytes, while they can be produced at low cost through economies of scale[21]. In addition, screen-printed electrochemical sensors provide excellent base platforms that can be modified with a variety of nanomaterials and structurally related materials without the need for pretreatment (such as electrode polishing and/or electrochemical pretreatment), which is common required for other electrode materials.

Without any question, it will help to expand the use of these detectors for more universal applications involving rapid and simple sample screening methods as well as free-enzyme approaches in order to decentralize analysis towards a "disposable nanotechnology" approach.

On the other hand, carbohydrates as important analytes and taking advantage of the catalytic properties of nickel and copper electrodes over these compounds[22-24] and using selected samples to demonstrate the analytical potency of the NWs have been strategically chosen.

The approaches most commonly used to determine carbohydrates are GC, HPLC, and capillary electrophoresis (CE)[25,26,27]. As it was already discussed before, the electrochemical determination of sugars is very useful, taking into account that it avoids some difficulties that arise from their lack of chromophores for photometric detection. The electrochemical detection of sugars is favored by the electrocatalytic effects of copper and nickel, which allow the direct detection of carbohydrates with high sensitivity[22]. Pulsed amperometric detection (PAD) is commonly employed, and a strong alkaline medium is necessary to achieve sufficient sensitivity toward carbohydrate anions[28]. Moreover, electrochemical techniques for carbohydrate analysis do not need a derivatization step, and they offer other technical advantages, such as high compatibility with nanomaterials and their inherent miniaturization. Nano- and screen-printed technologies are very attractive in this field, which remains underexploited in the analysis of real samples.

In consequence, we are proposing disposable electrochemical sensors based on NWs using carbon screen-printed electrodes (CSPEs). FIA was used to evaluate the performance of the disposable screen-printed based nanowires.

II.2.2. Electro synthesis and characterization of elemental nickel and bimetallic nickel-copper nanowires based-electrodes

Since both nickel and copper are suitable for the electrochemical detection of sugars, the electrosynthesis and characterization of elemental nickel and bimetallic nickel-copper nanowires were carefully carried out.

Firstly, MNWs were synthesized by an electrodeposition method using a porous template[3,29]. Anodic alumina oxide membrane (AAO) that was used as a template for nanowire growth was sputtered with gold in its branched side to act as the working electrode during the electrodeposition. For the synthesis of nickel nanowires, a thin layer of copper was deposited (−1V, 10 C) to fill the imperfections of the template in order to obtain a regular and tubular structure for the growth of the nickel nanowire, and then the last step was the electroplating of the nickel layer to form the nanowires (−1V, 45 C).

For the Ni-CuNWs, after the sacrificial copper layer (−1 V, 10 C) had been deposited to fill the imperfections of the template, a thinner nickel layer than used for the NiNWs was deposited (−1 V, 22.5 C), and then a copper layer with the same charge (−1 V, 22.5 C) was deposited in order to complete the synthesis of the bimetallic Ni-CuNWs.

In both electrosynthesis, the sacrificial copper layer was eliminated with $CuSO_4 \cdot 5H_2O$ solved in HCl 30% (v/v). For releasing the nanowires, AAO template was dissolved with NaOH 3M for 25 min and then the nanowires were collected in a microtube and rinsed several times with deionized water until a neutral pH was obtained. A magnet was used to help us in the process.

Secondly, morphological and compositional characterization of electrosynthetized MNWs was performed using scanning electronic microscopy (SEM), transmission electronic microscopy (TEM) and electronic dispersion spectrometry (EDS) techniques. **Figure II.7A** shows the SEM micrographs where a random distribution of individual NiNWs with a length of about 6 μm was clearly observed upon fabrication. Characterization by TEM revealed the real width of NiNWs about 330 nm as it is observed in **Figure II.7B.** Also, EDS analysis was performed in order to confirm the homogeneity of the whole nanowires. As expected, Cu (from sacrificial layer) was detected in one extreme of the NWs (at a distance about 0.2 μm). However, the EDS analysis at different NW zones (at distances of about 1 and 4.5 μm); indicated 100% of the metal along the material confirming the suitability of the NiNWs fabrication.

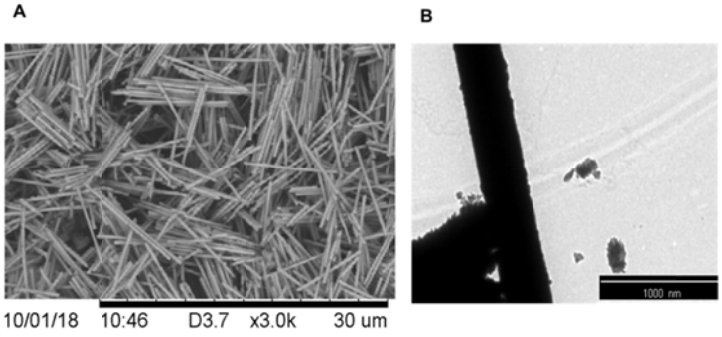

Figure II.7. (A) SEM micrographs of NiNWs (magnification 3000×). **(B)** TEM image of a single NiNW (magnification 8000×).

In addition, the influence of the deposited charges as well as the diameter of the pore of different membranes has also been explored.

Figure II.8 shows the micrographs obtained for NiNWs using different deposited charges (**A**; SEM) and alumina templates with different pore diameters (**B**; TEM). While adjusting the charge deposited

between 45 and 65 C allowed NWs with lengths ranging from 6 to 10 μm to be obtained, the use of alumina templates with different pore diameters led to NWs with roughly the same widths. Since these differences were not significant, an alumina template with a pore size of 200 nm and a deposited charge of 45 C were used during the electrosynthesis of both NWs (see **Figure II.8C** for SEM and TEM pictures of Ni-CuNWs). Under these conditions, both the Ni and the Ni-CuNWs were characterized by EDS, and the results obtained are listed in **Table II.3**. These results indicate the suitability of this fabrication process, since 97% of the metal in the NiNWs was Ni, and 50.6% and 49.4% of the metal in the Ni-CuNWs was Ni and Cu, respectively, as expected.

Table II.3. EDS analysis of MNWs

Metal (%)	NiNWs	Ni-CuNWs
Ni	96.6	50.6
Cu	3.4	49.4

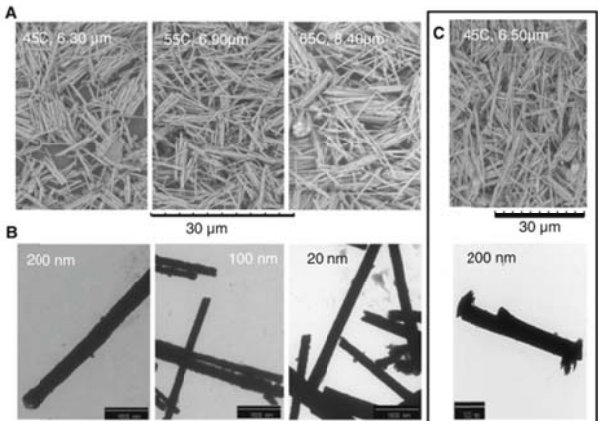

Figure II.8 (A) SEM micrographs of NiNWs (magnification 3000×), **(B)** TEM images of NiNWs (magnification 8000×), **(C)** SEM and TEM micrographs of Ni-CuNWs

Thirdly, the well-known electrocatalysis of MNWs over carbohydrates was firstly checked using cyclic voltammetry (CV). Anodic peaks at +0.70V and +0.55V and the cathodic peaks at −0.55V and −0.40V for NiNWs and Ni-bulk electrodes, vs. Ag and Ag/AgCl/KCl (3M) reference electrodes, respectively were found (voltammograms are not shown). Anodic and cathodic peaks corresponded to the oxidation of Ni(II) to Ni (III) and the reduction of Ni (III) to Ni (II), respectively. This redox reaction is responsible for the electrocatalytic properties of nickel electrodes over carbohydrates and amino acids[23,24,30,31,]. In consequence, these results indicated the electrocatalysis of NiNWs over carbohydrate sensing.

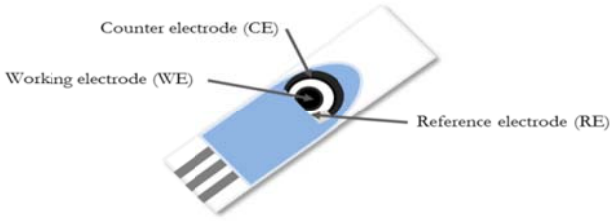

Figure II.9. Disposable platform integrating the three electrodes

Then, to build disposable amperometric detectors, different key-steps were systematically studied towards sensing of glucose and sucrose as target analytes. Analytical optimization was studied by modification of CSPE (integrating the three electrodes while dropping just 50 μL of sample, see **Figure II.9**), using FIA with a flow rate of 2.0mLmin^{-1}; 50 μL loop and under potentiostatic conditions of +0.70V vs. Ag reference electrode. Also, a permanent magnet was used in the cell in order to keep NiNWs on the surface under hydrodynamic regime. **Figure II.10A (a–d)** shows FIA signals for direct sensing of carbohydrates: on non-modified CSPE **(a)**, aligned non-activated NiNWs **(b)**, aligned and activated

NiNWs (at −1.5V for 600 s) **(c)**, and activated-washed NiNWs **(d)**. As expected, no signal was observed on the CSPE while a weak signal was observed on NiNWs modified electrodes. On the contrary, electrochemical activation of NiNWs becomes a critical variable as well, as it is observed in **Figure II. 10A (c)** with a signal improvement of about 20 times. Optimized activation conditions were performed using amperometry at −1.5V for 600 s (see **Table II.S1**). Interestingly, in a final optimization adjustment, signal decreased but signal/noise was improved (about 100%) when activated washed NiNWs were used **Figure II. 10A (d)**. **Table II.4** lists the quantitative data obtained in these studies.

Table II.4. Optimization of building disposable NiNWs detectors[1]

Electrode	Glucose			Sucrose		
	i ± s (μA)	**RSD (%)**	**S/N**	**i ± s (μA)**	**RSD (%)**	**S/N**
Bare	0.1 ± 0.1	3.7	3	0.02 ± 0.01	11.2	1
Non activated NW	0.9 ± 0.1	4.1	28	0.4 ± 0.1	2.8	11
Activated NW	21.1 ± 0.5	2.3	62	9.3 ± 0.1	1.4	27
Washed	16.4 ± 0.4	2.2	683	6.9 ± 0.1	2.2	288

[1] Values are average of five determinations. Glucose and sucrose are 0.5mM.

Evaluation of the influence of the magnetic field on analytical sensitivity was carefully studied. **Figure II. 10B** shows the signals obtained for target carbohydrates for different alignments of NiNWs in connection with the optical images regarding those orientations: **(a)** non oriented; **(b)** horizontally and **(c)** vertically oriented. Interestingly, vertical alignment of NiNWs depicting an architecture based on an array of microelectrodes of aggregated NiNWs with diameter ranging between 80 and 150 μm and a separation distance between 150 and 300 μm was observed; while in the horizontal alignment, NiNWs adopted a parallel configuration with respect to the electrode surface. When the magnet was

not used just a simple random distribution was noticed. It was also observed that when a magnetic field was applied during electrochemical activation step, sensitivity was increased in comparison to when no magnetic field was applied. This enhancement of sensitivity was noticed independently of the alignment used in **Figure II. 10B (b, c)** (for figures of the merit, see supporting information **Table II.S2**). Vertical position was chosen for set-up simplicity in all subsequent experiments before washing. After washing, as we have already mentioned before, signal-to-noise was improved. This fact could indicate an overabundance of NiNWs or that all of them were not involved in the electrocatalysis of carbohydrates while this high surface generated higher noise. Aliquot-volumes of well-dispersed NiNWs ranging between 5 and 20 µL were also examined with 15 µL being the optimum value with the highest sensitivity (see **Table II.S3**). Values above indicated saturated area and no increasing of signal were observed.

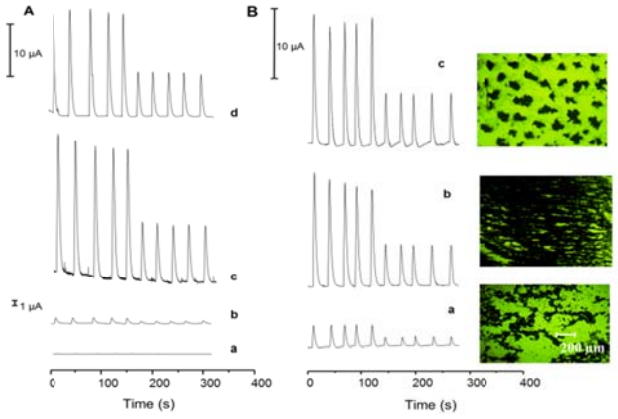

Figure II. 10. FIA signals for glucose and sucrose sensing **(A)**: **(a)** on CSPE; **(b)** CSPE-NiNWs; **(c)** activated CSPE-NiNWs and **(d)** activated and washed CSPE-NiNWs. Influence of alignment of NiNWs on analytical sensitivity **(B)**: **(a)** without magnet; **(b)** horizontal alignment and **(c)** vertical alignment. Experimental conditions: glucose and sucrose 0.5 mM; E= +0.7 V; F= 2 mL/min; Vinjection = 50 µL.

Under optimum conditions, the chemical state and the relative abundance of the elements on five electrodes were determined by XPS. The binding energies of core-levels of the elements are summarized in **Table II.S4**. The binding energy of the most intense Ni $2p_{3/2}$ component of the Ni 2p doublet appeared at ca. 855.4 eV which is characteristic of nickel oxide (Ni^{2+}). In agreement with this is the observation of a satellite line, at about 8 eV higher binding energy of each Ni 2p component, which is the fingerprint of Ni^{2+} ions. It is likely that Ni-nanowires exposed to ambient atmosphere quickly become oxidized. The atomic concentration of Ni on the electrode surface is around 0.9% calculated from the XPS spectra. The almost constant atomic Ni/C ratio for all samples (except one) confirms the reproducibility of the construction of NiNWs detectors.

II.2.3. Disposable electrochemical detectors based on elemental nickel nanowires for carbohydrate sensing

Analytical performance of NiNWs was studied using FIA under the previous optimized conditions. Firstly, repetitive injections of 0.5 mM glucose (n= 50) were performed using Ni-bulk and NiNWs electrodes under potentiostatic conditions taken from cyclic voltammograms (+0.50V for Ni-bulk electrode vs. Ag/AgCl (3M) and +0.70V for NiNWs vs. Ag electrode). Peak current of glucose was 21 μA and 20 μA at the Ni-bulk and NiNWs electrodes, respectively. Given that the atomic composition of NiNWs was only 0.9%, the current density at the NiNWs electrode was estimated to be about 65 times that at the Ni-bulk electrode under these current working FIA conditions. When the analysis was performed at +0.50V for NiNWs electrode, obviously peak current of glucose decreased to 10 μA. However, even under these potentiostatic conditions, the current density was estimated to be about 20 times higher in the NiNWs. The RSDs obtained when NiNWs were used (*intra*-electrode precision), was less than 7% compared with the RSDs of 14% obtained at the Ni-bulk electrode and in consequence no significant loss was observed in the peak current signal with consecutive glucose injections. Also, *inter*-NiNWs electrodes precision was evaluated obtaining good RSDs values less than 10% (n= 5). XPS confirmed the good reproducibility obtained during their construction since similar spectrum profiles and quantitative compositions were obtained when the different electrodes were examined. (See **Table II.S4**). These findings indicated a very good performance for NiNWs detectors depicting extremely high current density with the additional value of simplicity, miniaturization, extremely low nickel amount and further disposability.

NiNWs-concentration dependence was also studied. **Figure II.11** shows the FIA signals under the above conditions; inserted into the graph is the respective calibration curves for glucose determination.

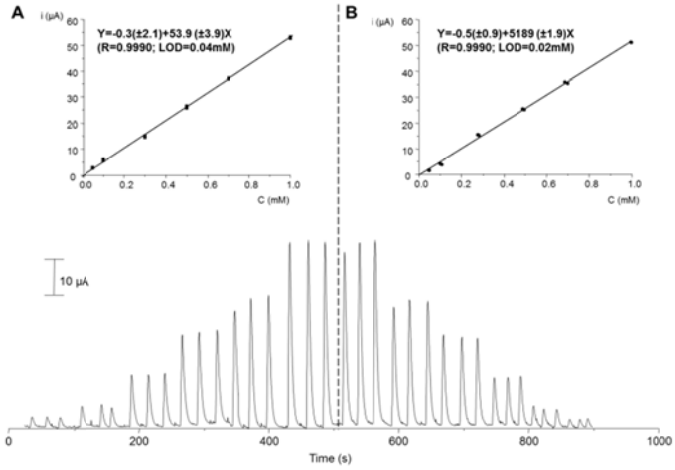

Figure II.11. External glucose calibrations **(A** and **B)**. Linear range: 0.05–1 mM. Inset: linear regression for both analyses. Other conditions are as listed in **Figure II.10.**

It can be seen that no memory effect is observed and also there is a high reproducibility giving an excellent analytical performance because identical intercepts, slopes and LODs were obtained for both calibration graphs. LODs obtained in our work (20 μM) were similar to those reported by other authors for similar NWs[17]. The analytical response of NiNWs to different carbohydrate structures was also explored for galactose, fructose, sucrose, lactose and inulin with sensitivity factors of 36.2, 36.4, 17.8, 20.6, and 48.8 μA/mM, respectively. Sensitivity was similar in each carbohydrate class, being higher for monosaccharides than disaccharides. Also, fast and reliable responses of NiNWs to the different carbohydrate structures assayed with excellent peak shapes, signal/ noise characteristics and very good precision (RSD≤3%) were clearly obtained (see **Table II.S5**).

Analytical performance was also evaluated using real samples. Firstly, analytical evaluation of NiNWs for determination of total carbohydrates as sample screening method was proposed using target samples strategically selected with very different total carbohydrate contents. **Figure II.12** shows FIA signals for selected runs of glucose (as control), caffeine (as prominent no sugar compound in the samples), and regular (diluted) and light (non-diluted) cokes.

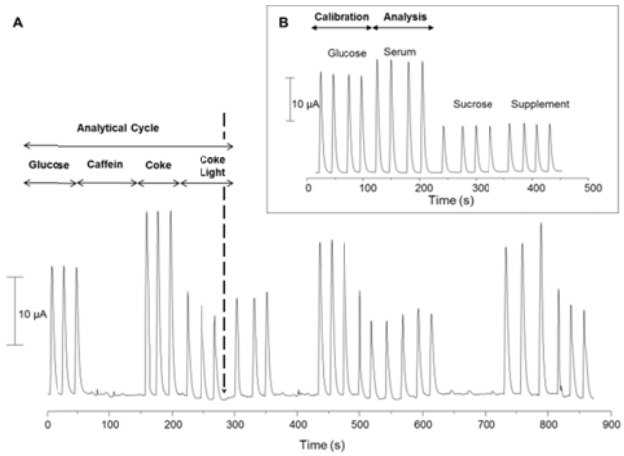

Figure II.12. FIA signals for sample screening analysis. **(A)** Injections of glucose (0.5 mM), caffeine (0.6 mM), regular coke (dilution 1/500, v/v) and light coke (direct injection). Inset: Simplified calibration and sequential determination of glucose and sucrose in serum and pharmaceutical, respectively **(B)**. Other conditions are as listed in **Figure II.10.**

NiNWs act as reliable sensors because while the expected glucose response was obtained, NiNWs did not give any analytical response during caffeine sensing. Also, a fast discriminated response for samples with different sugar content was clearly obtained (please, note that the dilution factor was 500 folds). This reliable behavior was also obtained when different cycle runs were performed where total carbohydrate signal was recovered and excellent precision was again achieved (see **Table II.S6**). In addition, total carbohydrate content in both beverages (coke

and coke light) was evaluated using glucose and glucose/sucrose mixture (50:50, w/w) as calibration standards. Interestingly, total carbohydrate levels were of 7.5 and 11.9 g/100mL for regular coke and 5 and 9 mg/100mL for coke light, using glucose and glucose/sucrose as standards, respectively. These values were in good agreement with those reported of 10.6 g/100mL and zero for coke and coke light for "total sugars", respectively. Precision was also very good with RSDs values less than 4% (n = 3). Also, the time employed in the 36 determinations was about 14 min and it indicated a very high throughput analysis (2–3 analyses per minute!). These results opened new possibilities for these nanotools which can be used for methods where just a reliable binary response and a fast determination of total carbohydrates is highly required.

Since linearity was demonstrated for all target carbohydrates (R^2 ≥0.990) and intercepts were statistically zero (−0.3±2.1, 1.0±1.1 for glucose and sucrose, respectively, α= 0.05) a simplified calibration protocol was also proposed. Firstly, upon injection of carbohydrate standard, the calibration factor (defined as $f_{carbohydrate}$= $Signal_{carbohydrate}$/[Carbohydrate standard]) is obtained and then, the sample injection is carried out. Then, the carbohydrate index is estimated as CI= $Signal_{sample}/f_{carbohydrate}$. **Figure II.12B** (inset) illustrates the proposed strategy depicting FIA signals for analytical cycles corresponding to the calibration of individual carbohydrate standard and its sequential determination in the sample for glucose and sucrose, respectively. **Table II.5** lists analytical figures of merit including calibration factor, precision and recoveries obtained during quantitative analysis using this strategy. Excellent precision for the simplified calibration approach and for the analysis of the samples with RSDs less than 2% were obtained. In addition, a high

recovery was yielded during the analysis of the samples indicating the suitability of the approach.

Table II.5. Analytical figures of quantitative analysis using simplified calibration approach

Simplified calibration[1]	**Glucose**	**Sucrose**
RSD (%)	1.8	1.2
Calibration factor (μA/mM)	46.9	22.5
Analysis of Sample	**Serum**	**Supplement**
RSD (%)	1.1	1.5
Concentration expected[2] (mM)	0.50	0.50
Concentration found[3] (mM)	0.57	0.51
Recovery[4] (%)	114	102

[1] Standard concentration 0.5mM; [2]Reference value in sample (given by manufacturer); [3]Concentration obtained using simplified calibration approach [4]Versus nominal value given by manufacturer

This simplified calibration approach had important advantages such as the dramatic decreasing of the analysis time and also, it can be suitably regarding target sample analysis. Indeed, that concentration of standard can be strategically chosen closer to the sample expecting an improvement in analytical features such as precision and accuracy since calibration and analysis are performed under repeatable conditions. In addition, simplified calibration solves the potential lack of *inter* electrodes reproducibility, allowing an extremely easy operation for performing quality control by the customer in the field.

II.2.4. Electrochemical monosaccharide index in honeys using nickel and nickel-copper nanowires

Next it was aimed to demonstrate the analytical potency of screen-printed electrochemical detectors based on NiNWs and nickel-copper nanowires (Ni-CuNWs) for the fast and reliable assessment of total sugars by comparing the results obtained using such NWs with those afforded by a well-established HPLC. Analyses of ten selected honeys were also carried out to demonstrate the reliability of this new method. Combining screen-printed and a nanotechnology on a board containing simple and miniaturized instrumentation is expected to open up new approaches to food electroanalysis.

In this case, CSPEs were modified using both Ni and Ni-CuNWs in order to create the electrochemical detectors. **Figure II.13** shows fiagrams obtained for glucose and sucrose on unmodified CSPE (**a**) as well as on electrochemically activated NiNWs (**b**) and Ni-CuNWs (**c**). As expected, no signal was observed on the unmodified CSPE, while well-defined signals were obtained on both NW-modified electrodes.

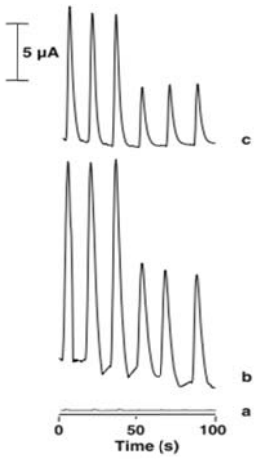

Figure II.13 Fiagrams of glucose and sucrose (0.5 mM each) on **(a)** CSPE, **(b)** NiNWs and **(c)** Ni-CuNWs. Other conditions are as listed in **Figure II.10.**

Firstly, the analytical performance obtained with both NWs was studied in detail. The analytical features of the calibration graphs for each individual sugar solution as well as the standard mixture of glucose:fructose (50:50 w/w, simulating sugar honey composition) are listed in **Table II.6**. Interestingly, both NWs gave similar analytical performances with the individual sugar solutions and the standard mixture, including very linear concentration dependences ($r \geq 0.99$), similar sensitivities, and an intercept that was statistically zero in all cases examined. In addition, the LODs and LOQs were estimated using the 3.3×S/N and 10×S/N criteria, respectively. Another important feature was the very good precision obtained (RSD≤ 5%), and the results were found to be independent of the NW composition and the composition of the sugar solution assayed, as listed in **Table II.6**. **Figure II.14** shows the calibration signals obtained for the concentration range assayed using both NiNWs and Ni-CuNWs. Very good peak shapes due to fast electronic transfer and very good signal-to-noise characteristics were clearly observed, in agreement with the results listed in **Tables II.6** and **II.7**.

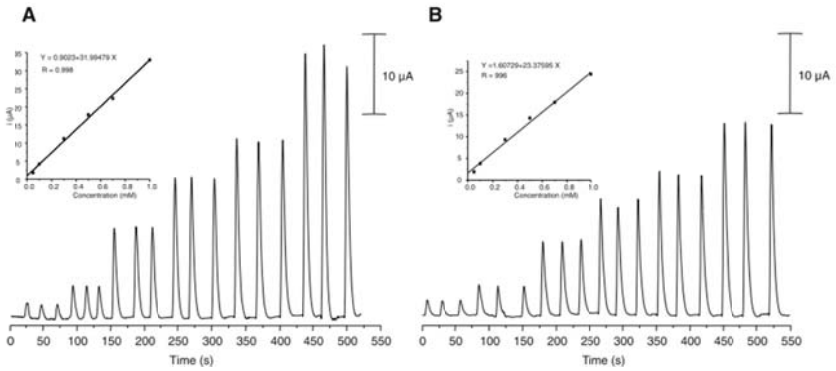

Figure II.14. External glucose/fructose calibrations performed using NiNWs **(A)** and Ni-CuNWs **(B)**. Linear range: 0.05–1 mM. Inset: linear regressions for both analyses. Other conditions are as listed in **Figure II.10.**

Table II.6. Precision in glucose-fructose calibration using NWs (%, n=3).

Glucose/Fructose concentration (mM)	Ni	Ni-Cu
0.05	0.58	1.61
0.10	0.51	0.73
0.30	0.77	1.04
0.50	0.59	4.19
0.70	0.85	1.15
1.00	4.26	0.88

Table II.7. Analytical characteristics of the calibration graphs employing both MNWs (α= 0.05, n=6).

Sugar Standard	NiNWs						Ni-CuNWs					
	Linear Range (mM)	r	$a \pm ts_a$ (μA)	$b \pm ts_b$ (μA/mM)	LOD (mM)	LOQ (mM)	Linear Range (mM)	r	$a \pm ts_a$ (μA)	$b \pm ts_b$ (μA/mM)	LOD (mM)	LOQ (mM)
Glucose	0.05-1.00	0.998	1.27 ± 1.63	41.45 ± 2.94	0.06	0.18	0.05-1.00	0.996	1.17 ± 1.47	27.28 ± 2.65	0.08	0.25
Fructose	0.05-1.00	0.999	1.57 ± 0.75	30.96 ± 1.35	0.04	0.11	0.05-1.00	0.999	1.00 ± 0.77	30.49 ± 1.39	0.04	0.12
Glucose/ Fructose (50:50) w/w)	0.05-1.00	0.999	0.58 ± 0.86	31.94 ± 1.55	0.04	0.13	0.05-1.00	0.996	1.61 ± 1.16	23.38 ± 2.08	0.08	0.23

Secondly, the ten honeys that had previously been characterized[32] were sequentially analyzed on the board of the same electrode. Because of the excellent features observed on the calibration graphs (linearity was demonstrated, the intercepts were statistically zero, and similar sensitivities were noted for all standards), as it was already proposed before, a simplified calibration approach based on a one-point calibration using a mixture of glucose/fructose (50:50 w/w) as standard was proposed. Again, the simplified calibration protocol was established by injecting in the standard mixture in order to calculate the calibration factor via $F_{\text{glucose/fructose}}$= $\text{signal}_{\text{glucose/fructose}}$/[glucose/fructose]. The samples were then injected in and the total sugar content (TS) was estimated via TS= signal sample/$F_{\text{glucose/fructose}}$.

Table II.8 lists the total sugar contents obtained for the ten target honeys using both the NiNWs and the Ni-CuNWs. The total sugar contents obtained by HPLC-RI (as the sum of the individually determined glucose and fructose contents) are also included. Very good repeatability was obtained, with RSD values of less than 6% (n=3); the results were also observed to be independent of the NWs used and the honey analyzed. However, when the sugar approach was compared with those obtained by the HPLC-RI method, high systematic errors of up to 50% were noted. Also, the error was seen to increase with the number of analyses. To solve this inconvenience, a fast calibration was performed immediately prior to each subsequent analysis. Interestingly, when this was done, the systematic errors obtained were much lower (see also **Table II.8**). Using this strategy, the results obtained using both NWs were in good agreement with the

HPLC-RI method, and both the NiNWs and the Ni-CuNWs yielded similar errors; thus, the electroanalytical approach exhibited very good accuracy.

Figure II.15 illustrates selected FIA signals obtained for NiNWs and Ni-CuNWs. On the one hand, **Figure II.15A** and **B** show the analytical signals from three selected honeys (honey samples 2, 4, and 6 in **Table II.8**) obtained using Ni-CuNWs according to both calibration strategies [calibration was either performed only once before the sequential analysis for all ten honeys (**A**), or immediately prior to the analysis of each honey (**B**)]. As observed, when calibration was performed only once, a clear decrease in signal was observed when each honey was analyzed (**A**). As expected, this decrease in sample signal was also observed in calibration signal; however, it did not affect to the accuracy of results as it is observed in **Table II.8**. Also, similar signals were obtained for the standards and samples because the concentration of the standard and the sample dilution were strategically chosen to produce signals in the middle of the linear calibration range. In order to highlight the impressive performance of this novel electrocatalytic sugar detection approach, **Figure II.15c** shows the FIA signals on the board of just one modified electrode with NiNWs during multiple honey analyses, each preceded by a calibration, where both analytical steps were performed in triplicate.

Table II.8. Total sugars in honey samples analysis using NiNWs and Ni-CuNWs.

Honey	HPLC-RI[1]	NiNWs			Ni-CuNWs						
	Total (%)	Total (%)[2]	Er (%)	Calibration factor (μA/mM)	Total (%)[3]	Er (%)	Total (%)[1]	Er (%)	Calibration factor (μA/mM)	Total (%)[3]	Er (%)
1	68.9	74.9 ±1.4	8.6	40.1	74.9 ± 1.4	8.6	70.4 ± 0.6	2.1	50.0	70.4 ± 0.6	2.1
2*	64.5	60.1 ± 0.9	-6.8	38.4	62.7 ± 1.0	-2.8	64.4 ± 2.6	-0.2	47.1	68.4 ± 2.8	6.0
3	64.9	52.6 ± 0.8	-19.0	33.8	62.3 ± 0.9	-4.1	55.0 ± 4.7	-15.2	43.6	63.1 ± 5.4	-2.9
4*	63.2	47.4 ± 0.9	-25.1	31.9	59.4 ± 1.1	-6.1	48.9 ± 0.3	-22.6	43.4	56.4 ± 0.4	-10.9
5	72.7	57.3 ± 4.1	-21.3	36.1	63.5 ± 4.6	-12.7	46.4 ± 2.8	-36.2	33.7	68.7 ± 4.1	-5.5
6*	66.1	48.1 ± 0.8	-27.2	28.9	66.7 ± 1.2	1.0	37.9 ± 0.4	-42.6	31.5	60.1 ± 0.7	-9.0
7	63.9	43.7 ± 2.6	-31.6	30.4	57.6 ± 3.4	-9.8	42.8 ± 0.5	-33.1	36.0	59.4 ± 0.6	-7.1
8	69.4	38.1 ± 2.2	-45.2	23.6	64.6 ± 3.7	-7.0	41.4 ± 0.7	-40.4	35.1	59.5 ± 0.1	-14.3
9	70.2	57.3 ± 1.9	-18.3	36.7	62.6 ± 2.0	-10.8	46.9 ± 2.0	-33.2	35.3	66.4 ± 2.8	-5.4
10	64.5	50.3 ± 0.8	-21.9	30.5	66.0 ± 1.0	2.4	35.1 ± 0.7	-45.6	35.2	56.6 ± 1.2	-12.2

[1] Obtained by sum of the individual ones of glucose and fructose. [2] Employing only a calibration factor at the beginning. [3] Employing a calibration factor for each sample.

* Analyzed samples shown on **Figure II.14.**

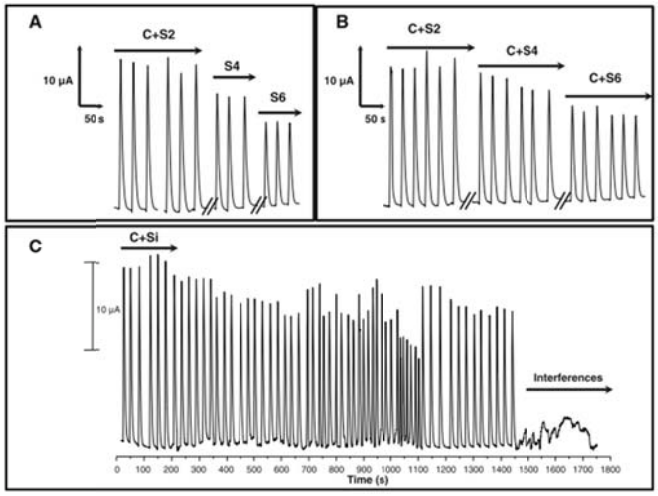

Figure II.15. Illustration of the signals obtained from the analysis of honey samples using Ni-CuNWs **(A–B)** and NiNWs **(C)**,along with calibration **(A**: calibration and the subsequent analysis of all samples; **B–C**: each sample analysis was preceded by a calibration). C + S2–S6 glucose/fructose calibration and analysis of honey samples 2, 4, and 6, respectively; C + Si glucose/fructose calibration and analysis of honey samples 1–10. Other conditions are as listed in **Figure II.10.**

While, conceptually speaking, the selectivity of this approach was inherently demonstrated by its very good accuracy**,** interferences from polyphenols and other compounds such as ascorbic acid were also studied. No interference was observed, as shown in **Figure II.15C**. These results were extremely interesting, because this approach possesses inherent selectivity that is governed by the catalytic material used, in contrast to expensive enzyme reagents. Therefore, this novel non enzymatic approach has the additional advantages of economy and simplicity of application by non-specialist users in the field. As well as this improved analytical reliability, the simplified calibration strategy utilized has important advantages: it simplifies the overall process, and it dramatically decreases the analysis time, thus allowing high throughput (60 samples can be processed in about 25 min,

yielding a rate of 2 samples min^{-1}, on the board of just one electrode without any loss of performance; see **Figure II.15c**).

Although both NWs exhibited excellent analytical performance, the NiNWs are considered preferable due to their simplicity of fabrication, as only one electroplating solution is required. As it was discussed before, the excellent analytical performance of the NiNWs was reinforced by comparing them with a bulk Ni electrode. Indeed, since the NiNWs contained only 0.9% Ni, the current density obtained on the NW surface is much higher than that obtained on bulk Ni (about 60 times greater)[33]. These findings demonstrate that the magnetic manipulation and assembly of these NiNWs, with their large active surfaces, open the door to new, enhanced sensors, and a wide range of novel sensing operations. This is not possible using bulk Ni. Also, NiNWs are disposable and highly compatible (in terms of scale) with microfluidic analytical systems, while bulk Ni is neither.

The extremely small amount of NWs used in the detector was probably the reason for the performance loss observed when several samples with high sugar contents were analyzed. This fact indicates that nanotools should be handled with care when a large number of relatively concentrated samples are examined (quality control). However, it should be pointed out that this is not a disadvantage, since the detectors are disposable. Therefore, NWs represent a valuable alternative to the HPLC-RI approach, offering simplicity, sensitivity, and selectivity for total sugar assessment, and avoiding the need for expensive instrumentation and time-consuming SPE extraction– HPLC column separation.

In resume, because of the excellent analytical performance obtained with this novel electroanalytic detector, we propose that the term "electrochemical monosaccharide index" should be employed to describe

the total monosaccharide content in the target sample, thus avoiding the need to use specific columns for individual monosaccharide determination.

II.2.5. Conclusions

These works shows the analytical potency of a simple, easy, user friendly, low-cost, and modern electroanalytical technique that utilizes nanomaterials on disposable screen printed platforms to determine the total monosaccharide contents of target samples. Electrochemical detectors based on NiNWs and Ni-CuNWs nanowires were shown to provide excellent analytical performance in terms of fast analytical response, analyte class selectivity, calibration performance, and reliability during the analysis of the samples. NWs are a novel, reliable, and disposable free-enzyme nanotool, and provide a valuable alternative to other more sophisticated and expensive techniques (such as HPLC) used for total sugar assessment. In addition, under the philosophy of "disposable nanotools", the simplified calibration protocol proposed was an elegant and pertinent strategy because it will help us move ahead to "in-field" testing and subsequent decentralization of fast and reliable analysis. Indeed, it allows the customer to perform a calibration and/or quality control and analysis of target sample in a very simple, fast and cheap way with additional reliability. This novel approach could be used not only as a routine method in common labs but also in decentralized and *in situ* analyses. The term "electrochemical monosaccharide index" was also proposed as a way to describe the total monosaccharide content in the target samples.

II.2.6 Experimental Section

II.2.6.1 Apparatus

The scanning electron microscopy (SEM) micrograph was performed on a Hitachi TM-1000 (Tokyo, Japan) with qualitative and quantitative energy-dispersive X-ray spectrometry (EDS) system Swift-ED for TM-1000 form Oxford Instruments (Oxford, UK). Aluminum mount stubs used for the SEM analysis were obtained from electron microscopy sciences (Hatfield, UK). The transmission electron microscopy (TEM) micrograph was performed on a ZEISS EM10C (Germany).

Photoelectron spectra (XPS) were obtained with a VG Escalab 200R spectrometer equipped with a hemispherical electron analyzer (pass energy of 50 eV) and an MgKα ($h\upsilon$ = 1254.6 eV, 1 eV= 1.6302×10^{-19} J) X-ray source, powered at 120 W. The kinetic energies of photoelectrons were measured using a hemispherical electron analyzer working in the constant pass energy mode. The background pressure in the analysis chamber was kept below 2×10^{-8} mbar during data acquisition. The XPS data signals were taken in increments of 0.1 eV with dwell times of 50 ms. Binding energies were calibrated relative to the C 1s peak at 284.9 eV. High resolution spectra envelopes were obtained by curve fitting synthetic peak components using the software "XPS peak". The raw data were used with no preliminary smoothing. Symmetric Gaussian–Lorentzian product functions were used to approximate the line shapes of the fitting components. Atomic ratios were computed from experimental intensity ratios and normalized by atomic sensitivity factors[34]

The magnetic orientation of NiNW was monitored using an inverted optical microscope working in bright field for optical images capture. For this purpose, a model system was designed using a glass slide

and setting a magnet below it (1.1cm separation distance as in the flow cell). 8 μL of 10mg·mL^{-1} NiNW suspension was deposited on the glass slide and the NiNWs were orientated in vertical or horizontal position turning the magnet 90º. The images were captured using the CCD camera of the microscope.

The optical images of nickel nanowires were taken using an inverted microscope Motic AE31 (Xiamen, China). The digital images from the microscope were acquired with a Moticam 3000 CCD camera and Motic Images advanced 3.2 (from Motic, Xiamen, China). X-ray photoelectron spectroscopy (XPS) data using a VG Escalab 200R (Thermo Fischer Scientific Inc., Waltham, MA, USA).

Autolab PGSTAT 12 potentiostat (Eco Chemie, The Netherlands) with a standard three-electrode system was used for the electroplating and amperometric detection. An Ag/AgCl electrode in saturated KCl solution was used as the reference electrode and a platinum wire as the counter electrode.

II.2.6.2 Materials and Methods

Materials employed for the NiNWs and Ni-CuNWs fabrication were: $CuSO_4 \cdot 5H_2O$ for the sacrificial layer and the copper layer in the Ni-CuNWs, and a mixture of $NiCl_2 \cdot 6H_2O$/$NiSO_4 \cdot 6H_2O$ for the nickel electrodeposition. All solutions were dissolved in H_3BO_3 20 g·L^{-1}. For removing the sacrificial layer a $CuSO_4 \cdot 5H_2O$ in HCl 30% (v/v) was used. Filtration alumina membranes with a plastic ring, 25 mm diameter, 0.2, 0.1 and 0.02 μm of pore diameter and 60 μm thicknesses were purchased from Whatman (England).

CSPE integrating the three electrodes system, (carbon counter and working electrode 4 mm in diameter) and silver reference electrode and miniaturized flow cell were purchased from Dropsens (Oviedo, Spain). Nickel disk electrode 3 mm in diameter was purchased from BASi (Bioanalytical Systems) (West Lafayette, USA)

Carbohydrate and samples were analyzed using a FIA system (with a flow rate of 2 $mL \cdot min^{-1}$ and a loop of 50 μL) and a CSPE modified with NWs integrating the three electrodes. The measurements were carried out in amperometric mode at +0.7 V.

Electrode modification and activation were performed as follows. Firstly, we introduced the CSPE in the flow cell and under it, the magnet that serves to avoid the leaching of NWs and also to align and orientate the nanowires (in order to increase the surface). Two cylindrical magnets (2×4200 G) with a diameter of 22 mm and 10 mm height were used to align the NiNWs. Then, we dropped 35 μL of the buffer solution and then we added 15 μL of the corresponding NWs suspension (10 $mg \cdot mL^{-1}$) over the working electrode in order to achieve the necessary volume to get the three electrodes covered. The nickel and nickel-copper modified electrodes were activated by amperometry (at −1.5 V; 600 s; NaOH 0.1M) before sample analysis. This process allows the formation of nickel oxide species on the nanowire's surface which are responsible for the catalytic oxidation of carbohydrates[18,24]. Then the overabundance of nanowires is retired from the electrode surface by cleaning it with deionized water.

Glucose, fructose, galactose, lactose, sucrose and inulin were purchased from Sigma Chemical Co. (St. Louis, MO). Sueroral (Glucose serum containing 15 g/L glucose) and Neobrufen 600 (containing 3.30 g of sucrose) were acquired in a local pharmacy (Madrid, Spain). Coke (energy

value 42 kcal, total sugar 10.6 g/100 mL; E-150d, E338) and coke light (energy value 0.2 kcal, E-150d, E952, E-950, E-951, E-338) soft drinks were acquired in a local supermarket. For both, sample and standards, 10 mL of 50 mM solutions were prepared for all carbohydrates and then the necessary dilutions were done in order to obtain the desired concentration. All solutions were prepared dissolving the corresponding weight in 10 mL of buffer solution. An aliquot of 160 μL from Sueroral was taken for analyses into a final volume of 25 mL and 360 mg of Neobrufen (±0.1 mg) were dissolved into a final volume of 10 mL. Beverages were suitably sonicated and then coke was diluted (50 μL into 25 mL) prior to analysis while coke light was directly injected for analysis. All stock solutions of standards were dissolved in NaOH 0.1 M.

Honey samples were obtained through IMIDRA (an agroalimentary institute located in Madrid, Spain) and were previously characterized using a HPLC-RI method in which glucose and fructose contents were extracted by SPE with Sep-Pak C18 filters (Waters), and subsequently analyzed by HPLC using a RECEX RCM-Monosaccharide precolumn and column (Phenomenex) at 90 °C, and using a K-2301 refractive index detector. Elution was performed using water (HPLC grade). The appropriate amount of each honey was dissolved into a final volume of 10 mL to produce the stock solutions, and then the necessary dilutions were performed to achieve the desired concentrations. All stock solutions of the standards were dissolved in NaOH 0.1 M eluent at a flow rate of 1.0 mL min^{-1} [35].

Standards and samples were prepared daily.

All chemicals used in buffer preparation and in supporting electrolytes were reagent grade.

All experiments were performed at room temperature.

II.2.7. References

[1] E. Roduner, Size matters: why nanomaterials are different, Chem. Soc. Rev. 35 (2006) 583–592.

[2] J. Wang, Nanomaterial-based electrochemical biosensors, Analyst 130 (2005) 421–426.

[3] V.P. Menon, C.R. Martin, Fabrication and Evaluation of Nanoelectrode Ensembles, Anal. Chem. 67 (1995) 1920–1928.

[4] P. Ugo, L.M. Moretto, F. Vezza, Ionomer-Coated Electrodes and Nanoelectrode Ensembles as Electrochemical Environmental Sensors: Recent Advances and Prospects, Chem. Phys. Chem. 3 (2002) 917–925.

[5] J. Li, X.Q. Lin, Electrocatalytic reduction of nitrite at polypyrrole nanowire–platinum nanocluster modified glassy carbon electrode, Microchem. Journal 87 (2007) 41–46.

[6] L. Liu, J.F. Song, P.F. Yu, B. Cui, A novel electrochemical sensing system for inosine and its application for inosine determination in pharmaceuticals and human serum, Electrochem. Comm. 8 (2006) 1521–1526.

[7] D.B. Luo, J.F. Zhi, Fabrication and electrochemical behaviour of vertically aligned boron-doped diamond nanorod forest electrodes, Electrochem. Comm. 11 (2009) 1093–1096.

[8] F.L. Qu, A.W. Shi, M.H. Yang, G. Shen, R. Yu, Preparation and characterization of Prussian blue nanowire array and bioapplication for glucose biosensing, Anal. Chim. Acta 605 (2007) 28–33.

[9] E. Piccin, R. Laocharoensuk, J. Burdick, E. Carrilho, J. Wang, Adaptive Nanowires for Switchable Microchip Devices, Anal. Chem. 79 (2007) 4720-4723.

[10] C.M. Hangarter, N.V. Myung, Magnetic Alignment of Nanowires, Chem. Mater. 17 (2005) 1320–1324.

[11] M. Tanase, L.A. Bauer, A. Hultgren, D.M. Silevitch, L. Sun, D.H. Reich, P.C. Searson, G.J. Meyer, Magnetic Alignment of Fluorescent Nanowires, Nano Lett. 1 (2001) 155–158.

[12] J. Wang, Adaptive nanowires for on demand control of electrochemical microsystems, Electroanal. 20 (2008) 611-615.

[13] J. Wang, M. Scampicchio, R. Laocharoensuk, F. Valentini, O. González-García, J. Burdick, Magnetic Tuning of the Electrochemical Reactivity through Controlled Surface Orientation of Catalytic Nanowires, J. Am. Chem. Soc. 128 (2006) 4562–4563.

[14] O.A. Loaiza, R. Laocharoensuk, J. Burdick, M. Rodriguez, J. Pingarron, M. Pedrero, J. Wang, Adaptive Orientation of Multifunctional Nanowires for Magnetic Control of Bioelectrocatalytic Processes, Angew Chemie Int. Ed. 46 (2007) 1508–1511.

[15] R. Laocharoensuk, A. Bulbarello, S.B. Hocevar, S. Mannino, B. Ogorevc, J. Wang, On-Demand Protection of Electrochemical Sensors Based on Adaptive Nanowires, J. Am. Chem. Soc. 129 (2007) 7774–7775.

[16] B. Tao, J. Zhang, S. Hui, L. Wan, An amperometric ethanol sensor based on a Pd-Ni/SiNWs electrode, Sensor actuat. B 142 (2009) 298-303.

[17] Tao, B., Zhang, J., Hui, S., Chena, X., Wan, L. "An electrochemical methanol sensor based on a Pd–Ni/SiNWs catalytic electrode" Electrochimica Acta 55 (2010) 5019–5023.

[18] N.D. Hoa, N.V. Quy, H. Jung, D. Kim, H. Kim, S. Hong, Synthesis of porous CuO nanowires and its application to hydrogen detection, Sensor Actuat. B 146 (2010) 266–272.

[19] J.P. Metters, R.O. Kadara, C.E. Banks, New directions in screen printed electroanalytical sensor: an overview of recent developments, Analyst 136 (2011) 1067–1076

[20] K.Z. Brainina, Electroanalysis: from laboratory to field versions. Anal. Chem. 56 (2001) 303–312.

[21] J.P. Hart, S.A. Wring, Recent developments in the design and application of screen-printed electrochemical sensors for biomedical, environmental and industrial analyses, Trends Anal. Chem. 16 (1997) 89–103

[22] M. Vidotti, C.D. Cerri, R.F. Carvalhal, J.C. Dias, R.K. Mendes, S.I. Córdoba de Torresi, L.T. Kubota, Nickel hydroxide electrodes as amperometric detectors for carbohydrates in flow injection analysis and liquid chromatography, J. Electroanal. Chem. 636 (2009) 18–23.

[23] J. Wang, G. Chen, M.P. Chatrathi, Nickel Amperometric Detector Prepared by Electroless Deposition for Microchip Electrophoretic Measurement of Alcohols and Sugars, Electroanal. 16 (2004) 1603–1608.

[24] C. Zhao, C. Shao, M. Li, K. Jiao, Flow-injection analysis of glucose without enzyme based on electrocatalytic oxidation of glucose at a nickel electrode, Talanta 71 (2007) 1769–1773.

[25] C. Martínez Montero, M.C. Rodríguez Dodero, D.A. Guillén Sánchez, C.G. Barroso, Analysis of Low Molecular Weight Carbohydrates in Food and Beverages: A Review, Chromatographia 59 2004 15–30.

[26] M. Herrero, V. García-Cabañas, C. Simo, A. Cifuentes, Recent advances in the application of capillary electromigration methods for food analysis and Foodomics, Electrophoresis 31 (2010) 205–228.

[27] D.J. Harvey, Derivatization of carbohydrates for analysis by chromatography, electrophoresis and mass spectrometry, J. Chromatogr. B 879 (2011) 1196–1225.

[28] J. Wang, Electrochemical detection for capillary electrophoresis microchips: a review, Electroanal. 7 (2005) 1133–1140.

[29] A. Bulbarello, S. Sattayasamitsathit, A.G. Crevillen, J. Burdick, S. Mannino, P. Kanatharana, P. Thavarungkul, A. Escarpa, J. Wang, Striped Alloy Nanowire Optical Reflectance Barcodes Prepared from a Single Plating Solution, Small 4 (2008) 597-600.

[30] I.G. Casella, M. Gatta, T.R.I. Cataldi, Amperometric determination of underivatized amino acids at a nickel-modified gold electrode by anion-exchange chromatography, J. of Chromatography A 878 (2000) 57–67.

[31] T. You, O. Niwa, Z. Chen, K. Hayashi, M. Tomita, S. Hirono, An Amperometric Detector Formed of Highly Dispersed Ni Nanoparticles Embedded in a Graphite-like Carbon Film Electrode for Sugar Determination, Anal. Chem. 75 (2003) 5191–5196.

[32] M. Ávila, A.G. Crevillén, M.C. González, A. Escarpa, L.V. Hortigüela, C.L. Carretero, R.A. Pérez-Martín, Electroanalytical approach to evaluate antioxidant capacity in honeys: proposal of antioxidant index. Electroanal. 18 (2006)1821–1826

[33] M. García, A. Escarpa, Disposable electrochemical detectors based on nickel nanowires for carbohydrate sensing, Biosens. Bioelectron. 26 (2011) 2527–2533.

[34] C.D. Wagner, L.E. Davis, M.V. Zeller, J.A. Taylor, R.H. Raymond, L.H. Gale, Empirical atomic sensitivity factors for quantitative analysis by electron spectroscopy for chemical analysis, Surf. Int. Anal. 3 (1981) 211-225.

[35] R.A. Pérez, M.T. Iglesias, E. Puedo, M. González, C. De Lorenzo, Amino Acid composition and antioxidant capacity of Spanish honeys. J. Agric. Food Chem. 55 (2007) 360–365

II.2.8. Supporting information

Table II.S1. Optimization of NiNWs electrochemical activation[1]

Time (s)	Glucose		Sucrose	
	i ± S (μA)	RSD (%)	i ± S (μA)	RSD (%)
300	12.7 ± 0.3	2.1	4.6 ± 0.1	3.3
600	19.6 ± 1.3	6.6	9.9 ± 0.2	1.6
900	19.6 ± 1.1	5.7	10.8 ± 0.5	5.1

[1] Values are average of five determinations. Glucose and sucrose are 0.5mM.

Table II.S2. Influence of alignment of NiNWs[1]

Alignment	Glucose		Sucrose	
	i ± S (μA)	RSD (%)	i ± S (μA)	RSD (%)
Vertical	19.9 ± 0.7	3.4	8.2 ± 0.1	1.6
Horizontal	16.9 ± 1.1	6.3	6.7 ± 0.1	1.6
No oriented	3.5 ± 0.1	1.9	1.4 ± 0.1	2.0

[1] Values are average of five determinations. Glucose and sucrose are 0.5mM.

Table II.S3. Optimization of volume of NiNWs[1]

Volume (μL)	Glucose		Sucrose	
	i (μA)	RSD (%)	i (μA)	RSD (%)
5	13.7 ± 0.6	4.2	5.7 ± 0.1	1.7
10	16.4 ± 0.2	1.5	7.7 ± 0.1	1.9
15	29.4 ± 0.3	1.0	15.3 ± 0.3	1.7
20	29.7 ± 0.6	2.1	14.9 ± 0.1	0.3

[1] Values are average of five determinations. Glucose and sucrose are 0.5mM.

Table II.S4 Binding energies (eV) and surface atomic ratios

Sample	C1s	$Ni2p_{3/2}$	$Cu2p_{3/2}$	Ni/C at
1	284.8	855.2	934.1	0.0079
2	284.8	855.3	934.0	0.0084
3	284.8	855.4	934.2	0.0135
4	284.8	855.3	934.0	0.0078
5	284.8	855.3	934.1	0.0026

Table II.S5. Electrochemical sensing of different carbohydrate structures on NiNWs.

Carbohydrate[1]	i ± s[2] (μA)	RSD (%)	f [3](μA/mM)
Glucose	18.8 ± 0.5	2.9	37.6
Galactose	18.1 ± 0.2	1.3	36.2
Fructose	18.2 ± 0.2	1.2	36.4
Sucrose	8.9 ± 0.2	1.9	17.8
Lactose	10.3 ± 0.1	0.8	20.6
Inulin	24.4 ± 0.4	1.6	48.8

[1] 0.5mM, [2] Mean values ± standard deviation, n=3. [3] Calibration factor

Table II.S6. Precision in sample screening analysis[1]

Cycle	Standard/Sample	i ± s (μA)	RSD (%)
1	Glucose	18.8 ± 0.2	1.0
	Caffeine	ND	ND
	Coke[1]	27.1 ± 0.1	0.2
	Light-Coke[2]	13.7 ± 1.5	11.1
2	Glucose	14.8 ± 0.5	3.3
	Caffeine	ND	ND
	Coke[1]	22.7 ± 0.3	1.1
	Light-Coke[2]	12.7 ± 2.2	17.3
3	Glucose	12.3 ± 0.6	4.5
	Caffeine	ND	ND
	Coke[1]	23.2 ± 2.0	8.6
	Light-Coke[2]	13.9 ± 1.3	9.1

[1] Glucose 0.5mM; Coke as sugar drink with a 1/500 dilution, [2] Light coke as free sugar drink without any dilution

II.3 Microfluidic chips with electrochemical detection based on nickel and copper nanowires for carbohydrate sensing

II.3.1. Introduction and objectives

As we have stated in **section II.1.6,** microfluidic technology seeks to improve analytical performance by reducing the analysis time, decreasing the consumption of sample and reagents, diminishing the risk of contamination and increasing reliability, functionality and sensitivity through automation, integrating multiplexing analysis, and especially portability to provide the possibility of point-of-care applications[1-3].

One of the most important "products" of microfluidic-LOC technology is the termed microfluidic chips (MC). Since electrokinetics is a very common principle for fluidic pumping and manipulation, these MCs are very often used as microchips electrophoresis (ME). Strictly speaking, microfluidic chip format (MC or ME) is an analytical microsystem constituted at least by an injector (where a sample plug is critically loaded) and separation microchannels (where separation of analytes is performed) interfaced suitably to reservoirs (where different solutions/samples are deposited). Microchannels and reservoirs are fabricated in microchips using photolithography or micromolding to form channels for sample injection, separation, and analyte detection. Once all solutions, including those of the samples, are loaded, the samples are typically transferred electrokinetically into an injector region. Then their components are separated by application of a high voltage, and afterwards detected with a suitable detection system. Microchip approach eliminates the necessity of most fluidic connections that otherwise link microfluidic components. Avoiding such connections greatly reduces sample dispersion, delay times, and dead volumes between the different microchip compartments, therefore, significantly increasing the separation power of such integrated miniaturized systems.

The typical layout of a MC or ME (both a simple cross T-injector (**A**), and a twin-T injector (**B**)) is depicted in **Figure II.16.** It has a network of channels with widths varying from 10 to 100 μm with typical straight separation channels between 3 and 10 cm. In a typical set-up, buffer solutions are introduced on sample (S), running buffer (RB) and waste (W) reservoirs. The reservoir volume is often defined by their capacities (100-250μL). Electric fields are applied to the reservoirs by high voltage power supplies (1-5kV), and platinum electrodes are placed in the reservoirs for injection and separation because samples are normally electrokinetically driven into the network channels.

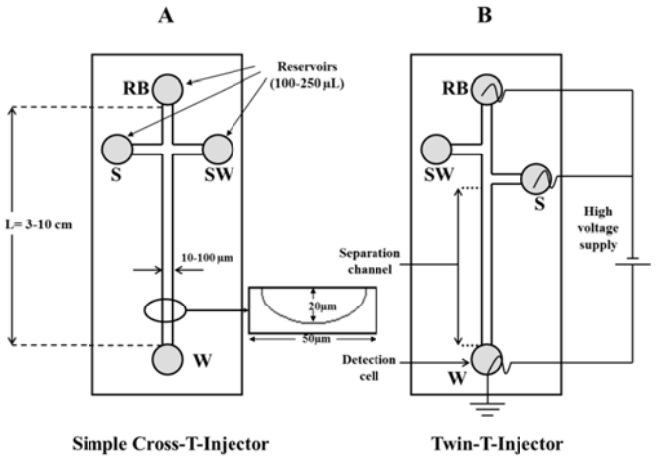

Figure II.16. Typical layouts of MC: **(A)** Simple cross T-injector and **(B)** Twin- T injector.

MCs (or ME) are mainly fabricated using glass and polymer substrates. Glass substrates are the most common because of their good optical properties (optically transparent, which allows optical detection and visual inspection), resistant to many chemicals, well-understood surface characteristics (exhibit an EOF close to fused silica ≈$9.5x10^{-4}$ cm^2/Vs at pH>9), dielectric properties (possibility of working with the high voltages

used in capillary electrophoresis) and well-developed microfabrication methods (adapted from silicon microfabrication industry). Other advantages of glass are its hardness, high thermal stability and biocompatibility (wide range of applications: DNA separations, enzyme/immunoassays, cell biology and small molecules).

Polymeric substrates have mainly comprised poly(methylmethacrylate) (PMMA) (fabricated by injection moulding or hot embossing) and poly(dimethylsiloxane) (PDMS) (fabricated by casting). These materials have found favour due to the ease of fabrication. PDMS has widely been discussed due to several characteristics: (i) optical transparency; it is suitable for optical detection down to 320 nm; (ii) it cures at low temperatures and moulding can easily be replicated through the process of prototyping, master formation, and soft lithography; (iii) it can seal reversible to itself and other materials by van der Waals contact with the clear smooth surface at room temperature; (iv) its surface chemistry can be controlled to form EOF using a plasma technique.

Basically, two fluidic manipulations have to be used in MC: injection of a defined plug of sample and their analyte separation. Without question, a very important fluidic handling function is the ability to dispense very well defined and small volumes of solutions (in order to keep selectivity constant) with reproducibility. Especially, the injection of a well-defined, reproducible injection plug into the separation channel is of paramount importance to find the right trade-off between separation efficiency and detection sensitivity. Also, the reduced injection volumes used in microchip format (pL) help maintain resolution. These small volumes are very important in many analytical applications. The easiest injection procedure is the no pinched approach which is shown in **Figure II.17** (in general, it is

the common strategy used). This principle can be carried out using just a single power supply. A high voltage is applied to the sample reservoir for a short time with the electrochemical reservoir held at ground (*injection*). Sample is introduced directly into the separation channel by electrokinetic injection. After the injection is completed, the high voltage is switched back to the buffer reservoir and the separation is initiated (*run/separation*). This approach does not use pushback voltages to keep sample into the main separation channel and can result in irreproducible injections and large plugs.

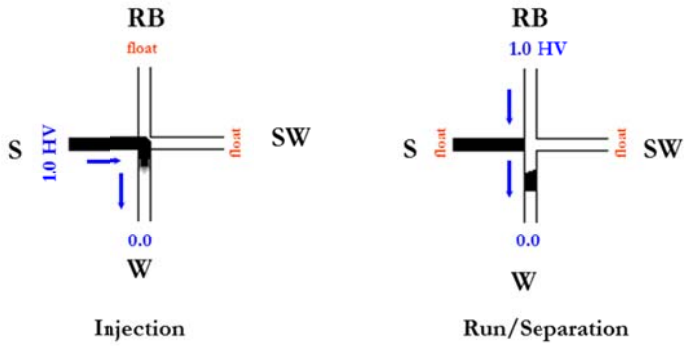

Figure II.17. Electrokinetic injection protocol

On the other hand, as it was discussed in section II.1.6., ED has been proven as an ideal and valuable technique to be incorporated in miniaturized devices, due to its inherent ease for miniaturization without loss of performance and high sensitivity and compatibility with the micro- and nano-technologies[4,5]. When used in the electrochemical detectors of MCs, nanomaterials can significantly improve a chip's analytical performance[4,6,7]. The scale of a typical nanomaterial is compatible with the scale of MC, and nanomaterials can offer high currents because of their large surface areas, thereby enabling large-scale redox conversion, which

increases the analytical sensitivity, resists passivation, and yields very good performance reproducibility.

Additionally, the detector design should ensure well-defined mass transport, minimal band broadening and electrical isolation (decoupling) from the high separation voltage (typically 1-5 kV). The latter is attributed to the fact that the current associated with the high separation voltage is usually several orders of magnitude larger than that measured at the electrochemical detector. High sensitivity, selectivity (via the applied potential and electrode material), simple handling, long-term stability, and rigidity are additional requirements.

In a conceptual way, the main approaches proposed have been taking into account the relative position between both working electrode-separation channel where the configurations can be classified as: *end-channel*, *in-channel* and *off-channel* detection **(Figure II.18)**. In *end-channel* detection (both externally mounted and internally mounted), the electrode is placed just outside of the separation channel. For *in-channel* detection, the electrode is placed directly in the separation channel, and *off-channel* detection involves grounding the separation voltage before it reaches the detector by means of a decoupler.

End-channel detection involves the alignment of the electrode at the end of the channel (tens of micrometers) and it means that the electrode is outside the channel. Separation voltage has a minimal influence on the potential applied in an electrochemical detector because most of the voltage is dropped across of the channel[8,9]. The main advantage of this design is that no decoupler is necessary, and that the whole system is simpler and more rugged because the channel is all in one piece. However, the main disadvantage is a loss of separation efficiency, due to the relatively short

length of the channel and the large distance between the end of the channel and the working electrode. This separation distance is also crucial for the noise signal obtained and it can lead to a complete loss of the analytical current. This approach has been used in this Thesis.

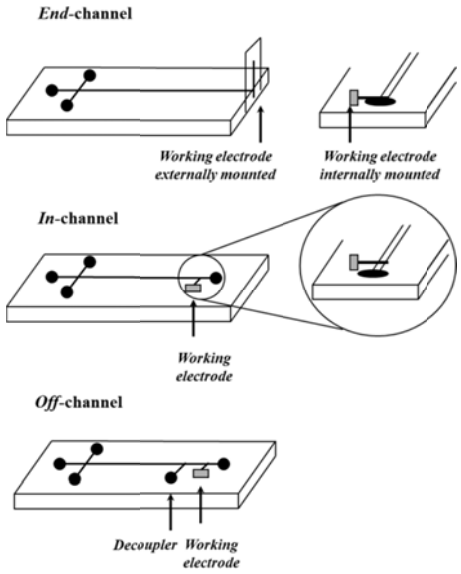

Figure II.18. Electrochemical **d**etection configurations in microfluidic chip systems[10].

Finally, as it was outlined in the chapter section II.1.7, while the use of MNWs as modifiers for amperometric sensors for carbohydrates detection has already been reported[11-16], however, the coupling between MC and NWs has been addressed in lesser extension[16]. Therefore, the aim of following works is the design of electrochemical detectors based on nickel and copper nanowires coupled to microfluidic-LOC systems for carbohydrate sensing.

II.3.2. Electro synthesis and characterization of nickel and copper nanowires based-electrodes

In addition to NiNWs, elemental copper nanowires (CuNWs) have also been explored coupled to microfluidic-LOC systems. CuNWs were also synthesized by an electrodeposition method using a porous template. For these CuNWs, the protocol is essentially the same, after the sacrificial copper layer deposited to fill the imperfections, an intermediate platinum layer was then deposited (-0.5 V, 3 C) to separate the sacrificial copper layer from the copper nanowires layer and also protect this last layer during the sacrificial layer removal. Finally, the copper layer itself was deposited (-1V, 30C).

The electrosynthesized CuNWs were also morphologically and compositionally characterized using SEM and EDS techniques. A homogeneous dispersion of the as-fabricated well defined individual electrosynthesized CuNWs, with an average length of 6 μm and a width of 300 nm was obtained in both cases. EDS analyses were performed in order to confirm the homogeneity of the whole nanowires. As expected, Pt (used in the separation layer) was detected during the EDS analysis. However, the EDS analysis indicated almost 100% of copper along the distributed material, confirming the convenience of the CuNWs electrochemical fabrication technique. For NiNWs, as it was discussed in section II.2.2., EDS revealed a composition very close to 100% of Ni indicating the complete removal of the sacrificial layer.

Then, the carbon screen-printed electrodes (CSPE) (10x1 mm, see Figure II.19A) were cast on the electrode surface by placing a 2 μL drop of the corresponding NWs suspension (10 mg/mL of nickel or copper). **Figure II.19** illustrates the analytical characterization of the CSPE-NWs based electrodes. **Figure II.19A** shows the field emission scanning electron

microscopy (FESEM) images of CSPEs modified with NWs. A random distribution of NiNWs **(a)** and CuNWs **(b)** over a CSPE at the background with well-defined morphology was displayed. From the inspection of the FESEM images CuNWs seem to be more uniform and rougher than nickel ones. In addition, electrochemical surface area for CSPE-NWs based electrodes was estimated by chronocoulometry as it shown in **Figure II.19B**. The CSPE presents a specific area about 6 mm^2. A surface three times higher than the original for NiNWs modified electrode (20.3 mm^2) and twice larger for CuNWs modified electrode (12.6 mm^2), was estimated.

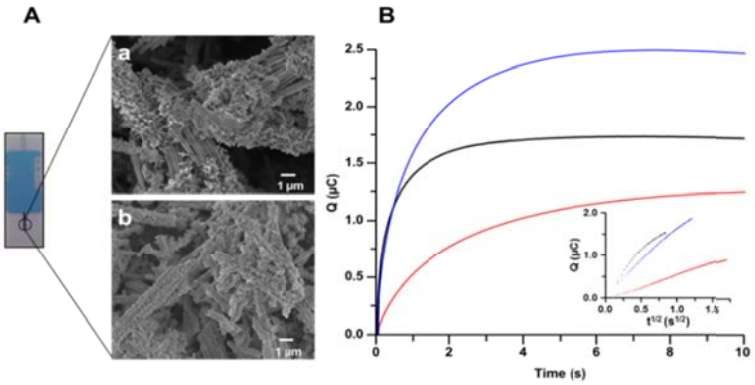

Figure II.19. Analytical characterization of screen-printed nanowire-based detectors. **(A)** CSPE and FESEM images of NiNWs **(a)** and CuNWs **(b)** (magnification 3000x). **(B)** Chronocoulometric charge-time plots for the reduction of 0.45 mM $K_3[Fe(CN)_6]$ in 0.1 M PBS (pH=7.4). NiNWs modified electrode (Blue line), CuNWs modified electrode (Black line) and bare electrode (red line). Inset in **(B)**: Chronocoulometric plots of the charge versus $t^{1/2}$.

II.3.3. Microfluidic electrochemical sensor for inulin detection

Inulin is a fructo-oligosaccharide containing up to 35 fructose units linked via β-1,2-glycosidic bonds with a high significance in the agro-food and clinical fields becoming an important carbohydrate with several benefits in human health. Inulin is a storage carbohydrate present in plant roots and tubers, being a source of fructose as well as dietary fiber constituting part of several functional foods to promote the appearance of beneficial flora microorganisms. It is important to mention that inulin has also a minimum increase of blood sugar being suitable as a sweetener for diabetics; this is because inulin is indigestible for humans and remains almost intact until reach the intestinal flora[17]. In addition, clinically, inulin has unique properties that allow its use for the determination of the glomerular filtration rate, to check the appropriate functioning of kidneys[18- 20].

Regarding analytical determination of inulin, several approaches involving both biosensor and separation approaches have been reported in selected literature. Firstly, since selective inulin detection without interference of free-fructose is required; commonly its determination has been performed using enzymes for its hydrolysis. Inulin is hydrolysed to its fructose former units and then the total monosaccharide content is determined in parallel. The amount of inulin is determined by calculating the difference between total fructose (obtained after hydrolysis) and free fructose (present in the raw sample). Then, the assessment of both fractions is commonly performed using HPLC coupled to different detectors like refractive index (RI)[21-23], UV[18, 20, 24, 25]], fluorimetric[19]. Secondly, electrochemical biosensors have also been employed for inulin and fructose determination using an interesting bienzymatic biosensor integrating both enzymes. Manso et al. developed an interesting biosensor combining two enzymes, inulinase and fructose dehydrogenase, to achieve the degradation

of inulin into its former units and subsequently carry out the determination of the hydrolysed fructose[26]. However, in this approach, the amount of inulin is also determined by calculating the difference of fructose present in the sample before (free fructose) and after the hydrolysis (total fructose). Thirdly, a different approach that overcomes the necessity of enzymes involves the use of a specific carbohydrates HPLC column coupled to refractive index detection[23].

As an alternative to these approaches, in this work we have developed an enzymeless electrochemical microfluidic sensor for inulin detection.

II.3.3.1. Analytical performance of the microfluidic sensor

As it was stated in the introduction, the determination of inulin in presence of free fructose become a very interesting alternative to the reported approaches since it will allows the individual and selective assessment of each fraction. Conceptually speaking, we hypothesize that the inherent selectivity and sensitivity of MC-MNWs, towards inulin and fructose detection become an interesting enzymeless approach that could allow the fast and simultaneous detection of inulin in presence of fructose avoiding the use of enzymes. To this end, the separation of inulin and fructose was explored on the MC-NWs adopting an *end-channel* configuration.

Figure II.20 shows the inulin structure **(A)** and the microfluidic electrochemical sensing of the inulin and fructose using Ni and CuNWs modified electrodes and a bare CSPE as control **(B).** A separation of inulin and fructose was achieved in less than 300s with a good resolution ($R_{Inu-Fruc}$=1.3) under optimized chemical (20 mM NaOH + 10 mM H_3BO_3, pH 12), electrokinetic (injection voltage +1500 V for 5 s; separation voltage +1000 V), and detection (+0.70 V in 20 mM NaOH + 10 mM H_3BO_3, pH 12) conditions. Detection of inulin and fructose displayed well-defined peaks at 164.3 ± 3.5 s and 215.2 ± 4.4 s, respectively; with an excellent precision in migration times (RSDs≤3%; n=3) and in peak heights (RSDs≤8%; n=3). In addition, no signal was obtained when the bare electrode was used confirming the selective electro catalysis of these materials towards the target analytes detection.

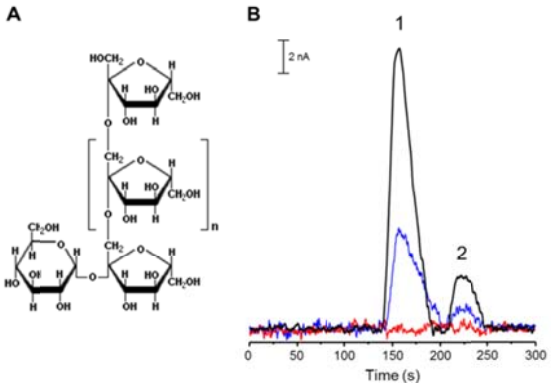

Figure II.20. (A) Chemical structure of inulin **(B)** Microfluidic sensing of inulin and fructose using NWs. From top to down: CuNWs, NiNWs and bare electrode. Peaks: **(1)** Inulin, 25 μM **(2)** Fructose, 200 μM. Separation conditions: 20 mM NaOH + 10 mM H_3BO_3, pH 12; separation voltage of +1000 V. Injection conditions: 5 s, +1500 V. Detection conditions: 20 mM NaOH + 10 mM H_3BO_3, pH 12 and detection potential +0.70 V.

Interestingly, clear differences were noticed, where the highest inulin sensitivity (0.40 nA/μM) with a good signal-to-noise characteristics (S/N up to 25) was obtained using CuNWs in comparison with it found for NiNWs (0.15 nA/μM, S/N up to 10). A very good *intra*-electrode repeatability with RSDs<8% (n=5) and *inter*-electrode reproducibility with RSDs<9% (n=4) were also obtained; indicating an excellent stability of the electrochemical detector. Because of the superior analytical performance of CuNWs, they were employed in the subsequent works.

Regarding the optimization process, both the separation and electrochemical detection of carbohydrates required a strong alkaline media. A 20 mM NaOH + 10 mM H_3BO_3, at pH=12 permitted the sensitive detection of well-defined analyte peaks with a good resolution ($R_{Inu\text{-}Fruc}$=1.3) and an optimum separation time of 300 s. Different buffers with different ionic strengths but always keeping the necessary high strong basic pH (20 mM NaOH; 20 mM NaOH +1 mM H_3BO_3) were also tested to achieve the analytes separation with a sensitive detection but peaks became not well

defined. The strong basic pK_as for both analytes (inulin 11.8/12.3 and fructose 10.3) explain the necessity of an alkaline media to achieve the separation accordingly to their charge-mass ratio. Elution order was due at the working pH (pH=12) inulin is almost neutral or partially one negative charged and fructose present one negative charge being in addition much smaller in molecular weight.

The separation voltage affects both the analyte resolution and the current signals. As expected, increasing the voltage from +1000 V to +2000 V (in 500 V steps), decreased the migration times for analytes (from 165 s to 145 s and from 215 s to 180 s, for inulin and fructose respectively) as well as peak-to-peak resolution (from $R_{Inulin\text{-}Fructose}$=1.3 to $R_{Inulin\text{-}Fructose}$=0.6). A separation voltage of +1000 V was the most favourable due to a short analysis time and the optimum Rs conditions.

Under previous optimize chemical (20 mM NaOH + 10 mM H_3BO_3, pH 12) and electrokinetic (injection voltage +1500 V for 5 s; separation voltage +1000 V) conditions, hydrodynamic voltammograms (HDVs) were also constructed as it is shown in **Figure II.21.** The electrooxidation of carbohydrates at copper electrodes in alkaline media involves the reaction of the carbohydrate with the copper oxides present at the surface with a two electron exchange in which the copper oxide is reduced and as a result the carbohydrate is chemically oxidized, the subsequent re-oxidation of the oxides provides the analytical signal. Both compounds displayed no response below +0.40 V. The response rises gradually between +0.40 V and +0.80 V, after which it levels off. A very well defined sigmoidal curve was obtained with an $E_{1/2}$= +0.65 V for both inulin and fructose. A detection potential of +0.70 V offered the best signal-to-noise characteristics, S/N= 48 versus an S/N= 14 obtained at

+0.80 V. These findings informed about the success of the end-channel electrochemical detector coupling.

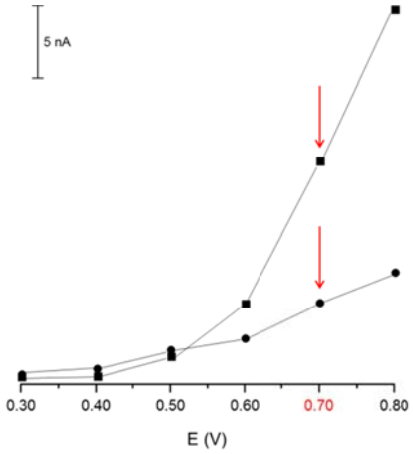

Figure II.21. Hydrodynamic voltammograms (—■—Inulin,—●—Fructose). Other conditions are as listed in **Figure II.20.**

II.3.3.2. Quantitative analysis of inulin in selected samples

Quantitatively, CuNWs displayed well defined concentration dependence as it is illustrated in **Figure II.22**. Indeed, well defined peaks proportional to the analyte concentration were observed for both analytes. The resulting calibration plots were highly linear ($r \geq 0.990$) in the concentration ranges assayed (see inset **Figure II.22**). Interestingly, despite their complex structure, inulin performance was excellent showing impress sensitivity in comparison with its monomer fructose (almost 40 times higher). Combining the high sensitivity of the CuNWs with its low noise level (1 nA) resulted in an excellent LOD for inulin of 3μM (S/N=3). Also, excellent precision was obtained with independence of the concentration assayed (RSD<3% and RSD<8%, for migration times and oxidation currents, respectively). **Figure II.22** (inset) also shows inulin detection in a selected real sample where a good signal-to-noise characteristics was also obtained (S/N =13) even during the analysis of a real matrix. Interestingly, no signal was obtained when the bare electrode was used confirming the selective electro catalysis of these materials towards the target analytes detection during the analysis of real samples.

Table II.9 summarizes the quantitative results obtained during the analysis of selected samples. Firstly, **Table II.9** lists the high agreement between the migration times obtained in the analysis of samples in comparison with those found for standards with an excellent precision RSDs < 3% for the migration times. The quantitative levels obtained for inulin in the samples, were in high agreement with those declared by the manufacturer. Indeed, excellent quantitative and reproducible recoveries (97-113%; RSDs<4%) were achieved during the samples analysis indicating a very good reliability of the approach.

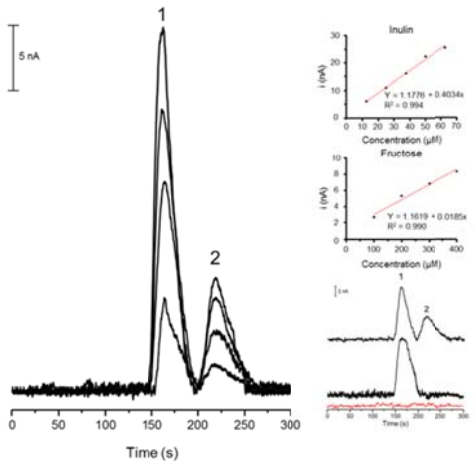

Figure II.22. Inulin and fructose calibration using MC-CuNWs. Inset: Sample analysis**.** Peaks: **(1)** Inulin, **(2)** Fructose. Red line corresponds to the analysis using a bare electrode. Other conditions are as listed in **Figure II.20.**

Table II.9. Quantitative analysis of inulin in selected samples[1]

Analytical feature		**Inulin**	**Fructose**
Standard	**tm±S (s)[1]**	164.3 ± 3.5	215.2 ± 4.4
	RSD (%)	2.3	2.1
Sample 1	**tm±S (s)[2]**	164.5 ± 1.9	N.D.
	RSD (%)	1.2	N.D.
	Recovery (%)	97 ± 1	N.D.
Sample 2	**tm±S (s)**	178.9 ± 4.7	N.D.
	RSD (%)	2.6	N.D.
	Recovery (%)	113 ± 4	N.D.

[1] Values are expressed as Mean values ± standard deviation (n=3)

Finally and in comparison with previous literature, classified selected works for inulin determination are listed in **Table II.10** accordingly to biosensor and HPLC approaches**.** Most of them involve the use of enzymes for inulin hydrolysis previous HPLC determination and in consequence

longer analysis times and/or more complex instrumentation than used in the current work are needed. Indeed, the approach presented here is a faster and simpler alternative to enzyme based assays. Also, our approach exhibited competitive LODs for inulin in comparison to those found in the literature involving the use of enzymes but allowing the direct inulin determination without the necessity of the common employment of enzymes for inulin hydrolysis or the necessity of specific carbohydrates HPLC columns reducing the complexity of the whole process and as a result the total analysis time and costs. In addition, the LOD obtained for inulin was also suitable for its application to analyze complex clinical samples where the levels of inulin are typically in the range 5-30 μM.

Table II.10. Selected works for inulin determination

Approach	Method	Sample	Analysis time (min)	LOD (μM)	Remarks		Ref
					Strengths	Weakness	
Biosensor	Enzymatic-UV	Vegetables and Dietary supplements	30	-	Simple method, easily implemented on an automatic centrifugal analyser	Inulin is calculated by difference between total and free fructose	37
	Enzymatic-UV	Cereal products Processed food	23	1 %	Use simpler instrumentation	Inulin is calculated by difference between total and free fructose	38
	Enzymatic-UV	Serum and Urine	15	1.0	Clinical samples	Sample pretreatment	33
	Enzymatic-Fluorimetric	Plasma	--	0.74	Excellent LOD in clinical samples	Inulin is calculated by difference between total and free fructose. Need derivatization for fructose determination	32
	Enzymatic-Amperometric	Chicory powder Prebiotic food	2	0.66	Bienzyme architecture	Inulin is calculated by difference between total and free fructose	39
Separation	HPLC- Diode array	Blood and Urine	7	0.2	Simple instrumentation	Acid inulin hydrolysis	31
	HPLC-Refractive index	Meat	15	0.82 μg	Good recovery in samples	Sample incubation Multiple fructose determination	34
	HPLC-Refractive index	Cereals Dairy products	--	10	No hydrolysis	Specific HPLC column	36
	HPLC-Refractive index	Sweetening products	10	-	High applicability for routine analysis	Sample pretreatment Inulin is calculated by difference between total and free fructose.	35
Microfluidic	Amperometric	Dietary supplements	5	3	Selective and fast enzymeless approach	No automation	This work

II.3.3.3. Conclusions

The strategically driven inherent selectivity of MC-CuNWs has allowed a novel and creative enzymeless approach for microfluidic sensing of inulin, a complex polysaccharide involved in food and clinical fields. This approach becomes an interesting alternative to the employment of enzymes or the necessity of sophisticated HPLC approaches with the additional inherent advantages derived from microfluidic technology such as rapid analysis times and extremely low sample and reagents consumption. Inulin determination in a selected samples was also carried out with good reproducible recoveries (97-113%, RSDs<4%) indicating an excellent method´s reliability. Interestingly inulin detection exhibited impress sensitivity and excellent LOD become very valuable and it opened novel avenues for its detection in urine samples as well. Additionally, to our best knowledge, this is the first report involving MC-NWs coupling and one of the fewest ones using direct electrochemistry for inulin detection. Therefore, it is possible that the work presented here could open novel avenues for complex carbohydrates detection such as glycan or glycoproteins.

II.3.4. Microfluidic chips using copper nanowires for fast and reliable determination of monosaccharides in honey samples

Despite of the inherent difficulties in the analysis of real samples, ME technology in general and ME-ED in particular, has demonstrated to be a powerful tool in food analysis which has been critically revised from the early times when the first works were appeared[27-29]. Although microchip technology is emerging from important food analysis fields such as analysis of antioxidants, detection of frauds, toxics and allergens; the coupling between ME and nano-technologies has not reached the expected impact in the field. In addition, while the coupling of ME with CNTs has been explored[30,31], no reports with MNWs have been described in the agro-food sector.

Previously, in **section II.2.4**, carbohydrates detection using CSPEs modified with nickel and nickel/copper NWs was a very useful tool for quantitative determination of total carbohydrate content in honey samples using a miniaturized flow injection analysis system[13]. However, although the analytical performance was impressive, only total sugar indexes were assessed.

As a consequence and as a natural step ahead; in this work, the CuNWs were combined to a ME to find the selectivity provided through the ME separation to achieve the accurate measurement of individual carbohydrates in the samples. The analytical reliability of ME-CuNWs for the fast and reliable assessment of carbohydrates in honey samples was demonstrated by comparison with the results obtained using HPLC-RI as reference method.

II.3.4.1. Separation and detection of glucose and fructose

Figure II.23 illustrates the ME layout, a CSPE-CuNWs and an image of the detection reservoir **(A)** and the microchip electropherograms of glucose and fructose in both standards as well as in the nine analysed honeys (H-1-H-9) **(B)** under optimized separation (20 mM NaOH + 10 mM H_3BO_3, pH=12; separation voltage +1000 V) and detection (E= +0.70 V in 20 mM NaOH + 10 mM H_3BO_3, pH=12) conditions. Detection of glucose and fructose was carried out in less than 250s displaying well-defined peaks at 159.3 ± 3.2 s and 210.7 ± 3.7 s, respectively. An excellent precision in migration times and oxidation currents with RSDs values under 2% and 6% (n=3); respectively, was also recorded. Good S/N characteristics were obtained during the analysis of standards (noise level < 0.6 nA and S/N ratios ranging between 8 and 32). In addition, no signal was obtained when the bare electrode was used confirming the selective electro catalysis of these materials towards the target analytes detection (see control in **Figure II.23B**).

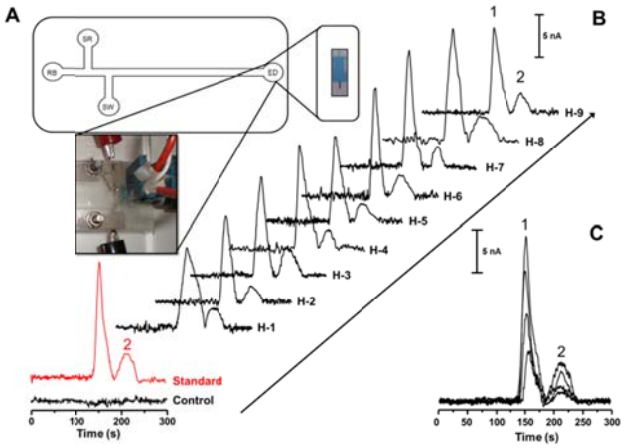

Figure II.23. (A) Microchip and CSPE layouts and image of the detection reservoir. RB: running buffer reservoir, SR: sample reservoir, SW: sample waste reservoir, ED: electrochemical detection cell. **(B)** Microchip electropherograms on CSPE-CuNWs for glucose and fructose detection in honey samples. Standards analysis is shown in red. No signal is observed when a bare electrode is used (bottom electrophoregram). **(C)** External glucose and fructose calibration plots

Peaks: **(1)** Glucose, **(2)** Fructose. Separation conditions: 20 mM NaOH + 10 mM H_3BO_3, pH 12; separation voltage of +1000 V. Injection conditions: 5 s, +1500 V. Detection conditions: 20 mM NaOH + 10 mM H_3BO_3, pH 12 and detection potential +0.70 V.

A 20 mM NaOH + 10 mM H_3BO_3, medium at pH=12 was also carefully adjusted to obtain sensitive analyte detection with the best resolution (Rs=1.5) in the shortest time (250 s). The pKas for both analytes (glucose 11.3 and fructose 10.3) explain the necessity of an alkaline media to achieve the separation accordingly to their charge-mass ratio. Elution order was due to the negative charge of both analytes at working pH=12 and the extra interactions due to the complexation of the carbohydrates with the borate buffer. In these interactions, hydroxyl groups in a planar position of the carbohydrates form complexes with borate ions increasing its size in a considerable manner and therefore modifying its electrophoretic mobility, as it happens in glucose but not in fructose[32-34]. Electrochemical detection

has often been considered incompatible with the combination of the high voltages applied in the electrophoretic separations and sensitive electrochemical detectors have been seen as a conflict. However, it has been found that with appropriate designs of the detector cell the separation voltage does not interfere with the electrochemical measurement. The suitability of the *end-channel* coupling between a ME and a CSPE-CuNWs was demonstrated towards the influence of the separation voltage on the detected response. The separation voltage affected both the analyte resolution and the current signals. As expected, increasing the voltage from +750 V to +1500 V decreased the migration times for analytes (from 185 s to 80 s and from 270 s to 110 s, for glucose and fructose respectively) as well as peak-to-peak resolution from 1.5 to 0.4, being +1000 V the most suitable separation potential, due to a resolution good enough in peaks separation in a shorter time.

Under previous optimized chemical (20 mM NaOH + 10 mM H_3BO_3, pH 12) and electrokinetic (injection voltage +1500 V for 5 s; separation voltage +1000 V) conditions, hydrodynamic voltammograms (HDVs) were also constructed as it is shown in **Figure II.24**. The electro-oxidation of carbohydrates at copper electrodes in alkaline media involves the reaction of the carbohydrate with the copper oxides present at the surface with a two electron exchange in which the copper oxide is reduced. As a result the carbohydrate is chemically oxidized; the subsequent re-oxidation of the oxides provides the analytical signal. Both compounds displayed no response below +0.20 V. The response rises gradually between +0.30 V and +0.70 V, after which it levels off. A well-defined sigmoidal curve was obtained with an $E_{1/2}$= +0.65 V for both glucose and fructose. The detection potential (+0.70 V) was selected because of the best S/N

characteristics (S/N= 32). These findings informed about the success of the end-channel electrochemical detector coupling.

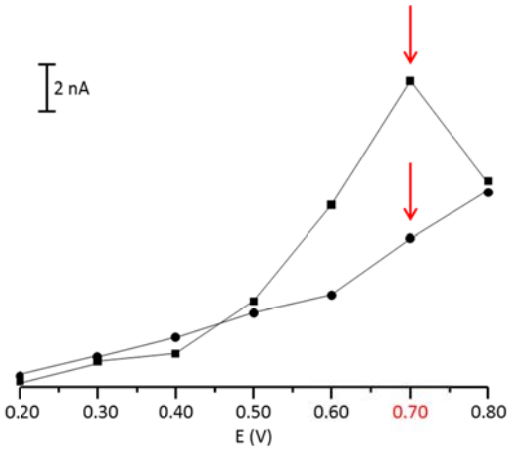

Figure II.24. Hydrodynamic voltammograms (–■–Glucose,–●–Fructose). Other conditions are as listed in **Figure II.23.**

II.3.4.2. Quantitative analysis of glucose and fructose

Quantitatively, CSPE-CuNWs displayed well-defined concentration dependence as it is illustrated in **Figure II.23C. Table II.11** lists the analytical characteristics of the resulting calibration graphs. The resulting calibration plots were highly linear ($r \geq 0.990$) in the concentration ranges assayed. Interestingly, glucose exhibited a sensitivity 15 times higher than fructose despite both are monosaccharides. Combining the high sensitivity of the CuNWs with its low noise level resulted in suitable LODs about micro molar levels (S/N=3). Also, excellent precision was obtained with independence of the concentration assayed (RSD<2% and RSD<6%, for migration times and oxidation currents, respectively).

Table II.11. Analytical characteristics of the method

Analyte	Linear range (μM)	R^2	Intercept a ± t Sa (nA)	Slope b ± t Sb ($nA \cdot \mu M^{-1}$)	LOD (μM)
Glucose	50 - 200	0.995	1.97 ± 1.61	0.086 ± 0.012	4
Fructose	100 - 400	0.998	-0.01 ± 0.26	0.012 ± 0.001	23

Figure II.23B also shows overlapped the microchip electropherograms for all the honey samples analysed (H1-H9). A good signal to noise characteristics were also obtained even during the analysis of a complex matrix (noise level < 1 nA and S/N ratios ranging between 18 and 33). During the analysis of honey samples, interestingly, no signal was obtained when the bare electrode was used confirming the selective electro catalysis of these materials towards the target analytes detection obtaining identical control profiles than those found when standards were used (see control on **Figure II.23B**).

Table II.12 shows the precision obtained in the quantitative analysis of honey samples. Firstly, an excellent precision was obtained for the migration times (RSD<2% for both glucose and fructose) indicating a high electro osmotic flow (EOF) stability. Secondly, without exception, the migration times for glucose and fructose were in agreement with those obtained for the standards. Thirdly, low RSD values in the oxidation currents (RSD<7% for glucose and RSD<9% for fructose) were also obtained demonstrating the suitability of the approach for the sample analysis despite the complexity of the studied samples.

Table II.13 lists quantitatively in detail the individual glucose and fructose contents as well as the total monosaccharide obtained using both ME-CuNWs and HPLC-RI approaches. From a detailed inspection of these results, it is clearly seen that ME-CuNWs provided very accurate results when comparing them to those obtained by the method used as reference. The errors obtained during the determination were under 11% in the case of glucose and under 8% in the case of fructose. Regarding to the total carbohydrates content the error values were under 9% demonstrating in all cases the potency of the approach for individual and total carbohydrates content determination. Taking into account the samples complexity due to the presence of a great variety of components, such as, phenolic compounds, vitamins or aminoacids, it is remarkable the accuracy and precision obtained for both, each individual carbohydrate and the total carbohydrate content in all the nine samples studied. Overall selectivity (ME separation plus selective CuNWs detection towards sugars) allowed the accurate determination of each individual glucose and fructose fraction as it was clearly demonstrated.

In our previous approach, electrochemical detectors based on NiNWs and bimetallic Ni-CuNWs nanowires have demonstrated an

excellent analytical performance in terms of fast analytical response, class-selectivity towards the analytes involved, calibration performance and reliability during the analysis of a the selected honey samples studied[13]. However, the approach proposed here added the selectivity provided by the individual sugar determination in comparison with the only total sugar content ("Electrochemical Monosaccharide Index") previously reported. Also, in comparison with literature[14, 35-37], our work presented not only good LODs (lower than other similar approaches) but also reducing analysis times (from times >20 min to 4 min) with simpler instrumentation. However, this approach needs still a full-automation for the future use in the labs.

Table II.12. Precision in the quantitative determination of glucose and fructose in honey samples[1]

HONEY	**GLUCOSE** (159.3±3.2 s)[2]				**FRUCTOSE** (210.7±3.7 s)[2]			
	tm ± S (s)	**RSD (%)**	**i ± S (nA)**	**RSD (%)**	**tm ± S (s)**	**RSD (%)**	**i ± S (nA)**	**RSD (%)**
H-1	161.7 ± 1.4	0.9	15.2 ± 0.5	3.4	212.8 ± 2.5	1.2	3.7 ± 0.2	5.8
H-2	158.5 ± 2.0	1.3	17.8 ± 0.8	4.7	211.3 ± 2.8	1.3	3.7 ± 0.3	8.0
H-3	156.3 ± 1.6	1.0	19.8 ± 0.6	3.2	209.4 ± 3.8	1.8	3.7 ± 0.1	0.4
H-4	157.3 ± 0.9	0.6	20.5 ± 1.3	6.2	212.4 ± 0.9	0.4	3.7 ± 0.3	9.0
H-5	154.6 ± 0.4	0.3	18.0 ± 0.8	4.4	213.9 ± 1.4	0.7	3.6 ± 0.1	3.6
H-6	160.5 ± 0.8	0.5	21.8 ± 0.6	2.9	212.4 ± 2.4	1.1	3.8 ± 0.2	5.0
H-7	162.9 ± 2.0	1.3	22.6 ± 1.2	5.4	214.2 ± 2.3	1.1	3.8 ± 0.3	6.8
H-8	163.7 ± 1.1	0.7	22.5 ± 0.9	3.9	211.7 ± 2.3	1.1	3.7 ± 0.1	3.5
H-9	164.7 ± 1.0	0.6	16.9 ± 0.6	3.8	218.4 ± 3.7	1.7	3.8 ± 0.2	4.4

[1] Values are expressed as Mean values ± standard deviation (n=3). [2] Migration times for standards.

Table II.13. Determination of glucose and fructose in honey samples[1]

HONEY	GLUCOSE (%)			FRUCTOSE (%)			TOTAL CARBOHYDRATES (%)		
	ME-Cu NWs	HPLC-RI[2]	Er (%)	ME-Cu NWs	HPLC-RI[2]	Er (%)	ME-Cu NWs	HPLC-RI[2]	Er (%)
H-1	23.1 ± 2.6	23.9	3.2	47.1 ± 4.9	45.0	4.7	70.2 ± 5.6	68.9	1.9
H-2	24.9 ± 1.3	23.9	4.1	42.1 ± 3.8	40.6	3.7	66.9 ± 4.0	64.5	3.7
H-3	25.8 ± 0.9	27.4	5.8	38.9 ± 0.2	37.5	3.7	64.6 ± 0.9	64.9	0.4
H-4	25.6 ± 1.8	27.5	6.8	37.4 ± 3.4	35.7	4.8	63.0 ± 3.8	63.2	0.3
H-5	26.7 ± 1.3	29.7	9.9	44.0 ± 1.6	43.1	2.2	70.7 ± 2.1	72.7	2.8
H-6	29.9 ± 1.0	27.1	10.2	42.0 ± 2.1	39.0	7.8	71.8 ± 2.3	66.1	8.7
H-7	31.7 ± 1.9	29.8	6.4	42.7 ± 2.9	39.6	7.7	74.3 ± 3.4	69.4	7.0
H-8	29.5 ± 1.3	33.0	10.6	38.9 ± 1.4	37.2	4.8	68.4 ± 1.9	70.2	2.5
H-9	23.4 ± 1.0	23.9	2.1	43.4 ± 1.9	40.6	6.9	66.7 ± 2.2	64.5	3.5

[1] Values are expressed as Mean values ± standard deviation (n=3). [2] RSDS<7% (n=3)

II.3.4.3. Conclusions

This work clearly shows the potential of ME-CuNWs for fast, reliable and still simple route for analysis of sugars in honeys. The values obtained using ME-CuNWs in comparison with those obtained by HPLC-RI were highly in agreement with errors and RSDs below 10% demonstrating the accuracy and precision of the approach. In addition, the proposed ME-CuNWs approach in comparison with the reference HPC-RI method allowed a faster analysis times, cheaper instrumentation, competitive LODs and avoided the use of toxic solvents becoming an environmental friendly approach. The excellent results obtained during the analysis of the samples studied confirms the analytical potency of ME-CuNWs approach, enhancing the maturity of the microchip technology and opening new avenues for future implementation of applications in the field of food analysis. More robust, simplest and full-disposable ME devices are being developed in our lab for future implementation of this technology in the agro-food sector.

II.3.5 Copper nanowires immobilized on the boards of microfluidic chips for the rapid and simultaneous diagnosis of galactosemia diseases in newborn urine samples

Galactosemia is a rare disease, with a prevalence of 1 in about 50.000 people, in which exists a metabolic disorder associated with intolerance to galactose. The consequences of the disease can become fatal if it is not discovered during the firsts days of life, therefore a neonatal screening is highly needed in order to detect the disorder before it starts to show symptoms and avoid irreversible damages to the patient. The galactosemia metabolic pathway is shown in the **scheme 1**. Three types of galactosemia are related to malfunctions in the following enzymes: the failure of galactose 1-phosphate uridyltransferase (GALT) produces the most severe and common form of the disease, type I galactosemia (classic galactosemia), which could lead to develop liver disease, cataracts, mental retardation or even death. When galactokinase (GALK) is under malfunctioning, produces the type II form of the disease; and the failure of uridine diphosphate galactose-4-epimerase (GALE), produces the rarest type III form of the disease. These enzyme deficiencies result in heightened levels of galactose 1-phosphate (Gal 1-P) and galactose (Gal), Gal, and Gal 1-P/Gal/ uridyl diphosphate galactose (UDP-Gal), which indicate galactosemias type I, II and III, respectively. As consequence, these metabolites become true biomarkers that permit the identification of the three types of the galactosemia diseases accordingly to the profile detected.

Scheme 1

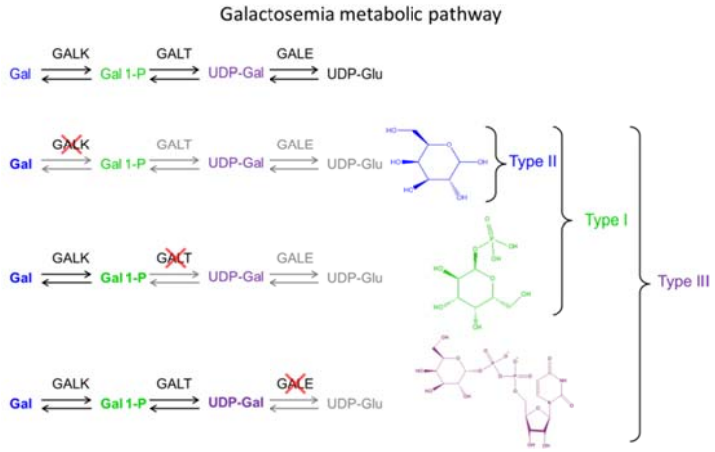

Nowadays the diagnosis of galactosemia is commonly performed through the measurement of the activity of the enzymes involved in the metabolic pathway determining their functioning using Beutler test or related protocols[38,39] or by measuring metabolites of the pathway, such as Gal and Gal 1-P, by microbiological methods as it is done in Paigen test[40]. Enzymatic colorimetric assays are also employed for the detection of Gal and Gal 1-P as an alternative using simpler instrumentation for a wider and cheaper implementation[40]. However, they tend to be susceptible to interference from other compounds in a complex sample. The determination of galactose has also been carried out assisted by the enzyme galactose oxidase in combination to ZnO nanorods as transducers[14] in a biosensor approach. Separation techniques such as HPLC or CE coupled to PAD or laser-induced fluorescence (LIF), have also been employed for determine the metabolites concentration in real samples[42-44]. However, these techniques usually involve longer analysis times due to the necessary sample pretreatment. Also, the simultaneous detection of the three biomarkers has not been reported.

More important, is the absence of screening methods in order to carry out earlier and faster diagnosis of galactosemia. Unfortunately, due to the low prevalence of the illness screening methods are not commonly employed around the world. Screening programs could avoid the undesired effects of the illness on the population. Without any question MC becomes not only a clear alternative to those previous approaches, but also a very unique screening method since it could allow the analysis in a fast and economic way, requiring only extremely low amounts of biological samples (microfluidic technology allows introducing minute amounts of samples using electrokinetic injection protocols) and also performing multiplexed analysis in future applications.

As consequence, this work is presented as a novel alternative to the approaches described above, based on the coupling of MC-CuNWs. Conceptually speaking, we hypothesize that the inherent selectivity and sensitivity of CuNWs, towards galactosemia metabolites detection in connection with MC selectivity could allow the fast and simultaneous detection of the three galactosemia biomarkers which implies the fast diagnosis of any galactosemia type in just one single analysis. It is important to remark that in this way, any form of the disease could be diagnosed in one analysis, saving time in contrast with other approaches in which a specific galactosemia analysis is performed only when determined signals of the illness appear.

This MC-NWs approach creatively assembles the advantages of rapid MC analysis using extremely low quantities of biological sample with a detection technique that does not rely on a chromophore signature as alternative to enzymatic approaches. Additionally the method requires urine samples, being less invasive for the baby.

This work has also sought to study an analysis system comprising an MC coupled to CuNWs for the rapid diagnosis of the three galactosemia profiles in newborn, healthy, or ill urine samples toward the detection of the specific metabolite profiles involving Gal 1-P, Gal, and UDP-Gal. The newborn urine samples were very unique due to the low prevalence of the illness. Selected precious urine samples collected from patients that had been previously diagnosed with the diseases were tested to validate the MC-CuNWs approach. To the best of our knowledge, this is the first report of MC-NWs based approach in the field of galactosemia diagnosis.

II.3.5.1. Simultaneous detection of galactosemia biomarkers

Accordingly to **scheme 1,** the diagnosis of galactosemia requires the simultaneous detection of the different metabolite profiles to determine the specific type of galactosemia, which become as true biomarkers of the disease. Indeed, galactosemia type I should be diagnosed towards the simultaneous detection of Gal 1-P (specific biomarker) and Gal (accumulated biomarker); type II towards the detection of Gal (specific biomarker) and type III towards the simultaneous detection of accumulated Gal 1-P and Gal as well as UDP-Gal as specific biomarker of this profile.

Figure II.25 illustrates the scheme for simultaneous detection of galactosemia biomarkers on the MC layout **(A)** and the simulated galactosemia profiles using standards mixtures accordingly, obtained under previously optimized separation (NaOH 3 mM, pH=11.5; separation voltage +750 V), injection (+1500 V for 5s) and detection (E=+0.70 V in NaOH 3 mM, pH=11.5) conditions **(B)** within a time period of less than 350 s. Interestingly, no signal was obtained when the bare electrode was used confirming the selective electro catalysis of these materials towards the galactosemia metabolites detection.

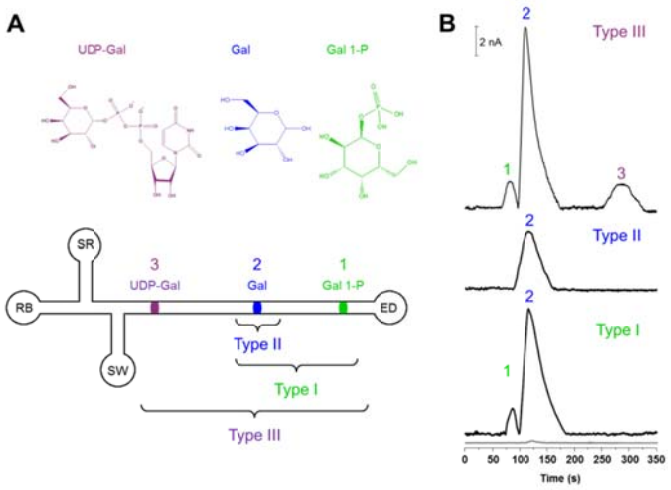

Figure II.25. (A) Scheme for simultaneous detection of galactosemia biomarkers on the microfluidic chip layout. RB: running buffer reservoir, SR: sample reservoir, SW: sample waste reservoir, ED: electrochemical detection cell. **(B)** Typical galactosemia profiles obtained using the MC-CuNWs. Type I peaks: **(1)** Gal 1-P 400 μM **(2)** Gal 200 μM; Type II peaks: **(2)** Gal 200 μM; Type III peaks: **(1)** Gal 1-P 400 μM **(2)** Gal 100 μM **(3)** UDP-Gal 400 μM. The analyses were performed using a CuNWs modified electrode. The gray line corresponds to the analysis using a bare electrode. Separation conditions: NaOH (3 mM, pH 11.5) and a separation voltage of +750 V. Injection conditions: +1500 V for 5 s. Detection conditions: E= +0.70 V in NaOH (3 mM, pH 11.5).

As it is listed in **Table II.14**, galactosemia type I was identified by the detection of Gal 1-P and Gal as earlier metabolite in the galactose metabolic pathway, which displayed well-defined peaks at 83.5 ± 2.0 s and 114.1 ± 3.7 s, respectively. The detection of galactosemia type II was achieved through the detection of Gal, which yielded a well-defined peak that migrated at 117.2 ± 1.0 s. UDP-Gal was detected at higher migration times, 287.7 ± 2.2 s, as a specific biomarker of the rarest form of galactosemia, type III. Accordingly, type III galactosemia was confirmed towards the detection of Gal 1-P (85.9 ± 4.1 s) and Gal (116.1 ± 3.1 s). An excellent precision in migration times (RSDs ≤5%) and in peak heights (RSDs ≤6%) (n=5) were also observed. In addition, a very good *intra-*

electrode repeatability with RSDs<8% (n=10) and *inter*-electrode reproducibility with RSDs<12% (n=5) were obtained; indicated an excellent stability of the electrochemical detector. These excellent values informed not only about the high resistance to fouling, but also about the stability of the CuNWs distribution on the electrode as it was supported with the FESEM results previously discussed.

Table II.14. Precision obtained in the simultaneous detection of galactosemia biomarkers (n=5).

Analytical feature	Type I		Type II	Type III		
	Gal 1-P	**Gal**	**Gal**	**Gal 1-P**	**Gal**	**UDP-Gal**
tm±S (s)	83.3±1.0	114.5±2.2	117.2±0.9	85.9±4.1	116.1±3.1	287.7±2.2
RSD (%)	1.2	1.9	0.8	4.8	2.6	0.8
i ± s (nA)	1.9±0.1	9.4±0.3	4.2±0.1	1.8±0.1	12.4±0.1	1.8±0.1
RSD (%)	5.7	3.0	2.7	5.5	0.3	5.1

In an effort to simplify the analytical procedures, we have identified a common set of conditions that may be applied to either analytical route. The chemical and electrokinetic conditions were evaluated to achieve the separation of target biomarkers within the shortest period of time. A 3 mM NaOH media (pH=11.5) permitted the sensitive detection of well-defined analyte peaks with an excellent resolution ($R_{Gal\ 1\text{-}P\text{-}Gal}$ = 1.0; $R_{Gal\text{-}UDP\text{-}Gal}$= 2.6) and an optimum separation time of 350 s.

The suitability of the *end-channel* coupling between a MC and CuNWs was demonstrated, as shown in **Figure II.26A**, which examines the influence of the separation voltage on the detected response. The separation voltage affected both the analyte resolution and the current signal. As expected, by increasing the voltage from +500 V to +1000 V (in 250 V

steps (A-C)), the migration times for the target biomarkers decreased (from 135 s to 58 s, from 206 s to 90 s, and from 360 s to 208 s, for Gal 1-P, Gal, and UDP-Gal, respectively) as well as the peak-to-peak resolution ($R_{Gal\ 1\text{-}P\text{-}Gal}$ decreased from 1.5 to 0.8 and $R_{Gal\text{-}UDP\text{-}Gal}$ decreased from 4.1 to 1.9**)**. A separation voltage of +750 V was the most favorable due to a short analysis time and the optimum Rs conditions ($R_{Gal\ 1\text{-}P\text{-}Gal}$= 1.0 and $R_{Gal\text{-}UDP\text{-}Gal}$= 2.6). The peak-to-peak noise level increased from 0.09 to 0.15 nA upon changing the voltage between +500 V and +1000 V. From the inspection of **Figure II.26A**, the initial charging-current flat baseline indicated complete isolation at all separation voltages assayed. In addition, the linear dependence found between electrophoretic current and separation voltage (r=0.990) indicated a negligible Joule effect on the separation.

Optimal chemical and electrokinetic separation conditions (Na OH 3 mM, pH=11.5; separation voltage +750 V) were used to generate the hydrodynamic voltammograms (HDVs) using the CuNWs, as shown in **Figure II.26B**. The curves were collected stepwise under a separation voltage of +750 V by making +0.10 V changes in the detection potential. The three metabolites displayed no response below +0.20 V. The response gradually rose between +0.20 V and +0.70 V, after which the response leveled down. A very well-defined sigmoidal curve was obtained for all metabolites with $E_{1/2}$=+0.35 V, $E_{1/2}$=+0.35 V, and $E_{1/2}$=+0.55 V for Gal, Gal 1-P, and UDP-Gal, respectively. A detection potential of + 0.70 V offered the best signal-to-noise characteristics with ratios ranging from 15 to 80.

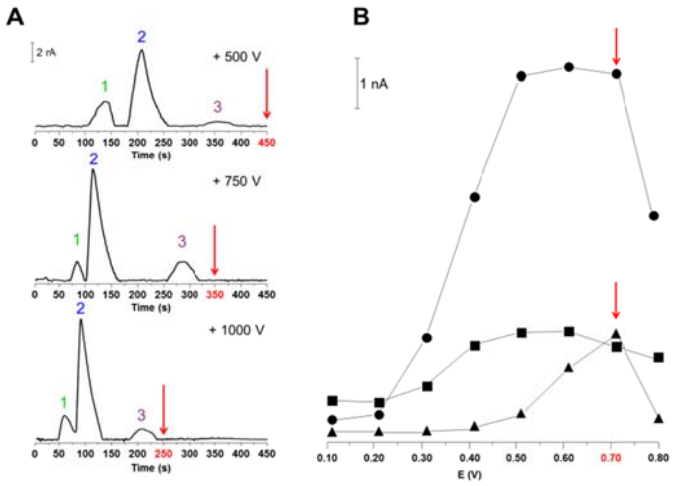

Figure II.26. (A) Influence of the separation voltage on the galactosemia metabolite separation, Peaks: **(1)** Gal 1-P 400 µM **(2)** Gal 100 µM **(3)** UDP-Gal 400 µM. **(B)** Hydrodynamic voltammograms of galactosemia metabolites (–■–Gal 1-P,–●–Galactose, –▲– UDP-Galactose) in NaOH 3 mM, pH 11.5. Separation voltage +750 V. Red arrows correspond to optimal time and detection potential. Other conditions are as listed in **Figure II.25.**

II.3.5.2. Diagnosis of galactosemias in newborn urine samples

Newborn urine samples, both healthy and ill, were analyzed in an effort to characterize the detection profiles corresponding to galactosemia types I, II, and III. The urine samples studied in this work are very unique as it was previously described. Urine samples are ideal for analysis because they can be obtained through non-invasive techniques, and in addition, the metabolites are present at higher levels than in the blood samples. Urine samples permit the detection of galactosemia in cases in which a blood sample cannot be used due to contamination from an undeclared transfusion or parenteral feeding[45].

Figure II.27 shows a complete analysis of urine samples from healthy and ill newborns. On the one hand, **Figure II.27A** displays the analysis results obtained from healthy urine samples. As expected, a galactosemia profile was not observed in the analysis of the healthy samples (black line), only a small quantity of glucose was detected. In contrast, galactosemia profiles were clearly observed in the strategically spiked urine samples (red line), which were clearly differentiated from the healthy urine profiles.

On the other hand, **Figure II.27B** displays the analysis results obtained from the newborn urine samples from patients who had been previously diagnosed with one of the three types of galactosemia. Types I, II, and III galactosemia were readily distinguished based on the detection of the specific and accumulated metabolite biomarkers in accordance to galactosemia pathway shown in scheme 1; Gal 1-P/Gal, Gal, and Gal 1-P/Gal/UDP-Gal, respectively.

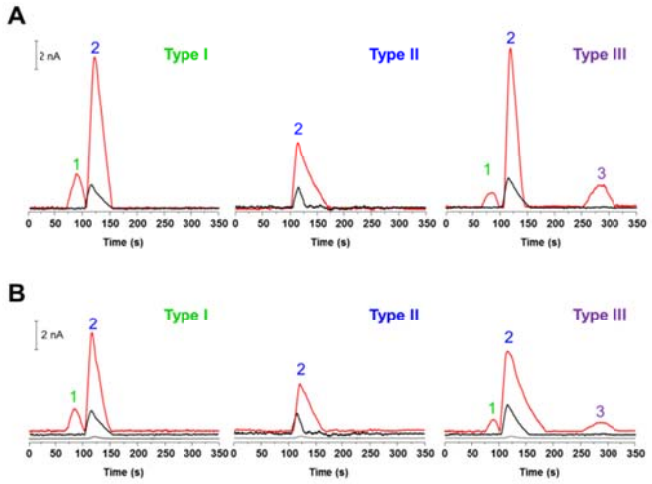

Figure II.27. Rapid detection of galactosemia profiles in urines samples obtained from healthy **(A)** and ill **(B)** newborns. **(A)** Analysis of healthy (black line) and spiked healthy newborn urine samples (red line). **(B)** Analysis of ill newborn urine samples (red line), each one corresponding to a different galactosemia profile. Analysis of healthy urine samples for comparison (black line). Analysis of ill newborn urine samples using a bare electrode (gray line). Peaks indicate the detection of: **(1)** Gal 1-P, **(2)** Gal and **(3)** UDP-Gal. Other conditions are as listed in **Figure II.25.**

A close examination of **Figure II.27B** reveals clear differences between healthy and ill urine samples, whereas no signal was observed in the absence of the CuNWs (**Figure II.27B** gray line). The analytical potency of the MCs, therefore, relied on the presence of CuNWs. In all cases, the analysis exhibited impressive signal-to-noise characteristics with ratios ranging from 7 to 65, and noise level < 0.15 nA.

In addition, the CuNWs based detectors displayed a concentration dependent response to the metabolites. Well-defined peaks were measured in proportion to the analyte concentration for all three target galactosemia metabolites. As listed in **Table II.15**, the calibration plots were highly linear ($r \geq 0.990$) within the concentration ranges assayed. Combining the high sensitivity of the CuNWs with their low noise levels yielded a suitable level

of detection at micromolar concentrations (S/N=3). The method developed here shows LOD's (16, 15 and 120 μM for Gal 1-P, Gal, and UDP-Gal, respectively) lower than cut-off values employed as reference in the illness (Gal 1-P > 0.4 mM and Gal > 1.4 mM). These values are in agreement with those found in the bibliography and also with the values set in the methods employed in screening programs in hospitals[46]. It is important to mention that commonly an abnormal value is far away from the cut-off value being the levels found in ill patients greatly amplified due to the malfunctioning of the enzymes and the accumulation produced.

Table II.15. Analytical characteristics of the method

Analyte	Linear range (μM)	R^2	a ± tSa (nA)	b ± tSb ($nA \cdot \mu M^{-1}$)	LOD (μM)
Gal 1-P	100-1000	0.999	0.294 ± 0.210	0.042 ± 0.003	16
Gal	50-400	0.998	0.072 ± 0.525	0.020 ± 0.002	15
UDP-Gal	100-1000	0.999	-0.144 ± 0.138	0.004 ± 0.002	120

Table II.16 summarizes the quantitative results obtained during the analysis of urine samples from healthy and ill newborns. Firstly, **Table II.16** lists the high agreement between the migration times obtained in the analysis of urine samples in comparison with those found for standards. In addition, an excellent precision with an RSD of < 4% for the migration times and a RSD of < 16% (n=5) for the oxidation currents was also obtained during the urine samples analysis indicating the suitability of the approach for analysis of real samples. **Table II.16** also lists the quantitative results obtained upon the analysis of the spiked healthy or ill urine samples. Excellent recoveries (93–107%) were achieved in the spiked healthy urine samples indicating a very good accuracy of the proposed approach. Since

the recovery precision was also excellent (RSDs of < 6%), the approach become very reliable to perform the simultaneous detection of all biomarkers involved in the illness.

In addition, the levels obtained for each specific biomarker in the ill urine samples agreed with the levels typically found in the urine samples for these diseases (Gal 1-P > 0.4 mM and/or Gal > 1.4mM), indicating that a galactosemia diagnosis may be achieved using the analysis results from the MC-Cu NW devices with reliability. Also, since ill urine samples were previously diagnosed with a specific type of galactosemia, these results reveal the suitability of the approach and the real analytical potency of the MC-CuNWs as novel analytical screening tool for galactosemia diagnosis.

Table II.16. Analysis of urine samples from healthy and ill newborns

Analytical feature		Type I		Type II	Type III		
		Gal 1-P	**Gal**	**Gal**	**Gal 1-P**	**Gal**	**UDP-Gal**
Standards	**tm±S (s)**	83.3 ± 1.0	114.5 ± 2.2	117.2 ± 0.9	85.9 ± 4.1	116.1 ± 3.1	287.7 ± 2.2
	RSD (%)	1.2	1.9	0.8	4.8	2.6	0.8
Healthy Urines	**tm±S (s)**	83.0 ± 0.5	116.3 ± 0.9	115.6 ± 0.3	84.7 ± 2.8	125.1 ± 2.1	275.7 ± 2.2
	RSD (%)	0.6	0.8	0.3	3.3	1.7	0.8
	Recovery (%)	105.5 ± 4.6	106. 9 ± 5.3	93.2 ± 2.9	105.1 ± 2.8	102.9 ± 1.9	100.4 ± 1.8
Ill Urines	**tm±S (s)**	83.3 ± 3.1	117.3 ± 1.5	119.9 ± 2.1	84.3 ± 0.8	116.1 ± 0.5	284.3 ±3.6
	RSD (%)	3.7	1.3	1.8	1.0	0.4	1.3
	Concentration (mM)	15.2 ± 0.1	7.9 ± 0.5	8.4 ± 0.4	7.0 ± 0.2	2.8 ± 0.4	9.6 ± 0.7
	RSD (%)	0.8	6.0	4.9	3.5	15.7	7.6

Finally and in comparison with previous literature, the commonly employed methods are listed in **Table II.17.** Most of them employing blood samples (more invasive) and involving longer analysis times derived from the necessity of extraction, incubation or derivatization steps during the sample pretreatment. Also, detection of only one biomarker was commonly carried out. The approach presented here is an alternative to enzyme based assays being even more sensitive than other nanowires-enzyme based galactose sensors with the additional advantages of the simultaneous detection of the three target biomarkers involved in galactosemia diseases allowing the specific diagnosis of each type of galactosemia. Another clear advantage of our proposal is that microfluidic technology allows introducing minimum amounts of samples using electrokinetic injection protocols achieving the representativeness.

II.3.5.3. Conclusions

The inherent sensitivity and selectivity of CuNWs toward galactosemia metabolites in the context of MCs selectivity enables a novel and creative approach to the rapid, reliable and simultaneous diagnosis of the three types of galactosemia disease from an analysis of newborn urine samples. Types I, II, and III galactosemia profiles were identified through the detection of the specific biomarkers Gal 1-P, Gal, and UDP-Gal, with LOD's of 16, 15 and 120 μM respectively. The analysis results were obtained in less than 350 s with negligible sample consumption as well as with good signal-to-noise characteristics (>15, noise levels under 0.15 nA). Excellent accuracy (recoveries 93–107%) and stability of the electrochemical detector (*intra*-electrode repeatability with RSDs<8% (n=10) and *inter*-electrode reproducibility with RSDs<12% (n=5)) were additional revealed. The significance of the newborn urine samples studied confirms the analytical potency of the MC-CuNWs platforms, enhancing the maturity of the microchip technology and opens new avenues for future screening implementation applications in the field.

Table II.17. Analytical methods employed for galactosemia diagnosis.

Method	Sample	Analyte	Analysis Time (min)	LOD (µM)	Remarks	Ref
Fluorimetric	Blood	GALT activity	90	----	Beutler test adaption Need hemoglobin removal	38
Fluorimetric	Blood	Gal/ Gal 1-P	90	----	Beutler test adaption with tedious sample pretreatment	39
HPLC	Blood	Gal and GALK, GALT, GALE activity	----	----	Microbiological Paigen test and 3 different assays to evaluate the enzymes activity	40
Colorimetric	Blood	Gal 1-P	5 h	----	Long sample pretreatment	41
HPLC/PAD	Blood	Gal 1-P	4	1.15	Involves extraction of Gal 1-P	42
HPLC/PAD	Blood	Gal	5	0.14	Carbohydrates derivatization is not required, but needs a post-column to increase the pH and enhance the sensitivity	43
CE/ LIF	Urine	Gal	10	0.10	Requires carbohydrates derivatization	44
Potentiometric	-----	Gal	10 s[1]	1000	Biosensor immobilizing galactose oxidase on ZnO nanorods	14
MC-CuNWs	Urine	Gal 1-P/ Gal/UDP-Gal	6	15,16, 120	Simultaneous detection of the three biomarkers (350 s). Inherent selectivity of CuNWs towards carbohydrate detection	This work

[1] Response time of the sensor

II.3.6. Experimental Section

II.3.6.1 Electro synthesis and characterization of nanowires based electrodes

Alumina filtration membranes with a plastic ring, 25 mm diameter, 0.2 μm pore diameter, and 60 μm thicknesses were purchased from Whatman (England).

Materials employed for the NiNWs fabrication were: $CuSO_4 \cdot 5H_2O$ for the sacrificial layer, and a mixture of $NiCl_2 \cdot 6H_2O$/$NiSO_4 \cdot 6H_2O$ for the layer that formed the NiNWs. For the synthesis of the CuNWs the reagents were: $CuSO_4 \cdot 5H_2O$ for the sacrificial layer and also for the layer that formed the CuNWs, $H_2PtCl_6 \cdot xH_2O$ was used for the intermediate platinum layer needed to separate the sacrificial and the nanowires layers. Copper and Nickel working solutions were dissolved in H_3BO_3 20 g/L and the platinum solution was solved in HCl 0.1 M. The sacrificial layer was removed using a $CuSO_4 \cdot 5H_2O$ solution 30%v/v HCl in both cases. All chemicals used in buffer preparation and in supporting electrolytes were of reagent grade.

Nanowires were synthesized by an electrodeposition method using a porous template. An anodic alumina oxide membrane (AAO) was used as a template for nanowire growth. Gold was sputtered onto the branched side of the membrane to function as the working electrode during the electrodeposition steps. The AAO membrane was connected with an aluminium foil contact. An Ag/AgCl electrode and a platinum wire were used as reference and counter electrodes, respectively. The sputtered membrane was placed in the bottom of the plating. The NiNWs were synthesized, by first depositing a thin layer of copper (-1 V, 10 C) which filled any imperfection in the template to obtain a regular tubular structure for the growth of nickel nanowires and then, the nickel layer to form the

nanowires was deposited (-1 V, 45 C). For the CuNWs, the protocol was essentially the same, after the sacrificial copper layer deposited to fill the imperfections, an intermediate platinum layer was then deposited (-0.5 V, 3 C) to separate the sacrificial copper layer from the copper nanowires layer and also protect this last layer during the sacrificial layer removal. Finally, the copper layer itself was deposited (-1V, 30C).

The sacrificial copper layer was removed using $CuSO_4 \bullet 5H_2O$ in 30%v/v HCl. The nanowires were released by dissolving the AAO template in a 3 M NaOH solution for 25 minutes. The nanowires were rinsed several times with deionized water until a neutral pH was obtained. After rinsing with deionized water, centrifugation completed the separation and purification steps.

Then the carbon screen-printed electrodes (CSPE) (10x1 mm) were cast by placing on the electrode surface a 2µL drop of the corresponding nanowires suspension (Nickel or Copper) with a concentration of 10 mg/mL.

Scanning electron microscopy (SEM) was performed using a Hitachi TM-1000 (Tokyo, Japan). Qualitative and quantitative energy dispersive X-ray spectrometry (EDS) system Swift-ED for TM-1000 form oxford instruments (Oxford, UK) was also performed. Aluminum mount stubs were used for the SEM analysis and were obtained from Electron Microscopy Sciences (Hatfield, UK).

The electrodes surfaces were characterized by covering them with a 4-5 nm Au layer. The surfaces were then imaged by field emission scanning electron microscopy (FESEM) using a JEOL JSM6335F equipment working at 5 kV. The energy-dispersive X-ray spectroscopy (EDS) analysis was performed using 80 mm^2 X-max with a resolution of 127-5.9 eV.

The electrochemical effective surface area was estimated by the slope of the plot of Q vs. $t^{1/2}$, obtained by chronocoulometry, based on **Equation 1**, given by Anson[47] using 0.45 mM $K_3[Fe(CN)_6]$ in 0.1 M PBS (pH=7.4).

$$Q(t) = \frac{2nFAcD^{1/2}t^{1/2}}{\pi^{1/2}} + Q_{dl} + Q_{ads}$$

In this equation, A is the effective electrochemical surface area of the working electrode (cm^2), c is the concentration of the electroactive species (mol/cm^3), n is the number of transfer electron that is 1, and D is the diffusion coefficient, 7.6 x 10^{-6} cm^2s^{-1} [48]. Q_{dl} is double layer charge which could be eliminated by background subtraction and Q_{ads} is Faradaic charge.

Reagents and samples

Inulin and fructose were purchased from Sigma Chemical Co. (St. Louis, MO). 1 mL solutions 1 mM and 50 mM for inulin and fructose respectively were prepared, and then the necessary dilutions were performed in order to obtain the desired concentrations. The inulin samples assayed were *Inulac* (dietetic supplement containing 41.5% w/w of inulin) and *Dietabelt* (dietetic pills containing 67.2 mg each pill of 580 mg) which were acquired in local supermarkets. All solutions were prepared by dissolving the corresponding weight in 1 mL of buffer solution.

Glucose and fructose were purchased from Sigma Chemical Co. (St. Louis, MO). Honey samples were obtained through IMIDRA (an agroalimentary institute located in Madrid, Spain). Firstly, 1 mL stock solutions 50 mM for glucose and fructose were prepared in running buffer, and secondly working solutions for the studies were appropriately diluted in the running buffer. The running buffer used for sample preparation and as

electrophoretic buffer was 20 mM NaOH + 10 mM H_3BO_3, pH 12, which were purchased from fluka and Merck respectively. In all cases, high-quality water, purified in a Milli-Q system (Millipore, Bedford, MA, USA), was used.

Gal, Gal 1-P and UDP-Gal were purchased from Sigma Chemical Co. (St. Louis, MO). At first, they were dissolved in deionized water and secondly working solutions for the studies were appropriately diluted in NaOH pH 11.5, which was purchased from Merck. In all cases, high-quality water, purified in a Milli-Q system (Millipore, Bedford, MA, USA), was used.

Newborn urine samples previously diagnosed were obtained in collaboration with the Laboratorio de Metabolopatías of the Hospital Clínico (CHUS) in Santiago de Compostela (Galicia, Spain), which is conducting a Newborn Screening Program by collecting solid-phase urine samples and paired blood samples[49]. Urine samples were collected from newborns by placing a slip of Whatman 903 paper on the genitals and holding it in place with a napkin. This should be done immediately prior to collecting the blood sample because the stress induced by the latter causes the infant to urinate. The collection paper may subsequently be withdrawn and laid horizontal to dry. To avoid interference from contaminants, the infant should be clean and free of creams, oils, talc, or any other cosmetic. If the infant defecates during the operation in addition to urinating, the sample should be discarded, the infant cleaned, and the operation repeated with another paper slip (each newborn screening kit generally contains two). Although the first paper may not have been soiled with faeces, it may have been contaminated with faecal material taken up by the urine. The urine-impregnated paper slips require a 4 hour drying time at room temperature. Discs 6 mm in diameter were cut to obtain an aliquot of the sample. Each

slip corresponded to 10 μL[46]. Urine samples from newborns were presented on 6 mm discs of Whatman 903 paper. A disc was placed, with the help of tweezers, at the bottom of a 1.5 mL Eppendorf tube. A 0.5 mL volume of the running buffer was then added, and the extraction step proceeded over 10 minutes under agitation. The disc was later removed from the Eppendorf tube.

II.3.6.2. Microfluidic chip with electrochemical detection

The analytical microsystem set-up was originally reported and described elsewhere[50] and then adapted[51-54].

A double-T glass microchip manufactured by Micralyne (Model MC-BF4-TT100, Edmond, Canada) using wet chemical etching and thermal bonding techniques was used. The microchip consisted of a glass plate (88 mm X 16 mm), and the total length of the separation channel was 85 mm with a semicircular section of 50 μm wide and 20 μm deep. The joint formed by injection feature 5 mm side arms and a separation channel which together formed the shape of a double-T. The original waste reservoir was cut away, leaving the channel outlet open at the end of the chip to facilitate end-channel amperometric detection. The end-channel amperometric detector consisted of an Ag/AgCl electrode as reference electrode, a platinum wire as counter electrode, and a CSPE-nanowires modified electrode as the working electrode. Amperometric detection was performed using a Potentiostat Autolab PGSTAT12 from Eco Chemie. A LabSmith HVS448 High voltage sequencer with eight independent high-voltage channels and programmable sequencing capabilities over the range required for voltage manipulation (LabSmith, Livermore, CA) was used as the voltage source.

Microfluidic protocol: The channels of the glass microchip were treated prior to use by rinsing with 0.5 M NaOH for 40 min and deionized water for 10 min. This procedure was carefully monitored to obtain reproducible results. The running buffer reservoir and detection reservoir were filled with the running buffer. The sample reservoirs were either filled with the analytes or the corresponding samples using the running buffer as the carrier solution. A voltage of +1500 V was applied for 3 min to the buffer reservoir to fill the longitudinal channel, and the detection reservoir was grounded, leaving the others reservoirs floating. This procedure was performed on each sample reservoir for 60 s to facilitate the process of filling the injection channel (located between the longitudinal channel and the sample reservoir) and then a voltage was then applied for 3 min to the running buffer reservoir to eliminate the remains of any previously introduced samples from the longitudinal channel. Finally, the samples were injected by applying +1500 V for 5 s.

Amperometric detection: A detection voltage of +0.70 V was applied to the working electrode. A spacer (easily removable adhesive tape, 60 μm) was placed between the surface of the electrode and the channel outlet to reproducibly control the distance between the electrode and the separation channel and to avoid interference from the electrical field applied for the separation in the detector. All experiments were performed at room temperature.

Calculations: The resolution (R) was calculated using the following equation:

$$R = \frac{1.18 \times (t_2 - t_1)}{(w_1 + w_2)}$$

Where t_1 and t_2 are migration times of the corresponding analytes and w_1 and w_2 are the corresponding peak widths at the half height of two adjacent analyte bands.

Safety considerations: The high-voltage supply should be handled with extreme care in order to avoid electrical shock.

II.3.7 References

[1] M.L. Kovarik, D.M. Ornoff, A.T. Melvin, N.C. Dobes, Y. Wang, A.J. Dickinson, P.C. Gach, P.K. Shah, N.L. Allbritton, Micro Total Analysis Systems: Fundamental Advances and Applications in the Laboratory, Clinic, and Field, Anal. Chem. 85 (2012) 451-472.

[2] D. Mark, S. Haeberle, G. Roth, F. Von Stettenzab, R. Zengerle, Microfluidic lab-on-a-chip platforms: requirements, characteristics and applications, Chem. Soc. Rev. 39 (2010) 1153-1182.

[3] M. Hervás, M.A. López, A. Escarpa, Electrochemical immunosensing on board microfluidic chip platforms, Trac-Trend Anal. Chem. 31 (2012) 109-128.

[4] A. Escarpa, Food electroanalysis: sense and simplicity, The Chem. Rec. 12 (2012) 72-91.

[5] C.E. Banks, R.G. Compton, New electrodes for old: from carbon nanotubes to edge plane pyrolytic graphite, Analyst 131 (2006) 15-21.

[6] M. Pumera, Nanomaterials meet microfluidics, Chem. Commun. 47 (2011) 5671–5680.

[7] M. Pumera, A. Escarpa, Nanomaterials as electrochemical detectors in microfluidics and CE: Fundamentals, designs, and applications, Electrophoresis 30 (2009) 3315-3323.

[8] G.M. Whitesides, The origins and the future of microfluidics, Nature 442 (2006) 368-373.

[9] K-I. Ohno, K. Tachikawa, A. Manz, Microfluidics: Applications for analytical purposes in chemistry and biochemistry, Electrophoresis 29 (2008) 4443–4453.

[10] W.R. Vandaveer IV, S.A. Pasas, R.S. Martin, S.M. Lunte, Recent developments in amperometric detection for microchip capillary electrophoresis, Electrophoresis 23 (2002) 3667-3777.

[11] M. García, A. Escarpa, Disposable electrochemical detectors based on nickel nanowires for carbohydrate sensing, Biosens. Bioelectron. 26 (2011) 2527–2533.

[12] Y. Bai, J. Xu, H. Chen, Selective sensing of cysteine on manganese dioxide nanowires and chitosan modified glassy carbon electrodes, Biosens. Bioelectron. 24 (2009) 2985–2990.

[13] M. García, A. Escarpa, A class-selective and reliable electrochemical monosaccharide index in honeys, as determined using nickel and nickel-copper nanowires, Anal. Bioanal. Chem. 402 (2012) 945–953.

[14] K. Khun, Z.H. Ibupoto, O. Nur, M. Willander, Development of Galactose Biosensor Based on Functionalized ZnO Nanorods with Galactose Oxidase, J. Sens. (2012) 696247-696253.

[15] J. Huang, Z. Dong, Y. Li, J. Li, J. Wang, H. Yang, S. Li , S. Guo, J. Jin, R. Li, High performance non-enzymatic glucose biosensor based on copper nanowires-carbon nanotubes hybrid for intracellular glucose study, Sensor Actuat B 182 (2013) 618- 624.

[16] E. Piccin, R. Laocharoensuk, J. Burdick, E. Carrilho, J. Wang, Adaptive Nanowires for Switchable Microchip Devices, Anal. Chem. 79 (2007) 4720-4723.

[17] T. Barclay, M. Ginic-Markovic, P. Cooper, N. Petrovsky, Inulin - a versatile polysaccharide with multiple pharmaceutical and food chemical uses, J. Excipients and Food Chem. 1 (2010) 27-50.

[18] A. Pastore, S. Bernardini, L. Dello Strologo, G. Rizzoni, C. Cortese, G. Federici, Simultaneous determination of inulin and p-aminohippuric acid in plasma and urine by reversed-phase high-performance liquid chromatography J. Chromatogr. B 75 (2001) 1187-1191.

[19] T. Rikita, Y. Egawa, T. Seki, Fluorometric determination of inulin using 5-quinolineboronic acid and inulinase, Anal. Biochem. 426 (2012) 24-26.

[20] S. Kimata, K. Mizuguchi, S. Hattori, S. Teshima, Y. Orita, Evaluation of a new automated, enzymatic inulin assay using D-fructose dehydrogenase, Clin. Exp. Nephrol. 13 (2009) 341-349.

[21] S. Vendrell-Pascuas, A.I. Castellote-Bargallo, M.C. Lopez-Sabater, Determination of inulin in meat products by high-performance liquid chromatography with refractive index detection, J. Chromatogr. A (2000) 881, 591-597.

[22] H. Wang, Z. Zhang, L. Liang, S. Wen, C. Liu, X. Xu, A comparative study of high-performance liquid chromatography and colorimetric method for inulin determination, Eur. Food Res. Technol. 230 (2010) 701-706.

[23] A. Zuleta, M.E. Sambucetti, Inulin Determination for Food Labeling, J. Agr. Food Chem. 49 (2001) 4570-4572.

[24] K. Hofer, D. Jenewein, Enzymatic determination of inulin in food and dietary supplements, Eur. Food Res. Technol. 209 (1999) 423-427.

[25] M. Steegmans, S. Iliaens, H. Hoebregs, Enzymatic, Spectrophotometric Determination of Glucose, Fructose, Sucrose, and Inulin/Oligofructose in Foods, J. AOAC Int. 87 (2004) 1200-1207.

[26] J. Manso, M.L Mena, P. Yáñez-Sedeño, J.M. Pingarrón, , Bienzyme amperometric biosensor using gold nanoparticle-modified electrodes for the determination of inulin in foods, Anal. Biochem. 375 (2008) 345-353.

[27] A. Escarpa, M.C. González, A.G. Crevillén, A.J. Blasco, CE microchips: An opened gate to food analysis, Electrophoresis 28 (2007) 1002–1011.

[28] A. Escarpa, M.C. González, M.A.L. Gil, A.G. Crevillén, M. Hervás, M.García, Microchips for CE: Breakthroughs in real-world food analysis, Electrophoresis 29 (2008) 4852–4861.

[29] A. Martín, D. Vilela, A. Escarpa, Food analysis on microchip electrophoresis: An updated review, Electrophoresis 33 (2012) 2212-2227.

[30] A.G. Crevillén, M. Ávila, M. Pumera, M.C. González, A. Escarpa, Food Analysis on Microfluidic Devices Using Ultrasensitive Carbon Nanotubes Detectors, Anal. Chem. 79 (2007) 7408-7415.

[31] A.G. Crevillén, M. Pumera, M.C. González, A. Escarpa, Towards lab-on-a-chip approaches in real analytical domains based on microfluidic chips/electrochemical multi-walled carbon nanotube platforms, Lab Chip 9 (2009) 346-353.

[32] C.D. García, C.S. Henry, Direct Determination of Carbohydrates, Amino Acids, and Antibiotics by Microchip Electrophoresis with Pulsed Amperometric Detection, Anal. Chem. 75 (2003) 4778-4783.

[33] M. Stefansson, D. Westerlund, Capillary electrophoresis of glycoconjugates in alkaline media, J. Chromatogr. A 632 (1993) 195-200.

[34] S. Hoffstetter-Kuhn, A. Paulus, E. Gassmann, H.M. Widmer, Influence of borate complexation on the electrophoretic behavior of carbohydrates in capillary electrophoresis, Anal. Chem. 63 (1991) 1541-1547.

[35] J.C. Fanguy, C.S. Henry, Pulsed amperometric detection of carbohydrates on an electrophoretic microchip, Analyst 127 (2002) 1021-1023.

[36] M. Ávila, A.G. Crevillén, M.C. González, A. Escarpa, L.V. Hortigüela, C.L. Carretero, R.A. Pérez-Martín, Electroanalytical approach to evaluate antioxidant capacity in honeys: proposal of antioxidant index. Electroanal. 18 (2006)1821–1826

[37] J. Ye, R. Baldwin, Determination of carbohydrates, sugar acids and alditols by capillary electrophoresis and electrochemical detection at a copper electrode, J. Chromatogr. A 687 (1994) 141-148.

[38] H. Rhode, E. Elei, I. Taube, T. Podskarbi, A. Horn, Newborn screening for galactosemia: ultramicro assay for galactose-1-phosphate-uridyltransferase activity, Clin. Chim. Acta, 274 (1998) 71–87.

[39] A. Fujimoto, Y. Okano, T. Miyagi, G. Isshiki, T. Oura, Quantitative Beutler Test for Newborn Mass Screening of Galactosemia Using a Fluorometric Microplate Reader, Clin. Chem. 46 (2000) 806–810.

[40] Y. Nishimura, G. Tajima, A. Dwi Bahagia, A. Sakamoto, H. Ono, N. Sakura, K. Naito, M. Hamakawa, C. Yoshii, M. Kubota , K. Kobayashi, T. Saheki, Differential diagnosis of neonatal mild hypergalactosaemia detected by mass screening: Clinical signi¢cance of portal vein imaging, J. Inherit. Metab. Dis. 27 (2004) 11–18.

[41] F. Diepenbrock, R. Heckler, H. Schickling, T. Engelhard, D. Bock, J. Sander, Colorimetric Determination of Galactose and Galactose-l-Phosphate from Dried Blood, Clin. Biochem. 25 (1992) 37–39.

[42] J-S. Jeong, H-J. Kwon, H-R. Yoon, Y-M. Lee, T-Y. Choi, S-P. Hong, A pulsed amperometric detection method of galactose 1-phosphate for galactosemia diagnosis, Anal. Biochem. 376 (2008) 200–205.

[43] J-S. Jeong, H-R. Yoon, S-P. Hong, Development of a new diagnostic method for galactosemia by high-performance anion-exchange chromatography with pulsed amperometric detection, J. Chromtogr. A 1140 (2007) 157–162.

[44] C.J. Easley, L.J. Jin, K.B. Presto Elgstoen, E. Jellum, J.P. Landers, J.P. Ferrance, Capillary electrophoresis with laser-induced fluorescence detection for laboratory diagnosis of galactosemia, J. Chromtogr. A 1004 (2003) 29–37.

[45] J.R. Alonso-Fernández, M.I. Carpinteiro, J. Baleato, J. Fidalgo, Vertical sandwich-type continuous/evaporative TLC with fixed mobile phase volume for separating sugars of clinical relevance in paper-borne urine and blood samples in newborn screening, J. Clin. Lab. Anal. 24 (2010) 106–112.

[46] J.R. Alonso-Fernández, B. Patel, Dietary Sugars: Chemistry, Analysis, Function and Efects. In Food and Nutritional Components in Focus No. 3. Ed. Victor R Preedy. Royal Society of Chemistry, www.rsc.org., pp 186–207.

[47] F.C. Anson, Application of Potentiostatic Current Integration to the Study of the Adsorption of Cobalt (III)-(Ethylenedinitrilo(tetraacetate) on Mercury Electrodes, Anal. Chem. 36 (1964) 932-934.

[48] N.P.C. Stevens, M.B. Rooney, A.M. Bond, S.W. Feldberg, , A Comparison of Simulated and Experimental Voltammograms Obtained for the $[Fe(CN)_6]^{3-/4-}$ Couple in the Absence of Added Supporting Electrolyte at a Rotating Disk Electrode, J. Phys. Chem. A 105 (2001) 9085-9093.

[49] J.R. Alonso-Fernández, C. Colón, Newborn screening in Spain, with particular reference to Galicia: Echoes of Louis I. Woolf, Mol. Genet. Metab. 101 (2010) 95–98.

[50] J. Wang, B. Tian, E. Sahlin, Micromachined Electrophoresis Chips with Thick-Film Electrochemical Detectors, Anal. Chem. 71 (1999) 5436-5440.

[51] A.G. Crevillén, M. Pumera, M.C. González, A. Escarpa, Carbon nanotube disposable detectors in microchip capillary electrophoresis for water-soluble vitamin determination: Analytical possibilities in pharmaceutical quality control, Electrophoresis 29 (2008) 2997-3004.

[52] A.G. Crevillén, M. Ávila, M. Pumera, M.C. González, A. Escarpa, Food Analysis on Microfluidic Devices Using Ultrasensitive Carbon Nanotubes Detectors, Anal. Chem. 79 (2007) 7408-7415.

[53] J. Wang, M. Pumera, M.P. Chatrathi, A. Rodriguez, S. Spillman, R.S. Martin, S.M. Lunte, Thick-Film Electrochemical Detectors for Poly(dimethylsiloxane)-based Microchip Capillary Electrophoresis, Electroanal. 2002, 14, 1251-1255.

[54] D. Vilela, A. Ansón-Casaos, M.T. Martínez, M.C. González, A. Escarpa, High NIR-purity index single-walled carbon nanotubes for electrochemical sensing in microfluidic chips, Lab Chip 12 (2012) 2006-2014.

III. Synthesis and characterization of polymer/nickel/platinum micromotors for immunoassays in microfluidic systems

III.1. Micromotors for sensing and biosensing

Technology advances come from the observation of nature and the effort to create artificial analogues that could generate new nanotechnologies mimicking or improving natural structures or systems. Nanomotors have been inspired by natural motors such as kinesin motors. Kinesin is a protein that is able to move along microtube filaments powered by the hydrolysis of adenosine triphosphate (ATP) as it is illustrated in **Figure III.1)**. The energy released from the ATP hydrolysis results in linear or rotational movement induced by small conformational changes. These natural nanomotors are responsible of different functions such as transporting vesicles from de centre of the cellule to its periphery. This active movement is involved in several cellular functions including the transport of cellular cargo. This active transport is what attracted the scientists and make them think about the possibility of mimic it making customized transporters able to carry specific cargoes to a desired place. Inspired by the sophistication of nature biomotors and driven by pioneering contributions of Sen and Mallouk's team and Ozin's group [1-3], major efforts are currently being devoted to the design of efficient high-speed synthetic micro-/nanoscale motors that convert chemical energy into autonomous motion.

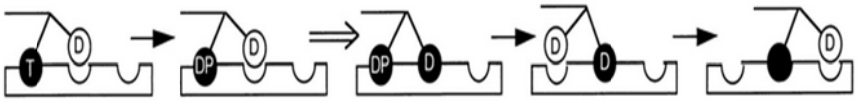

Figure III.1. Scheme of kinesin movement

According to the definition, micro/nanomotors are devices in the micro/nano scales capable of converting energy into movement and forces. Despite nanomotors have appeared recently on the bibliography there are a huge number of research papers related with them, so it is necessary to establish a classification, for example attending to the source

of energy that promotes the movement in the microstructure. The energy source is closely related to the microstructure shape, actually both shape and propulsion systems are connected.

Nanomotors can significantly improve the characteristic of common analytical systems through the impressive possibilities that they offer. As a result of the autonomous movement of these nanodevices the different steps of the analytical process can be performed in different places of the systems, allowing an increase in the sensitivity and selectivity. Such increase in sensitivity and selectivity is possible because of the nanomotor can develop each task in its optimum conditions even when each step has different ones by moving through different zones of the system searching for the best conditions for each step.

In the following section, different kinds of nanomotors are listed; they are classified by the source of energy and the resulting produced movement.

III.1.1. Self-electrophoretic propulsion-based micromotors

Catalytic nanomotors are a special kind of nanowires. Typically, these nanowires are synthesized by electrochemical template assisted methods to achieve the bimetallic structure needed; the synthesis takes place inside the pores of a membrane (i.e. AAO membrane). As it was described in Chapter II, in an easy and strategically defined manner, the nanowires synthesis is carried out in different steps. Briefly, firstly the electrochemical cell is filled with a gold solution to perform the electrodeposition of the first end of the nanowires and then the solution is changed for a platinum solution to complete the synthesis, extra layers can be included for magnetic control or for support further modifications, later on the template is removed to get the free nanowires.

The sequential deposition of the platinum and gold segments leads to asymmetric nanowires with spatially defined catalytic zones. Such asymmetry is essential for generating a directional force. The resulting nanomotors are propelled by electrocatalytic decomposition of the hydrogen peroxide fuel (on both ends of the wire), with oxidation to oxygen occurring at the platinum anode and its reduction to water on the gold cathode. This leads to a random autonomous non-Brownian movement toward their platinum end[1-5].

Additionally to the hydrogen peroxide reduction, the cathodic reaction on the gold segment involves also the four-electron reduction of oxygen to water. These cathodic reactions, along with the oxidation of the peroxide fuel at the platinum segment, result in electron flux within the wire (toward the gold segment) and generation of an electric field. These lead to electromigration of protons in the electrical double layer (surrounding the nanowire) from the platinum end to the gold end and to self-electrophoresis and as a result in the propulsion of the nanomotors. **Figure III.2** illustrates this phenomenon.

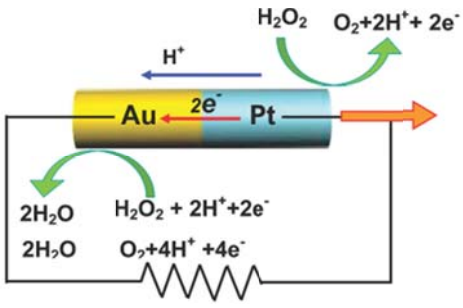

Figure III.2. Self-electrophoresis (bipolar electrochemical) mechanism for the propulsion of catalytic nanowire motors in the presence of hydrogen peroxide. The mechanism involves an internal electron flow from one end to the other end of the nanowire, along with migration of protons in the double layer surrounding the wires. Reprinted with permission from reference 4

In order to produce a controlled movement instead of a random one, to increase the potential applications of these nanostructures, it is necessary to include a control section. This control section can be achieved including a magnetic segment during the fabrication and through an external magnetic field provided by a Neodymium magnet the nanowires are aligned and remotely controlled[5].

Catalytic nanowires motors are influenced by gradients of the fuel concentration, moving to higher concentrations. An increment in the effectiveness of the reaction would lead in higher speed of the nanomotors and also in the generated force extending the possible applications of these devices. Different fuels (i.e. hydrazine) or nanowires composition (gold-silver alloys, CNT) have also been studied to improve their characteristics[6,7].

The attachment of the nanomotor to the target analyte can be accomplished through different strategies ranging from unspecific interactions like electrostatic or magnetic forces or specific bonding taking advantage of the sulphur affinity to gold surfaces or the biotin-streptavidin interaction.

It is highly desirable for future bio-applications not only fabricate a biocompatible nanomotor, that is affordable with the employment of gold or polymers, but also find a suitable fuel as source of energy due to the toxicity of hydrogen peroxide or hydrazine, that limits the potential biomedical applications of nanomotors. One interesting alternative to these fuels is to exploit the glucose that is present in high concentration in biological fluids using glucose oxidase to generate *in situ* the necessary hydrogen peroxide.

III.1.2. Bubble propulsion-based micromotors

III.1.2.1. Template assisted microtubes

Bubble propelled microstructures work using a similar principle as self-electrophoresis propelled micromotors, the decomposition of a fuel on a catalytic surface, but in this case the source of is not related to the generated gradients, the energy is provided by the bubble generation and the energy that these bubbles implement on the microstructure.

These micromotors are tubular micromotors consist of a polymer/Pt bilayer, present conical shape and the inner part correspond to the catalytic surface (Pt) where the decomposition takes place. Commonly hydrogen peroxide and platinum have been used and the decomposition of hydrogen peroxide using platinum as the catalytic surface generates oxygen bubbles. The conical shape of these microtubes and corresponding pressure differential assist the unidirectional expansion of the catalytically generated oxygen bubbles, and their release from one of the tubular openings thrusting the micromotor. Additionally, small amounts of surfactant are used to maintain the bubble development and promote their release.

Tubular micromotors have shown to be a considerable promise for diverse applications owing to their efficient bubble induced propulsion in complex media opening the alternative to move in real environments with higher ionic strength where catalytic nanowires cannot move. Moreover these micromotors are also synthesized using a bottom-up approach, a simplified membrane template electrodeposition protocol. The resulting micromotors displays some advantages apart from the low-cost mass production synthesis method, are commonly smaller than other typically found in the bibliography (i.e. rolled-up micromotors) and can

move even with low fuel concentration (0.2% H_2O_2) at high speeds (up to 1400 body lengths/s) which can be also used as a high towing force for transport diverse analytes. Body lengths/s is understood as how many times the micromotors are able to move its own size each second.

The basic bilayer scheme can be tailored to include different features like Ni and Au layers for their magnetic guidance and facile functionalization (i.e. with receptors), respectively. A creative modification of the outer Au surface by molecular bioreceptors, i.e. DNA probes[8], aptamers[9], antibodies[10], or lectins[11], has been shown useful for diverse target isolation sensing, drug and delivery[12] and environmental oil spills remediation[13] applications. Moreover, functionalized polymers can avoid the need of a gold surface and the SAM construction, this kind of polymers already present carboxy groups on their surface after its polymerization and are a real alternative to reduce the necessary steps in the modification of the micromotor achieving as a result at the end of the process higher speeds and towing force and in addition reducing the time necessary for the modification and the waste generated.

Recent progress in the field of synthetic nanomachines has opened the door to new and important applications[14-17]. For example, active transport by receptor-functionalized artificial nanomotors propelled in complex samples offers an attractive strategy for isolating target analytes[11,18].

Great efforts with the aim of construct micromotors which source of energy come from less aggressive chemicals are being done, the ultimate objective is fabricate micromotors which can extract the necessary energy for movement from harmless molecules like glucose by the introduction of enzymes, an intermediate approach was done by J.

Orozco et al.[19] in which the inner part of the tubular micromotor is formed by gold, and a catalase is attached through a self-assembled monolayer and EDC/NHS chemistry, avoiding in this case the employment of platinum, being that the catalase produces the oxygen bubbles by decomposing the hydrogen peroxide. In order to get even more biocompatible micromotors W. Gao et al.[20] developed a micromotor able to move in extreme acidic environments, without the need to any additional chemical fuel. The thrust is produced in this case by hydrogen bubbles due to the reduction of the protons in the media on the zinc surface, offering considerable potential for diverse biomedical applications including guided cargo transport in such an acid media like human stomach. **Figure III.3** Shows the schematic and images of these micromotors

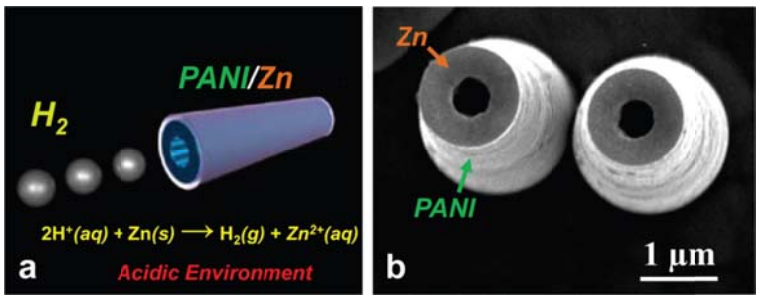

Figure III.3. Acid-driven PANI-Zn microrocket: **(a)** schematic of motion in an acidic environment; **(b)** SEM images of the top view of two PANI-Zn microtubes (prepared using a membrane with 2 µm diameter pores). Reprinted with permission from reference 21

As an alternative to the introduction of bio-receptors that are not adequate for harder environments, like high temperature, organic solvents or extreme pHs, Orozco et al.[21] proposed the synthesis of catalytic micromotors which polymeric layer is constituted by a molecularly imprinted polymer (MIP) including by this way artificial recognition sites. This a novel and creative approach for the integration of recognition sites

over the micromotor surface that can be tailored on-demand to the desired target molecule, by growing the polymer in the presence of the target molecule to generate the complementary cavities, and therefore expanding the possibilities for capture and transport a wide variety of important molecules for diverse applications.

III.1.2.2. Rolled-up microtubes

These catalytic microtube engines, pioneered by Mei and Schmidt, are extremely powerful catalytically propelled micromotors[22-24]. Rolled-up microtube engines commonly have an inner (catalytic) Pt surface, are typically 50-100 μm in length, and have an opening diameter of 5-10 μm[24].

Rolled-up microtubes are commonly prepared by top-down photolithography, glancing angled e-beam deposition and the stress-assisted rolling of functional nanomembranes on polymers into conical microtubes. The incorporation of an intermediate ferromagnetic (Ni, Fe or Co) layer during the fabrication process offers a precise magnetic guidance of their movement. The process is outlined in **Figure III.4.**

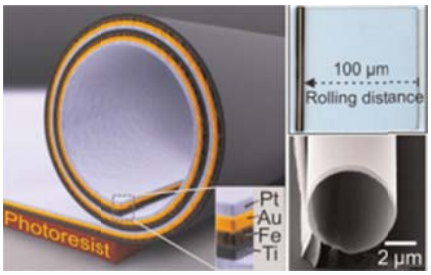

Figure III.4. Schematic diagram of a rolled-up microtube consisting of Pt/Au/Fe/Ti multilayers on a photoresist sacrificial layer **(left)**. Optical microscopy and SEM images of a rolled-up Pt/Au/Fe/Ti microtube **(right)**. Reprinted with permission from reference 24

III.1.3. Ultrasound propulsion-based micromotors

Despite recent advances in fuel-free microscale motors, there continues to be a need for a biocompatible energy source that can power micromotors, and acoustic energy is an interesting candidate for driving micromotors in fluids, including biological media. Ultrasound is an acoustic (sound) energy in the form of waves having a frequency above the human hearing range (i.e. frequencies above 20 kHz). Such high-frequency sound waves have minimal harmful effects on biological systems. Hoyos and Mallouk[25] describe exciting experiments in which ultrasonic acoustic waves can propel template grown metallic nanowires as fast as ~200 μm/s. The movement mechanism is based on the shape asymmetry of the rods. The asymmetric shape of the metal rods can lead to an asymmetric distribution of the acoustic pressure from the scattering of the incident acoustic waves at the metal surface. A locally induced pressure gradient associated with the concave end of the nanowires, leads to directional motion by a self-acoustophoresis.

Esener and Wang[26] have developed as well ultrasound driven micromotors or microbullets. These microbullets utilize the rapid expansion and vaporization of perfluorocarbon emulsion droplets confined to the microtubular machine interior triggered by an ultrasound pulse leading to an impressive speed of 6 m/s. **Figure III.5** illustrate theses aspects.

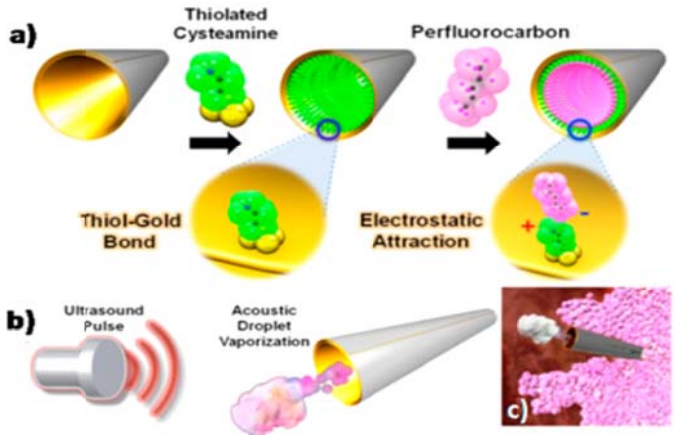

Figure III.5. (a) Preparation of the perfluorocarbon emulsion-loaded microbullets. **(b)** Schematic illustration of "microbullet" propulsion through acoustic droplet vaporization of the bound emulsion triggered by an ultrasound pulse. **(c)** Schematic of a "microbullet" penetrating into tissue for drug delivery. Reprinted with permission from reference 28

III.1.4. Magnetic propulsion-based micromotors

Magnetically controlled motion, inspired by the motility of prokaryotic and eukaryotic microorganisms represents another attractive route for addressing the challenge of nanoscale propulsion and accomplishing a fuel-free locomotion. Such nanoscale propulsion requires breaking the system symmetry by deforming the motor shape.

The controlled beating motion of artificial flagella consisting of helical tails was reported by Nelson[27] and Ghosh[28], but requires top down complex preparation routes involving advanced microfabrication facilities. An alternative reported by Wang's group is based on flexible metal nanowire swimmers[29]. The new three-segment nanowire (Au, Ag, Ni) motors were prepared using a template electrodeposition approach, then a partial dissolution of the central silver segment with hydrogen peroxide was done. A rotating magnetic field cause a cone shaped rotation of the Ni segment propelling the nanomotor and resembles microorganisms that use a rotation mechanism for their motion. **Figure III.6** shows a scheme of the nanowire swimmer and its movement.

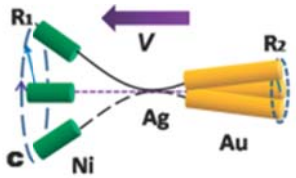

Figure III.6. Schematic of the magnetic swimmer moving "backward". Reprinted with permission from reference 31

The locomotion of the nanowire swimmer is attributed to the transfer of the magnetic energy into cyclic mechanical deformations. The flexible Ag bridge is essential for generating such cyclic mechanical deformations under an external rotating magnetic field. Additional advantages of these swimmers are the precise on/off motion control by

switching the magnetic field on/off, tailoring the nanomotor speed by varying the frequency of the applied field and the possibility of movement in high ionic strength environments.

Among other potential applications of these fuel-free nanomotors is important to remark the capability of load cargoes and the possibility of use this characteristic in drug-delivery. Gao et al.[30] demonstrated the pick-up and transport of a magnetic polymeric drug-loaded microsphere, using this kind of nanomotors, from a loading zone to a predetermined specific zone where the cargo is released to the target cancer cell.

Dual mode propulsion nanowire swimmers were also presented by Wang's group[31]. Here hybrid nanomotors are synthesized in a similar manner, but replacing the gold segment for a platinum-gold segment, being as a result catalytically active, as it is shown in **Figure III.7**.

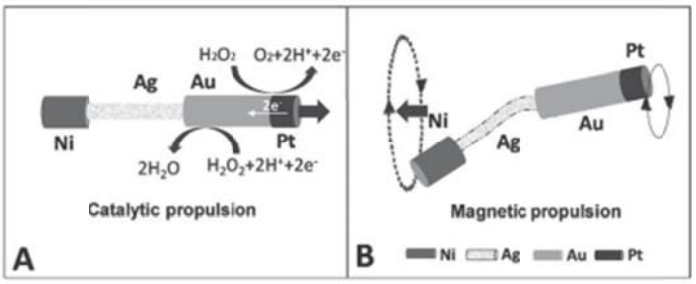

Figure III.7. Catalytic **(A)** and magnetic **(B)** propulsion of the hybrid nanomotor. Reprinted with permission from reference 33

The nanomotor can move with two different sources of energy broadening the scope of applications of these nanomotors taking advantage of each propulsion characteristics on demand. Catalytic and magnetic propulsion direct the nanomotor in opposite directions giving the nanomotor higher versatility. Additionally, the possibility of keep the

movement in high ionic strength, which is not achieved by catalytic nanomotors is allowed by switching on the magnetic propulsion.

III.1.5. Micromotors in lab-on-a-chip devices

The transport of desired cargoes represents an active research area that holds considerable promises in many fields, such as drug delivery, microfluidics and biosensing[32-36]. Once achieved faster nanowire motors and a precise motion control, these motors can be applied to the controlled transport of analytes inside a microfluidic platform avoiding the employment of pumps or external electrical fields for fluid movement and therefore enhancing the analytical capabilities of the lab-on-a-chip (LOC) technologies[32]. Controlled manipulation of cargo within microchannels is a promising alternative for multiple tasks like drug delivery or target isolation, separation and enrichment of different materials/analytes improving the microchip detection efficiency.

The remarkable cargo towing and manipulation capabilities of protein biomotors (like kinesin motor with neurotransmitter vesicles) have led to the introduction of chip-based nanoscale transport systems[27,28,37-41].

Particular attention has been given to the pick-up and guided transport of selected cargo by kinesin/MT-based motors within microchannels but they still require for the movement of the protein motor predefined tracks in the channels. For example Rios and Bachand[32] employed a kinesin motor for the active transport and simultaneous detection of multiple analytes in connection to the distinct spectral emission of quantum-dot nanocrystal tags of different sizes.

Newly developed synthetic catalytic micromotors are powerful, fast, stable, versatile and compatible with microsystems and their environments, being easily adapted to different LOC formats.

In LOC micromotor-based operations needs to be performed: recognition, transport and delivery.

Chemically-powered tubular microengines are particularly attractive for biomedical applications due to their efficient bubble-induced propulsion in relevant biological fluids[17,42]. These microengines are commonly prepared by thin-film rolled-up technology[16,17] or template electrodeposition[35]. Catalytic microtubes propel rapidly and efficiently and magnetic guidance can be achieved through the incorporation of an intermediate magnetic layer that can also be useful for capture of a magnetic cargo.

The capture of a target by a micromotor needs a recognition centre for loading the desired target, electrostatic forces between differently charged micromotor-target and magnetic attractions, taking advantage of the magnetic parts included on the micromotors for its controlled guiding, have been used, but when higher affinity is needed the streptavidin-biotin interaction can be incorporated as well as other bio receptors like, DNA probes, aptamers or antibodies.

Wang's team[13] also demonstrated that catalytic nanowire shuttles can readily pickup drug-loaded Poly-D,L-lactic-*co*-glycolic acid (PLGA) particles and liposomes and transport them to its final destination. Solovev et al.[43] demonstrated the use of microtubular (Ti/Fe/Pt) engines for the loading, transportation, and delivery of microscale objects, including colloidal microparticles and thin metallic nanoplates, by suction to the front of the microtube.

The next obvious step after the cargo pickup is its release, to complete the tasks intended for these devices. Despite less attention has been paid in this aspect, it is a crucial step to finally deliver the load in its

final destiny and also for the reutilization of the micromotors making possible multiple load/unload cycles. The unload process can be triggered by different stimuli, like chemical ones, when the micromotor moves to the deliver zone with different conditions that promote the link breakage between the micromotor and the analyte (i.e. pH change) or produced by an external source, like light, as it was demonstrated by Sen's group or magnetically producing a fast abrupt change in the micromotor direction to overcome the magnetic attraction and release the cargo[8].

In conclusion, extensive research has led an important increment in the diversity of catalytic micromotors whose properties are optimized for performing diverse operations in the nanoscale. Enhanced cargo-towing force, precise motion control, versatility and facile functionalization, have enabled impressive microchip applications towards the realization of autonomous motor-based on-chip transport systems. Thus, in this sense, functionalized synthetic catalytic nanomotors are particularly promising for realizing such autonomous LOC tasks. The employment of nanomotors could also enhance the "traditional" microfluidic systems, i.e. eliminating the need of fluid flow and providing numberless characteristics being the perfect synergy microsystems.

III.1.6. Future perspectives

To combine active targeting with precise guidance and control, future generation drug-delivery vehicles will require powerful propulsion and navigation capabilities in order to deliver payloads to predetermined body locations. Nanoshuttle carriers, transporting their drug payloads directly to diseased tissues, hold considerable promise for improving the therapeutic efficacy and reducing the side effects of toxic drugs. Such nanoshuttles should be able to be functionalized to carry large payloads of drugs, along with imaging moieties and targeting ligands to confer tissue specificity.

Artificial nano/microscale motors hold also considerable promise for diverse medical diagnostic applications[32,44]. Particularly attractive for such bioanalytical applications are new receptor functionalized artificial nanomotors, which are capable of capturing and isolating biological targets from unprocessed biological media[9-12,45].

The requirement of the common hydrogen peroxide fuel hinders some practical biomedical applications of catalytically propelled micro/nanomotors. Thus, a wide range of such applications, particularly in vivo applications, require other fuel sources.

Future microscale motors would require the identification of new in situ fuels in connection with new catalytic materials and reactions. A highly desired aspect of these microscale motors is the use of in situ fuel sources, being able to use the sample as fuel source. Ultimately, it would be beneficial to explore the sample matrix itself as the fuel source, obviating the need for adding external fuels and not compromising the viability of the biological target. Recent efforts have thus been directed at

exploring the use of the sample matrix (media or constituents) as the fuel[21].

Biocatalytic propulsion, powered by ensembles of multiple enzymes, has shown promise for moving microobjects in the presence of glucose fuel[39,46]. The abundant presence of glucose in body fluids makes it an attractive biocompatible fuel.

While impressive progress has been made over the past decade toward developing a wide range of synthetic fuel-driven and fuel-free nano/microscale machines, the realization of practical biomedical applications requires further improvement in their efficiency, power, performance, functionalization, versatility, sophistication, and biocompatibility

These miniature machines are likely to have profound impact upon diverse biomedical applications, including directed drug delivery, nanosurgery, biopsy, cell sorting, artery cleaning, or microchip bioassays. Artificial nanomotors are thus expected to advance from current initial proof-of-concept studies into practical in vitro and in vivo biomedical applications for further evaluation.

III.1.7. References

[1] W.F. Paxton, K.C. Kistler, C.C. Olmeda, A. Sen, S.K. St Angelo, Y.Y. Cao, T.E. Mallouk, P.E. Lammert, V.H. Crespi, Catalytic Nanomotors: Autonomous Movement of Striped Nanorods., J. Am. Chem. Soc. 126 (2004) 13424-13431.

[2] S. Fournier-Bidoz, A.C. Arsenault, I. Manners, G.A. Ozin, Synthetic Self-Propelled Nanorotors, Chem. Commun. 4 (2005) 441-443.

[3] G.A. Ozin, I. Manners, S. Fournier-Bidoz, A. Arsenault, Dream nanomachines, Adv. Mater. 17 (2005) 3011-3018.

[4] J. Wang, Can Man-Made Nanomachines Compete with Nature Biomotors?, ACS Nano 3 (2009) 4-9.

[5] T. R. Kline, W. F. Paxton, T. E. Mallouk and A. Sen, Catalytic Nanomotors: Remote-Controlled Autonomous Movement of Striped Metallic Nanorods, Angew. Chem., Int. Ed., 44 (2005) 744-746.

[6] R. Laocharoensuk, J. Burdick, J. Wang, CNT-Induced Acceleration of Catalytic Nanomotors, ACS Nano 2 (2008) 1069-1075.

[7] U. Demirok, R. Laocharoensuk, M. Manesh, J. Wang, Ultrafast Catalytic Alloy Nanomotors, Angew. Chem. Int. Ed. 47 (2008) 9349-9351.

[8] D. Kagan, S. Campuzano, S. Balasubramanian, F. Kuralay, G. Flechsig and J. Wang, Functionalized Micromachines for Selective and Rapid Isolation of Nucleic Acid Targets from Complex Samples, Nano Lett., 11 (2011) 2083-2087.

[9] J. Orozco, S. Campuzano, D. Kagan, M. Zhou, W. Gao and J. Wang, Dynamic Isolation and Unloading of Target Proteins by Aptamer-Modified Microtransporters, Anal. Chem. 83 (2011) 7962-7969.

[10] S. Balasubramanian, D. Kagan, C. J. Hu, S. Campuzano, M. J. Lobo-Casta~no, N. Lim, D. Y. Kang, M. Zimmerman, L. Zhang and J. Wang, Micromachine-Enabled Capture and Isolation of Cancer Cells in Complex Media, Angew. Chem., Int. Ed. 50 (2011) 4161-4164.

[11] S. Campuzano, J. Orozco, D. Kagan, M. Guix, W. Gao, S. Sattayasamitsathit, J. C. Claussen, A. Merkoçi and J. Wang, Bacterial Isolation by Lectin-Modified Microengines, Nano Lett. 12 (2012) 396-401.

[12] D. Kagan, R. Laocharoensuk, M. Zimmerman, C. Clawson, S. Balasubramanian, D. Kang, D. Bishop, S. Sattayasamitsathit, L. Zhang, J. Wang,

Rapid Delivery of Drug Carriers Propelled and Navigated by Catalytic Nanoshuttles, Small 6 (2010) 2741-2747.

[13] M. Guix, J. Orozco, M. García, W. Gao, S. Sattayasamitsathit, A. A. Merkoçi, A. Escarpa and J. Wang, Superhydrophobic Alkanethiol-Coated Microsubmarines for Effective Removal of Oil, ACS Nano 6 (2012) 4445-4451.

[14] T. E. Mallouk and A. Sen, Powering Nanorobots, Sci. Am. 5 (2009) 72-77.

[15] J. Wang, W. Gao, Nano/Microscale Motors: Biomedical Opportunities and Challenges ACS Nano 6 (2012) 5745-5751.

[16] Y. F. Mei, A. A. Solovev, S. Sanchez and O. G. Schmidt, Rolled-up nanotech on polymers: from basic perception to self-propelled catalytic microengines, Chem. Soc. Rev., 40 (2011) 2109-2119.

[17] S. Sengupta, M.E. Ibele, A. Sen, Fantastic Voyage: Designing Self-Powered Nanorobots, Angew. Chem., Int. Ed, 51 (2012) 8434-8445.

[18] S. Campuzano, D. Kagan, J. Orozco and J. Wang, Motion-driven sensing and biosensing using electrochemically propelled nanomotors, Analyst 136 (2011) 4621-4630.

[19] J. Orozco, V. García-Gradilla, M. D'Agostino, W. Gao, A. Cortés, J. Wang, Artificial Enzyme-Powered Microfish for Water-Quality Testing, ACS Nano 7 (2013) 818-824.

[20] W. Gao, A. Uygun, J. Wang, Hydrogen-Bubble-Propelled Zinc-Based Microrockets in Strongly Acidic Media" J. Am. Chem. Soc., 134 (2012) 897-900.

[21] J. Orozco, A. Cortés, G. Cheng, S. Sattayasamitsathit, W. Gao, X. Feng, Y. Shen, J. Wang, Molecularly Imprinted Polymer-Based Catalytic Micromotors for Selective Protein Transport, J. Am. Chem. Soc. 135 (2013) 5336−5339.

[22] Y.F. Mei, G.S. Huang, A.A. Solovev, E. Bermúdez Ureña, I. Mönch, F. Ding, T. Reindl, R.K.Y. Fu, P.K. Chu, O.G. Schmidt, Versatile approach for integrative and functionalized tubes by strain engineering of nanomembranes on polymers, Adv. Mater. 20 (2008) 4085-4090.

[23] A.A. Solovev, Y.F. Mei, E. Bermúdez Ureña, G.S. Huang, O.G. Schmidt, Catalytic Microtubular Jet Engines Self-Propelled by Accumulated Gas Bubbles, Small 5 (2009) 1688-1692.

[24] S. Sanchez, A.A. Solovev, S.M. Harazim, C. Deneke, Y.F. Mei, O.G. Schmidt, The smallest man-made jet engine, Chem. Rec. 11 (2011) 367-370.

[25] W. Wang, L.A. Castro, M. Hoyos, T.E. Mallouk, Autonomous Motion of Metallic Microrods Propelled by Ultrasound, ACS Nano 6 (2012) 6122-6132.

[26] D. Kagan, M.J. Benchimol, J.C. Claussen, E. Chuluun-Erdene, S.Esener, J. Wang, Acoustic Droplet Vaporization and Propulsion of Perfluorocarbon-Loaded Microbullets for Targeted Tissue Penetration and Deformation, Angew. Chem., Int. Ed. 51 (2012) 7519-7522.

[27] L. Zhang, J.J. Abbott, L.X. Dong, B.E. Kratochvil, D. Bell, B.J. Nelson, Artificial bacterial flagella: Fabrication and magnetic control, Appl. Phys. Lett. 94 (2009) 64107-64109.

[28] A. Ghosh, P. Fischer, Controlled Propulsion of Artificial Magnetic Nanostructured Propellers, Nano Lett, 9 (2009) 2243–2245.

[29] W. Gao, S. Sattayasamitsathit, K.M. Manesh, D. Weihs, J. Wang, Magnetically Powered Flexible Metal Nanowire Motors, J.Am.Chem.Soc. 132 (2010) 14403–14405.

[30] W. Gao, D. Kagan, O.S. Pak, C. Clawson, S. Campuzano, E. Chuluun-Erdene, E. Shipton, E.E. Fullerton, L. Zhang, E. Lauga, J. Wang, Cargo-Towing Fuel-Free Magnetic Nanoswimmers for Targeted Drug Delivery, Small 8 (2012) 460-467.

[31] W. Gao, K.M. Manesh, J. Hua, S. Sattayasamitsathit, J. Wang, Hybrid Nanomotor: A Catalytically/Magnetically Powered Adaptive Nanowire Swimmer, Small 7 (2011) 2047-2051.

[32] J. Burdick, R. Laocharoensuk, P.M. Wheat, J.D. Posner and J. Wang, Synthetic Nanomotors in Microchannel Networks: Directional Microchip Motion and Controlled Manipulation of Cargo, J. Am. Chem. Soc.130 (2008) 8164-8165.

[33] M. Burghard, A Freight Train of Nanotubes for Cargo Transport on the Nanoscale, Angew. Chem., Int. Ed., 47 (2008) 8565-8566.

[34] G.D. Bachand, S.B. Rivera, A. Carroll-Portillo, H. Hess and M. Bachand, Active Capture and Transport of Virus Particles Using a Biomolecular Motor-Driven, Nanoscale Antibody Sandwich Assay, Small 2 (2006) 381-385.

[35] C.T. Lin, M.T. Kao, K. Kurabayashi, E. Meyhofer, Efficient Designs for Powering Microscale Devices with Nanoscale Biomolecular Motors, Small 2 (2006) 281-287.

[36] J. Wang, Cargo-towing synthetic nanomachines: Towards active transport in microchip devices, Lab Chip 12 (2012) 1944-1950.

[37] C. Schmidt and V. Vogel, Molecular shuttles powered by motor proteins: loading and unloading stations for nanocargo integrated into one device, Lab Chip 10 (2010) 2195-2198.

[38] T. Kim, L.J. Cheng, M.S. Kao, E.F. Hasselbrink, L.J. Guo and E. Meyhöfer, Biomolecular motor-driven molecular sorter, Lab Chip 9 (2009) 1282-1285.

[39] L. Rios, G.D. Bachand, Multiplex transport and detection of cytokines using kinesin-driven molecular shuttles, Lab Chip 9 (2009) 1005-1010.

[40] S. Hiyama, Y. Moritani, R. Gojo, S. Takeuchi, K. Sutoh, Biomolecular-motor-based autonomous delivery of lipid vesicles as nano- or microscale reactors on a chip, Lab Chip 10 (2010) 2741-2748.

[41] H. Hess, J. Clemmens, D. Qin, J. Howard and V. Vogel, Light-Controlled Molecular Shuttles Made from Motor Proteins Carrying Cargo on Engineered Surfaces, Nano Lett. 1 (2001) 235-239.

[42] W. Gao, S. Sattayasamitsathit, J. Orozco, J. Wang, Highly Efficient Catalytic Microengines: Template Electrosynthesis of Polyaniline/Platinum Microtubes, J. Am. Chem. Soc. 133 (2011) 11862-11864.

[43] A.A. Solovev, S. Sanchez, M. Pumera, Y.F. Mei, O.G. Schmidt, Adv. Funct. Mater., Magnetic Control of Tubular Catalytic Microbots for the Transport, Assembly, and Delivery of Micro-objects 20 (2010) 2430-2435.

[44] M. García, J. Orozco, M. Guix, W. Gao, S. Sattayasamitsathit, A. Escarpa, A. MerkoÇi, J. Wang, Micromotor-based lab-on-chip immunoassays, Nanoscale 5 (2013) 1325-1331.

[45] S. Sanchez, A.A. Solovev, S. Schulze, O.G. Schmidt, Controlled Manipulation of Multiple Cells Using Catalytic Microbots, Chem. Commun. 47 (2011) 698–700.

[46] N. Mano, A. Heller, Bioelectrochemical Propulsion, J.Am.Chem.Soc. 127 (2005) 11574–11575.

III.2. Microfluidic-immunoassays based on micromotors

III.2.1. Introduction and objectives

The reliable identification, isolation and quantification of proteins holds an enormous potential to satisfy the growing demands in diverse fields, including medical diagnostics, food safety, forensic analysis, environmental monitoring and biodefense applications[1]. A wide variety of techniques are available for protein detection and purification. Particularly attention has been given to antibody-based standard ELISA protocols within multiple well plates,[2,3] although such assays often require long incubation times and multiple washing steps. Recent advances in the field of microanalytical systems have led to the development of LOC immunoassays, coupling the power of microchip devices with the high specificity and sensitivity of antigen–antibody interactions[4–8]. Yet, new efficient microchip immunoassays offering direct, simple and rapid isolation of target proteins are desired.

In this chapter, we present a novel 'on-the-fly' microchip sandwich immunoassay based on self-propelled antibody-functionalized artificial microtransporters able to perform each of the immunoassay steps in different reservoirs and providing direct visualization of the protein binding event. Biological motors and related motion-driven processes have demonstrated the ability to capture and transport target proteins along microtubule tracks in microchip devices.[9–11] One attractive example is a kinesin-powered 'smart dust' sensing device, containing antibody-functionalized microtubules, where the antigen capture and transport allow the replacement of the common washing steps.[11] Microtubule-based molecular shuttles, coupled to kinesin-coated microchannel tracks, were also used for motion based protein sorting.[9,10] However, practical utility of such kinesin-based microchip immunoassays is hindered by the limited operational stability and lifetime of biological motors in engineering

environments (associated with the rapid degradation of proteins outside biological environment) and by the necessity of preconfigured microlithographic tracks to guide their movement.[9,11]

The limitations of protein nanomotors have motivated the present study in which self-propelled antibody-functionalized artificial microtransporters have been incorporated for the first autonomous microchip device that integrates the protein capture, transport and detection operations within different separated zones. Synthetic catalytic nanomotors[12–17] are highly compatible with engineered microsystems and environments and can thus be readily adapted to different LOC formats.[18] Non-functionalized nanowire and microtube motors were used earlier for a guided movement and cargo-towing within complex microchannel networks of microchip devices.[19,20] Receptor functionalized artificial nanomotors can offer the selective isolation of biological targets from raw physiological fluids by capturing and transporting them to a clean environment.[21] While several self-propelled microtransporters have thus recently been described for isolating different biological targets,[22–25] there are no reports on the use of artificial micromotors for antibody-based protein immunoassays and related LOC protocols.

In the following sections we will demonstrate the first example of a LOC immunoassay based on the active transport of antibody-functionalized synthetic micromotors as it is shown in **Figure III.8**. As illustrated in **Figure III.8 I, A,** a simplified preparation of the functionalized microtransporters has been performed, relying on the presence of carboxy-terminated outermost polymeric layer of the template-deposited polymer/Ni/Pt microtubes. The resulting antibody-functionalized micromotors offer an 'on-the- fly' capture and transport of the target antigen and, in a second step, the pickup of a sphere-tagged secondary

antibody, thus demonstrating the efficiency of the different conjugation events held in each microchip reservoirs (**Figure III.8**, **II** (left)). Transport step thus replaces the washing steps common in traditional double antibody sandwich assays (DASA), in a manner analogous to kinesin-based 'smart dust' immunoassays[11]. Tagging the secondary antibody with the polymeric sphere offers a convenient direct visualization and detection of the immunoreactions. In a second approach, shown in **Figure III.8, II** (right), the functionalized microengine captures and transports the microsphere-tagged antigen through a microchannel network. Therefore, convenient optical visualization of the detection and transport events related to Staphylococcus aureus (S. aureus), used as target bacteria which contains protein A in its cell wall, is also achieved by using anti-protein A antibody-functionalized microengines. Such marriage of immunoassays, self-propelled artificial microtransporters, motion-based direct detection and microchip devices holds considerable promise for diverse applications of LOC systems.

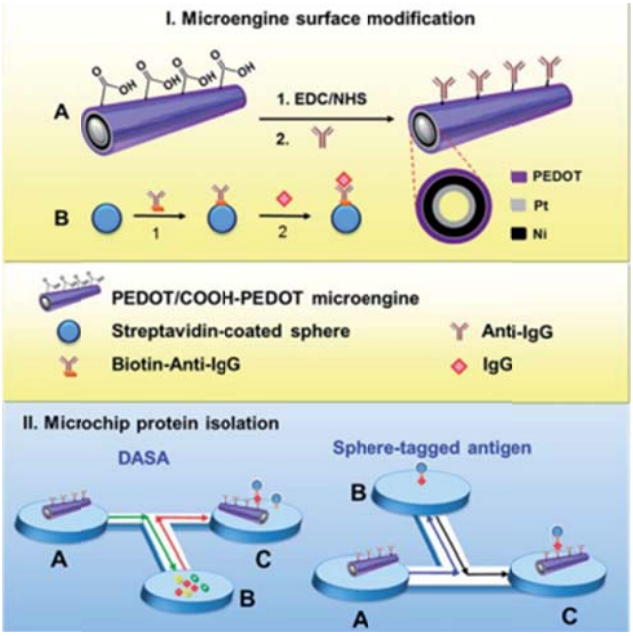

Figure III.8. Schematic of the micromotor-based microchip immunoassay. Microengine surface modification **(I)**: immobilization of anti-IgG on the COOH–PEDOT:PEDOT microengine surface **(A)**. Activation of the COOH groups through EDC/NHS chemistry **(1)** and immobilization of the anti-IgG antibody on the active moieties **(2)**. Modification of streptavidin-coated PP **(B)** with the biotinylated-anti-IgG antibody **(1)** and IgG antigen **(2)**. Micromotor-based microchip immunoassay **(II)**: in a DASA format, the anti-IgG-modified microengines are introduced into reservoir A and guided towards reservoir B, where they navigate for 10 min in a solution containing the target protein in the presence 10-fold non-target proteins. The modified microengine with the target protein is conducted to a third reservoir containing the tagged-PP. In a sphere tagged-antigen format, the anti-IgG-modified microengines are introduced in reservoir A and guided towards a reservoir B to pick-up the anti-IgG-modified PP and guided to reservoir C.

III.2.2. Immunoassay based on microtransporters

The new immuno-microtransporters were prepared by a template-based electrodeposition of multilayer PEDOT:COOH– PEDOT/Ni/Pt microtubes. **Figure III.8** depicts the surface modification of the microengine (I) along with a schematic of the tubular microtransporter and its corresponding cross-section. The outermost polymeric layer is synthesized by co-electropolymerization of PEDOT:PEDOT–COOH (from an electroplating solution containing an equimolar mixture of the monomers) followed by electrodeposition of the Ni and Pt metallic layers (from a Pt–Ni mixture electroplating solution). Whereas the inner Pt catalytic layer of the microtransporter is essential for generating the oxygen bubble thrust, the intermediate Ni layer is used for the magnetic guidance. The outermost PEDOT:COOH–PEDOT layer serves to anchor the antibody through the common carbodiimide (EDC)/N-hydroxysuccinimide (NHS) chemistry (**Figure III.8 IA**). Initial efforts involving a single COOH–PEDOT external layer resulted with numerous COOH groups exposed on the microtransporter outermost surface for subsequent functionalization step. However, the codeposition of a COOH–PEDOT:PEDOT was proved necessary to avoid adherence of the PEDOT-based microtransporters to the surface of a glass slide after the antibody functionalization. Electrochemical deposition conditions, such as composition of the electroplating solutions, applied current, potential and deposition time, were optimized (**Table III.S1)**. Carboxy moieties from the electropolymerized PEDOT:COOH–PEDOT external layer allow a direct functionalization of the resulting microengines, thereby obviating the need for e-beam deposition process of an outer gold layer and related clean room facilities. Unlike other microtubular engines, whose speed is greatly reduced after the e-beam gold deposition and further surface

PEDOT:PEDOT/Ni/Pt microtransporters (≈400 μm·s^{-1}) is not affected by this direct functionalization process. Furthermore, eliminating the need for self-assembled monolayers of alkanethiols[25,26] obviate potential poisoning of the inner Pt surface, hence ensuring high catalytic activity and therefore the efficient microtransporters movement. It should be noted that unlike earlier gold-based microengine functionalization schemes, involving modification of half of the outer surface, [25, 26] the present protocol allows the functionalization of the entire outer surface, as the carboxy moieties cover the entire outermost polymeric surface that will be coupled later to the antibody receptor.

The resulting polymer/Ni/Pt microtransporters propel efficiently *via* the expulsion of oxygen bubbles generated by the catalytic oxidation of hydrogen peroxide fuel at their inner Pt layer[27,28]. The template fabrication process results in 8 μm-long microtubes, similar to the scale of the particle-microsphere tag, which offers a convenient real-time optical visualization of the protein binding event. For example, the formation and movement of the immuno-sandwich complex can be readily visualized by tagging the secondary antibody with a microsphere tracer. **Figure III.8, II** illustrates the micromotor-based microchip immunoassay protein isolation protocol. All the capture-transport-tag-transport steps involved in the immunoassay protocol are thus carried out in the microfluidic device, hence replacing the capture-wash-tag-wash sequence common in conventional DASA protocols.

The ability of the micromotor to travel within a predetermined path along the microchip channels is crucial for the successful performance of the new LOC immunoassay protocol. **Figure III.9** and **Video S1** show the guided movement of the unmodified polymer/Ni/Pt microengine within different sections of the LOC microchannel network containing a PBS

solution along with the H_2O_2 fuel and sodium cholate (NaCh) surfactant. These images demonstrate the self-propelled micromotor departing from the reservoir (a), crossing the channel interconnecting reservoirs (b) and entering the T-shape cross-section while swimming within this junction (c). The generated oxygen bubbles are clearly noticeable during such autonomous movement inside the microchip, as previously reported for other microengines[20,23]. As indicated from the corresponding video, the microengine displays an efficient movement and advanced spatial motion control within the narrow channels and the different reservoirs in the microchip, reflecting the precise magnetic guidance associated with its intermediate Ni layer. Such advanced guided motion and efficient propulsion within the complex microchannel network meets the demands for the sandwich immunoassay and other complex microchip operations.

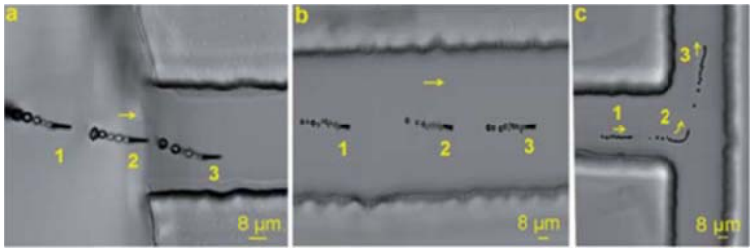

Figure III.9. Navigation of an unmodified COOH–PEDOT:PEDOT microengine within a LOC device. Different overlaid time lapse images (labeled as 1, 2, 3) of the microengine leaving a reservoir **(a)**, crossing the channel between two reservoirs **(b)** and entering the T-shape cross-section **(c)**. Arrows indicate the direction of the movement.

After demonstrating the precise microengine movement within the microchannel network, the microtransporters were functionalized with the corresponding antibody receptors to carry out the microchip immunoassays. In the first bioassay format, recognition of the target proteins was performed by functionalizing the microtransporters with the

antibody via EDC/NHS chemistry (**Figure III.8, IA**), followed by the detection of the target protein, which is conjugated to a secondary antibody functionalized with streptavidin-coated polystyrene particles (S-PP) (**Figure III.8, IB**). Therefore, the target binding event can be easily visualized by optical microscopy, as the antibody-modified microtransporter is efficiently picking-up the protein target conjugated secondary antibody-coated S-PP.

The microtransporter functionalization protocol was optimized for efficient protein–antibody interaction and locomotion. A highly reproducible loading protocol was accomplished by the systematic optimization of the experimental conditions involved in the recognition and labeling steps. Several variables, such as the amount of microtransporters, vortex speed (during the antibody functionalization), concentration and incubation time of the antibodies, were thus examined and optimized, as summarized in **Table III.S2**. The remaining amino moieties (after the modification) were blocked to minimize unspecific adsorption of the target proteins[21].

The specific capture of the target protein by the antibody modified microtransporters was first examined by using the LOC device. **Figure III. S1** and **Video S1** illustrates an anti-IgGmodi fied microtransporter leaving the microengines reservoir of a linear-shaped chip (a), passing through the interconnection channel (b) and arriving to the second reservoir (c), containing the IgG/anti-IgG-modified biotinylated S-PP. The modified microtransporter thus navigates into this second reservoir, capturing the S-PP-tagged-IgG and leaving the reservoir (d). Upon returning to the channel, the microengine-loaded with the tagged analyte-captures and transport three additional S-PP- tagged-proteins (e). This fact demonstrates the strong affinity of the antigen–antibody interaction and the high towing force of the modified microtransporter. **Figure III.10 a-d** and **Video S3** shows the

pick-up and transport of a single antigen-conjugated microsphere by the anti-IgG-modified microtransporter. This figure illustrates the functionalized motor approaching (a), contacting (b) and capturing and transporting (c) the antigen-coated S-PP within the microchip reservoir, followed by its entrance into a microchannel (d). The video shows the continuous transport of the protein–particle complex while crossing the entire reservoir (5 mm external diameter) at a speed of 44 μm s^{-1}, which is 50% slower compared to that observed without the complex. In contrast, no pickup and transport are observed in the control experiment of **Figure III.10 e-g** using the antibody-modified microtransporter and antibody-modified particle (in absence of the IgG antigen), despite the multiple direct motor-particle contacts.

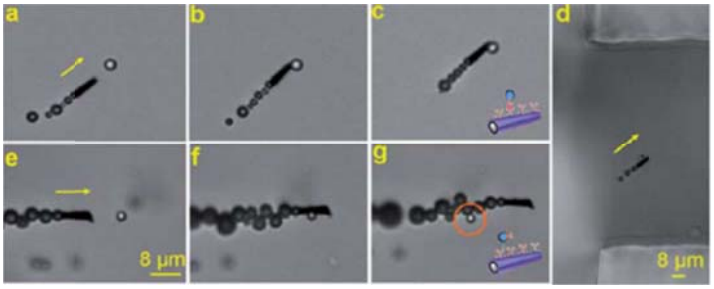

Figure III.10. (a–d) Anti-IgG-modified microengines approaching, contacting and capturing the IgG-antibody-modified particle complex. **(e–g)** Anti-IgG-modified microengines approaching, contacting but not capturing the antibody-modified particle (no IgG present; S-PP highlighted by an orange circle). It must be pointed out that the anti-IgG-modified S-PP is not pre-incubated with the IgG. All negative "controls" were performed on the surface of a glass slide.

Other control experiments are illustrated in Supporting Information (SI), **Figure III.S2** and **Video S4** (negative control 2). The modified microengine is shown first contacting but not capturing the unmodified PP (negative control 2; smaller size), while it is picking and transporting the

IgG-B–anti-IgG-modified S-PP complex (acting as "positive control", bigger size). These results demonstrate that the antibody-modified microtransporters are able to specifically capture the target protein, indicating the great potential of these immuno-microengines for transporting and isolating proteins in a LOC device. The different size of these tagged and untagged particles (≈2.0 μm vs. 0.85 μm, respectively), allows a clear optical real-time visualization and discrimination between the "positive" and "negative controls" during the motor navigation in one single experiment. The similar size scale of the microengines and tags facilitates the clear visualization of the binding events in real time (see **Figure III.10** and **Figure III.S2** and **Videos S2-S4**). This selective and rapid capture mechanism is attributed to the nearly instantaneous recognition of the proteins by the antibody-modified microengine (**Figure III.10 a-c**). The localized fluid convection associated with the microengine vortex effect leads to a fast protein binding event, as was demonstrated for other bioisolation strategies based on such machines[23]. Thus, unlike common immunoassays that require long incubation times (15–30 min)[2,8] the microengine-induced localized convection dramatically accelerates the binding process.

Additional control experiments were performed by using different assay formats to demonstrate that the surface confined antibody is solely responsible for the selective protein isolation (see the SI methods section for details). For example, **Figure III.S3 (A,a)** and **Video S4** (negative control 3) demonstrate that an unmodified "control" microengine (without the immobilized antibody) do not capture the IgG-B–anti-IgG-modified S-PP complex, even after multiple direct contacts. Furthermore, no capture of the particle–protein complex was observed for microtransporters without

COOH groups (on the outermost polymeric surface) that were incubated with the antibody (**Figure III.S3 (A,b)**) and **Video S4** (negative control 4).

An 'on-the-fly' DASA assay of the protein mixture was also carried out to confirm the high specificity of the surface-confined antibody towards the target protein. In such microchip sandwich immunoassay the target protein is first captured from a mixture of proteins by the anti-IgG modified microtransporters and later tagged with the S-PP tracer conjugated to the anti-IgG secondary antibody. The antibody-functionalized motors and spheres were placed in two different reservoirs of the T-shaped LOC device, with the third reservoir containing the 750 mg mL^{-1} of free IgG protein target along with a 10-fold excess of two other proteins, i.e., BSA and lysozyme (**Figure III.11**). A modified microtransporter thus travels from the modified-microengine reservoir (**Figure III.11,1**) to the sample reservoir containing the protein mixture (**Figure III.11, 2a**); following a 10 min incubation while the microengine is continuously swimming, it departs from the sample reservoir (**Figure III.11, 2b** and **3**) towards to the anti-IgG antibody reservoir (**Figure III.11, 4**). In this last compartment, the captured target protein (on the microtransporter) binds to the secondary antibody-modified particle (**Figure III.11** and **Video S5**), hence completing the microchip sandwich assay. These data clearly indicate the specific capture and transport of the target protein, reflecting the high affinity of the microtransporter surface antibody by the target protein and the effective minimization of non-specific binding due to the blocking of the remaining surface amino moieties after the antibody functionalization. In addition, the peroxide fuel and NaCh surfactant, essential for the microengine movement, do not compromise the specific protein-antibody interaction or the integrity of the bioreceptor coating.

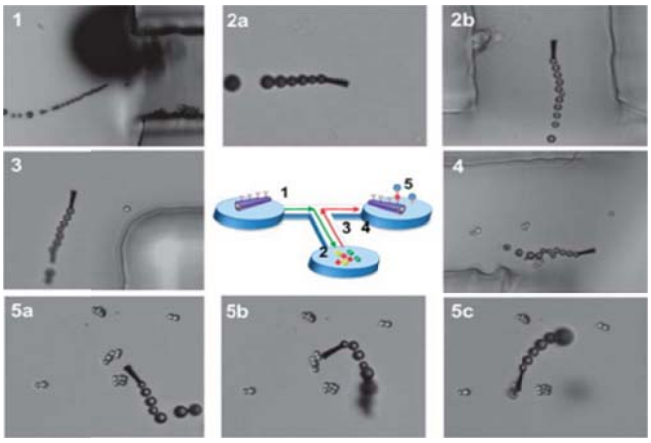

Figure III.11. 'On-the-fly' microchip sandwich immunoassay: capture and transport proteins by using a DASA format. Microtransporters are modified with anti-IgG antibody and placed in a reservoir; S-PP are modified with the anti-IgG antibody and placed in another reservoir of the T-shaped LOC device; the free target IgG protein along with a 10-fold excess (mg mL^{-1}) of BSA and lysozyme are added into the third reservoir. A modified microtransporter moves from the modified-microengine reservoir **(1)** to the one containing the protein mixture **(2a)** and after 10 min navigation is removed from the sample reservoir **(2b,3)** to the anti-IgG S- PP reservoir **(4)**. In this last compartment the protein target, confined on the modified microtransporter, captures the modified particles **(5a–c)**.

The experimental reproducibility was investigated by using 8 different batches of the modified microtransporters following the identical processing steps. All the modified microtransporters were able to rapidly capture the S-PP-tagged-targets, most often immediately, upon few contacts. This indicates that different batches of modified transporters display high protein capture efficiency and demonstrates the reliability of the fabrication, modification and movement steps involved in the entire process. The fast recognition and binding of the protein target indicates considerable promise for the rapid, direct and real time isolation of proteins.

Direct protein detection was tested by examining the ability of the antibody-modified microengines to recognize different quantities of the IgG target in the presence of a 10-fold excess of BSA and lysozyme. Capture and transport of the IgG was possible over the entire IgG concentration examined, i.e. from 20 to 750 mg mL^{-1}. **Figure III.S4** and the corresponding **Video S6** clearly illustrate that the functionalized microengines display an immediate 'on the fly' protein capture upon contacting the tagged-antigen present at the 20 mg mL^{-1} level, in the presence of a 10-fold excess of BSA and lysozyme proteins.

The practical application of the new immunomicrotransporter microchip approach was demonstrated also by the label-free detection of *Staphylococcus aureus* target bacteria (containing protein A in its cell wall).[29] As illustrated in **Figure III.12** and **Video S7** an anti-protein A antibody-modified microengine is able to recognize protein A from the cell wall of *Staphylococcus aureus* (*S. aureus*) while moving within the microchip. **Figure III.12 a–c** shows the modified microengine picking-up and loading this small, round, Gram-positive UTI-related bacteria and further leaving the reservoir containing the bacteria (**Figure III.12 d**). The bacteria dimension (around 2 μm) offers convenient direct optical visualization of the binding event. The specific binding of the anti-proteinA-modified microengines to *S. aureus* was also examined in PBS containing *S. aureus* target bacteria along with a 5-fold excess *Saccharomyces cerevisiae* (*S. cerevisiae*), a yeast specie frequently responsible for yeast infections and UTIs. SI, **Figure III.S5 a–c** and **Video S7** demonstrate the selective binding and transport of the small rod-shaped (≈2 μm length) *S. aureus* bacteria (delineated by green dotted circles). In contrast, the modified microengine does not capture the larger round-shaped *S. cerevisiae* cells (5 μm in diameter) even when multiple contacts occur (delineated by red dotted circles in the video and SI, **Figure**

III.S5 d–g). The distinctly different size of the target *S. aureus* and the *S. cerevisiae* control (2 μm vs. 5 μm, respectively), allows a clear optical visualization of the selective capture of the target cell and discrimination against non-target cells during the microengine movement (see **Video S8**). Note again that the similar size scale of the microengine and bacteria facilitates such real-time visualization of the binding event (see SI, **Figure III.S5 a–c** and **Video S8**). Such selective and rapid capture event is attributed to the nearly instantaneous recognition of the Protein A molecules on the bacterial cell wall by the anti-protein A- modified microengine (SI, **Figure III.S4 a–c**). Finally, capture and transport of the bacteria in an inoculated human urine samples was also demonstrated, as shown in **Figure III.12 e–g** and SI, **Video S9**.

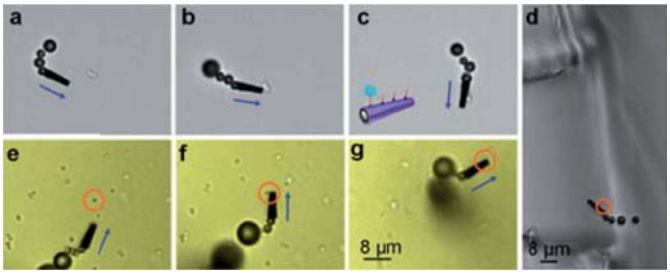

Figure III.12. Anti-ProtA-modified microtransporter approaching, contacting and loading S. aureus cells within a LOC device containing PBS **(a–d)**, and in a human urine media containing bacteria **(e–g)**, (experiments, on the surface of a glass slide). The target bacteria is highlighted by orange circles.

III.2.3. Conclusions

We have demonstrated the first example of microchip immunoassay protocols based on the movement of antibody-functionalized synthetic microtransporters within microchannel networks. New PEDOT:PEDOT–COOH/Ni/Pt immuno-microengines have thus been used for an 'on-the-fly' microchip DASA involving antibody-functionalized microtransporters including their directed capture and transport of target proteins along predetermined paths in the LOC system. Compared to common ELISA bioassays (in multiple well plates) the new motor-based immunoassay allows replacement of the common washing steps. Movement of the micrometer-size captured bacteria or sphere tag thus offer convenient direct real-time optical visualization of the protein binding event. Using different sizes of the microsphere tracers opens up the possibility of developing powerful chip-based multiplexed immunoassays involving different antibody-functionalized microtransporters. Such autonomous transport of antibody-functionalized nanomotors to 'on-the-fly' capture and isolate target proteins obviates the need for time-consuming and laborious multiple wash steps, hence greatly simplifying and accelerating the whole immunoassay protocol. Whenever needed, common regeneration procedures involving selected elution solutions[30,31], can be used for releasing the captured antigen and re-using the microengine. These results demonstrate the great potential of the antibody-modified microengines for the selective recognition, loading and isolation of target proteins and cells in a microchip device. Self-propelled immuno-microengines are expected to lead to new LOC bioanalytical microsystems with attractive protein isolation and detection capabilities, thus offering numerous opportunities in diverse areas, ranging from medical diagnostics to food safety.

III.2.4. Experimental Section

Self-propelled catalytic microengines in the microchannel were operated by filling the reservoirs and microchannel with a navigating solution consisting of a 2% NaCh/ 1% H_2O_2 mixture in PBS buffer solution (pH 7.2). Subsequently, microengines and particles were added into the reservoirs and were equilibrated until quiescent conditions were obtained. The movement of the microengines and all tasks were captured using the inverted optical microscope. Small quantities of either surfactant or fuel were further added when necessary. Such addition ensures not only the autonomous navigation of the microengines over prolonged time periods but also the absence of solution flow during the experiments (by maintaining the volume of mixture contained in the reservoirs).

Template electrochemical deposition of microtube was carried out with a CHI 661D potentiostat (CH Instruments, Austin, TX). An inverted optical microscope (Nikon Eclipse Instrument Inc. Ti-S/L100), coupled with a 20x objective, along with a Hamamatsu digital camera C11440 and a NIS-Elements AR 3.2 so-ware, were used for capturing movies at a frame rate of 20 frames per second. The speed of the microengines was tracked 1using a NIS-Elements tracking module and the results were statistically analyzed by using Origin software.

Synthesis of microtransporters: The multilayer microtubes were prepared using a common template directed electrodeposition protocol[28]. A cyclopore polycarbonate membrane, containing 2 μm maximum diameter conical-shaped micropores (Catalog no. 7060-2511; Whatman, Maidstone, UK), was employed as a template. A 75 nm gold film was first sputtered on one side of the porous membrane to serve as a working electrode using a Denton Discovery 18. Sputtering was performed at room temperature

under vacuum of $5x10^{-6}$ Torr, DC power 200 W and Ar was flowed at 3.1 mT. Rotation speed was 65 rpm along with a sputtering time of 90 s. A Pt wire and an Ag/AgCl with 3 M KCl were used as counter and reference electrodes, respectively. The membrane was then assembled in a plating cell with an aluminum foil serving as contact for the working electrode. PEDOT/PEDOT–COOH microtubes were electropolymerized up to 0.5 C at +0.85 V from a plating solution containing 7.5 mM of each monomer (EDOT and EDOT–COOH), 100 mM SDS and 7.5 mM KNO_3, all of them were prepared from Sigma-Aldrich reagents. Then, the metallic layers were deposited from a Pt-Ni mixture solution. The first Pt layer was deposited galvanostatically at -2 mA for 500 s to provide a smooth and high conductive surface after the polymer deposition and also improve the deposition of the next metallic layers. Afterwards the intermediate Ni layer was deposited amperometrically at -1.3 V for 4.0 C to achieve the magnetic properties that allow the micromotor guidance by properly orienting the magnetic field created by a simple neodymium magnet. Finally the catalytic inner Pt layer was deposited galvanostatically at -2 mA for 450 s. The Pt–Ni mixture solution was prepared by mixing the same volume of a commercial platinum solution (Platinum RTP; Technic Inc, Anaheim, CA) and a Nickel solution containing a mixture of 20 g L^{-1} $NiCl_2 \cdot 6H_2O$, 515 g L^{-1} $Ni(H_2NSO_3)_2 \cdot 4H_2O$, and 20 g L^{-1} H_3BO_3. To release the microengines from the template, the sputtered gold layer was completely removed by mechanical hand polishing with 3-4 μm alumina slurry. The membrane was then dissolved in methylene chloride for 10 min to completely release the microtubes. Finally, microengines were washed repeatedly with methylene chloride, followed by ethanol and ultrapure water (18.2 MΩ cm), three times of each, and collected by centrifugation at 6000 rpm for 3 min after each wash.

Microtransporters and particles functionalization: 1-Ethyl-3-(3-dimethylaminopropyl) carbodiimide (EDC)/Nhydroxysuccinimide (NHS) chemistry was used to activate the carboxyl-terminated groups from the polymer for conjugation with anti-Human IgG protein. For this purpose microengines were treated with 200 μl of a 0.1 M MES buffer solution pH 5.0 containing 20 mg EDC and 20 mg NHS for 15 min, washed with MES buffer 1 min and incubated with anti-Human IgG in PBS 1x pH 7.2 for 2 h. The excess of antibody were washed in PBS buffer (1x) pH 7.2 containing 0.05% of Tween 20. The remaining amine reactive-esters from the activated carboxylic groups were blocked with 1 M ethanolamine solution, pH 8.5, for 30 min and BSA 1% for 1 hour with a washing step in between in PBS 1x pH 7.2. In all the washing steps the microengines were centrifuged at 6000 rpm for 4 min. All the experiments were carried out under shaking at room temperature.

20 μl of streptavidin polystyrene particles were washed twice with B&W buffer and then incubated in 50 ml of 400 mg mL^{-1} biotin–anti-Human IgG antibody solution, for 15 min. The excess of reagents was washed with Milli-Q water and particles incubated with 50 ml IgG of 750 mg mL^{-1} IgG antigen solution, for 15 min. Finally the particles were washed with PBS buffer (1x) pH 7.2 containing 0.05% of Tween 20 and then resuspended in 20 μL PBS buffer (1x) for analysis.

III.2.5. References

[1] S.R. Weinberger, T.S. Morris and M. Pawlak, Recent trends in protein biochip technology, Pharmacogenomics 1 (2000) 395-416.

[2] M. Vandermeeren, M. Mercken, E. Vanmechelen, J. Six, A. Van de Voorde, J. Martin, P. Cras, Detection of Proteins in Normal and Alzheimer's Disease Cerebrospinal Fluid with a Sensitive Sandwich Enzyme-Linked Immunosorbent Assay, J. Neurochem. 61 (1993) 1828-1834.

[3] R.M. Lequin, Enzyme Immunoassay (EIA)/Enzyme-Linked Immunosorbent Assay (ELISA), Clin. Chem. 51 (2005) 2415-2418.

[4] N.H. Chiem and D.J. Harrison, Microchip systems for immunoassay: an integrated immunoreactor with electrophoretic separation for serum theophylline determination, Clin. Chem., 44 (1998) 591-598.

[5] J. Wang, A. Ibáñez, M.P. Chatrathi, A. Escarpa, Electrochemical Enzyme Immunoassays on Microchip Platforms, Anal. Chem. 73 (2001) 5323-5327.

[6] A.G. Crevillen, M. Hervás, M.A. López, M.C. González, A. Escarpa, Real sample analysis on microfluidic devices, Talanta 74 (2007) 342.

[7] A.E. Herr, A.V. Hatch, D.J. Throckmorton, H.M. Tran, J.S. Brennan, W.V. Giannobile, A.K. Singh, Microfluidic immunoassays as rapid saliva-based clinical diagnostics, Proc. Natl. Acad. Sci. U. S. A. 104 (2007) 104, 5268-5273.

[8] J.M. Nam, C.S. Thaxton, C.A. Mirkin, Nanoparticle-Based Bio-Bar Codes for the Ultrasensitive Detection of Proteins, Science 301 (2003) 1884-1886.

[9] G.D. Bachand, H. Hess, B. Ratna, P. Satird, V. Vogel, "Smart dust" biosensors powered by biomolecular motors, Lab Chip 9 (2009) 1661-1666.

[10] C.T. Lin, M.T. Kao, K. Kurabayashi, E. Meyhofer, Self-Contained, Biomolecular Motor-Driven Protein Sorting and Concentrating in an Ultrasensitive Microfluidic Chip, Nano Lett. 8 (2008) 1041-1046.

[11] T. Fischer, A. Agarwal, H. Hess, A smart dust biosensor powered by kinesin motors, Nat. Nanotechnol. 4 (2009) 162-166.

[12] T.E. Mallouk, A. Sen, Powering Nanorobots, Sci. Am. 5 (2009) 72-77.

[13] T. Mirkovic, N.S. Zacharia, G.D. Scholes, G.A. Ozin, Fuel for Thought: Chemically Powered Nanomotors Out-Swim Nature's Flagellated Bacteria, ACS Nano 4 (2010) 1782-1789.

[14] J. Wang, Can Man-Made Nanomachines Compete with Nature Biomotors?, ACS Nano 3 (2009) 4-9.

[15] T.R. Kline, W.F. Paxton, T.E. Mallouk, A. Sen, Catalytic Nanomotors: Remote-Controlled Autonomous Movement of Striped Metallic Nanorods, Angew. Chem., Int. Ed., 44 (2005) 744-746.

[16] Y.F. Mei, A.A. Solovev, S. Sanchez, O.G. Schmidt, Rolled-up nanotech on polymers: from basic perception to self-propelled catalytic microengines, Chem. Soc. Rev., 40 (2011) 2109-2119.

[17] S. Sanchez, M. Pumera, Nanorobots: The Ultimate Wireless Self-Propelled Sensing and Actuating Devices, Chem.-Asian J. 4 (2009) 1402-1410.

[18] J. Wang, Cargo-towing synthetic nanomachines: Towards active transport in microchip devices, Lab Chip 12 (2012) 1944-1950.

[19] J. Burdick, R. Laocharoensuk, P.M. Wheat, J.D. Posner, J. Wang, Synthetic Nanomotors in Microchannel Networks: Directional Microchip Motion and Controlled Manipulation of Cargo, J. Am. Chem. Soc.130 (2008) 8164-8165.

[20] S. Sanchez, A.A. Solovev, S.M. Harazim, O.G. Schmidt, Microbots Swimming in the Flowing Streams of Microfluidic Channels, J. Am. Chem. Soc. 133 (2011) 701-703.

[21] S. Campuzano, D. Kagan, J. Orozco, J. Wang, Motion-driven sensing and biosensing using electrochemically propelled nanomotors, Analyst 136 (2011) 4621-4630.

[22] S. Balasubramanian, D. Kagan, C.J. Hu, S. Campuzano, M.J. Lobo-Castaño, N. Lim, D.Y. Kang, M. Zimmerman, L. Zhang, J. Wang, Micromachine-Enabled Capture and Isolation of Cancer Cells in Complex Media, Angew. Chem., Int. Ed. 50 (2011) 4161-4164.

[23] D. Kagan, S. Campuzano, S. Balasubramanian, F. Kuralay, G. Flechsig, J. Wang, Functionalized Micromachines for Selective and Rapid Isolation of Nucleic Acid Targets from Complex Samples, Nano Lett., 11 (2011) 2083-2087.

[24] J. Orozco, S. Campuzano, D. Kagan, M. Zhou, W. Gao, J. Wang, Dynamic Isolation and Unloading of Target Proteins by Aptamer-Modified Microtransporters, Anal. Chem. 83 (2011) 7962-7969.

[25] S. Campuzano, J. Orozco, D. Kagan, M. Guix, W. Gao, S. Sattayasamitsathit, J.C. Claussen, A. Merkoçi, J. Wang, Bacterial Isolation by Lectin-Modified Microengines, Nano Lett. 12 (2012) 396-401.

[26] M. Guix, J. Orozco, M. García, W. Gao, S. Sattayasamitsathit, A. Merkoçi, A. Escarpa, J. Wang, Superhydrophobic Alkanethiol-Coated Microsubmarines for Effective Removal of Oil, ACS Nano 6 (2012) 4445-4451.

[27] W. Gao, S. Sattayasamitsathit, J. Orozco, J. Wang, Highly Efficient Catalytic Microengines: Template Electrosynthesis of Polyaniline/Platinum Microtubes, J. Am. Chem. Soc. 133 (2011) 11862-11864.

[28] W. Gao, S. Sattayasamitsathit, A. Uygun, A. Pei, A. Ponedal, J. Wang, Polymer-based tubular microbots: role of composition and preparation, Nanoscale 4 (2012) 2447-2453.

[29] B. Esteban-Fernández de Ávila, M. Pedrero, S. Campuzano, V. Escamilla-Gómez, J.M. Pingarrón, Sensitive and rapid amperometric magnetoimmunosensor for the determination of Staphylococcus aureus, Anal. Bioanal. Chem. 403 (2012) 917-925.

[30] R. Pei, X. Cui, X. Yang, E. Wang, Real-time immunoassay of antibody activity in serum by surface plasmon resonance biosensor, Talanta 53 (2000) 481-488.

[31] J.J. Gilligen, P. Schuck, A.L., Yergey, Mass Spectrometry after Capture and Small-Volume Elution of Analyte from a Surface Plasmon Resonance Biosensor, Anal. Chem. 74 (2002) 2041-2047.

III.2.6 Supporting information

Video S1. Guided movement of the unmodified polymer/Ni/Pt microengine within different sections of a LOC microchannel network containing a PBS solution along with the H_2O_2 fuel and NaCh surfactant.

Video S2. Anti-IgG-modified microtransporter capturing multiple S-PP-tagged-IgG.

Video S3. Pick-up and transport of a single antigen-coated microsphere by the anti-IgG-modified microtransporter.

Video S4. Negative controls.

Video S5. 'On-the-fly' DASA assay of protein mixture.

Video S6. 'On the fly' protein capture upon contacting the tagged-antigen present at the 20 μg/ml level, in the presence of a 10-fold excess of BSA and lysozyme proteins.

Video S7. Anti-proteinA antibody-modified microengine recognizing Protein-A from the cell wall of *Staphylococcus aureus (S. aureus)* while moving within the microchip.

Video S8. Selective binding and transport of the small rod-shaped (~2 μm length) *S. aureus* bacteria.

Video S9. Binding and transport of a *S. aureus* target cell in an urine sample.

Table III.S1. Optimal conditions for the fabrication of COOH-PEDOT:PEDOT/Pt/Ni/Pt microtransporters.

Layer	Electroplating solution	Electrochemical conditions
COOH-PEDOT:PEDOT	7.5 mM:7.5 mM, in 7.5 mM KNO_3 containing 100 mM SDS	+0.85 V, 0.5 C
Pt	commercial plating solution, see experimental section for details	-2 mA, 500 s
Ni		-1.3 V, -4.0 C
Pt		-2 mA, 450 s

Table III.S2. Optimal conditions for the functionalization of the COOH-PEDOT:PEDOT/Pt/Ni/Pt microtransporters.

Parameter	Optimal value
Concentration of capture antibody / μg/ml	750
Amount of microtransporters / mg	~ 0.60 ± 0.15
Vortex speed / r.p.m	1000
Concentration of tagging antibody / μg/ml	400

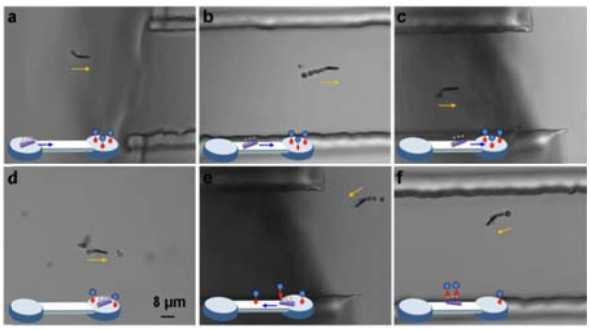

Figure III.S1. Anti-IgG-modified microtransporter leaving the microengines reservoir **(a)**, passing through the interconnecting section of a linear-shaped chip **(b)** and arriving to a second reservoir **(c)**, where IgG/anti-IgG-modified biotinylated S-PPs are present. Modified microtransporter navigated on this second reservoir, captured the S-PP-tagged-IgG **(d)** and left the reservoir **(e)**. When the microengine, coming back to the channel and loading the tagged analyte, found a cluster of three more S-PP-tagged-proteins was able to interact and pluck one of them from the cluster **(f)**.

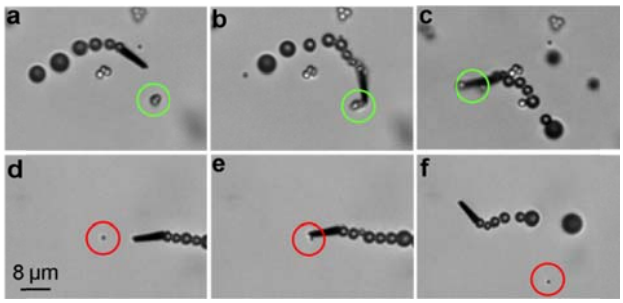

Figure III.S2. Modified microengine capturing and transporting a IgG-anti-IgG-modified-PP complex (delineated by green circles), and interacting (but not loading) with PP of smaller size (delineated by red circles).

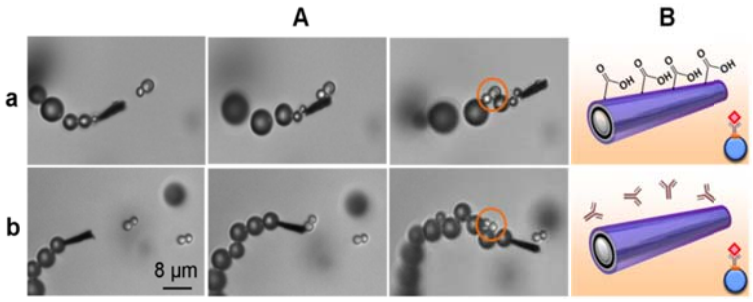

Figure III.S3. Interaction between nanomotors and AntiIgG-IgG-modified S-PP, navigating in a glass slide **(A)**. Negative controls: PEDOT/PEDOT-COOH **(a)** and PEDOT-anti-IgG-incubated nanomotors **(b)**, respectively. Corresponding sketches for **(a)** and **(b)** and modified S-PP (B), respectively. Contacted but unloaded particles, highlighted by an orange circle.

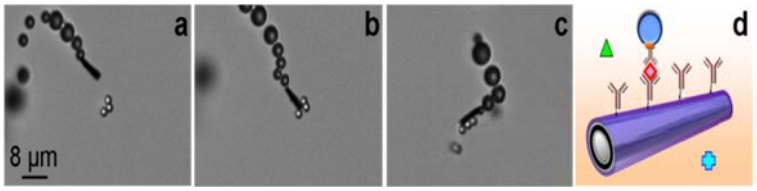

Figure III.S4. Anti-IgG-functionalized-microtransporters displaying an immediate 'on the fly' protein capture upon contacting the tagged-IgG target being present in a concentration of 20 µg/ml in the presence of a 10-fold excess of BSA and lysozyme proteins (Experiments performed on a glass slide). IgG, BSA and lysozyme, red rhombus, green triangle and blue cross, respectively.

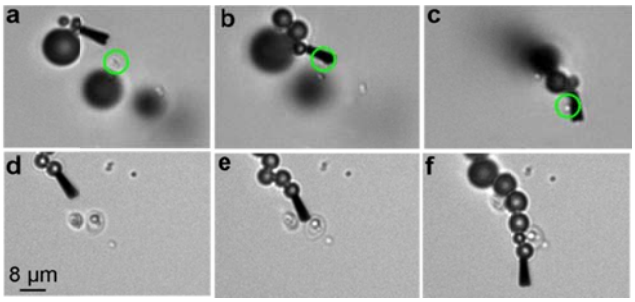

Figure III.S5. Selective binding and transport of the small rod-shaped (~2 µm length) *S. aureus* bacteria (delineated by green dotted circles) *vs* the bigger round-shaped *S. cerevisiae* cells (unlabeled, ~5 µm in diameter), unloaded even when after multiple contacts with the antiproteinA-modifed microtransporter.

IV. General conclusions

The studied one-dimensional materials –nickel and copper nanowires and micromotors– have demonstrated to be very powerful analytical tools to improve the biodetection of target molecules in both, agro-food and clinical fields, using miniaturized flow injection analysis and microfluidic systems based in *lab-on-a-chip* (LOC) technology. The inherent advantages of microfluidic systems such as, fast analysis and very low sample and reagents consumption and in addition those derived from the high specific surface of the studied nanomaterials, have been creative and synergicly exploited.

On the one hand, the electrosynthesis of nickel and copper nanowires using alumina membranes as templates has allowed obtain nanowires with reproducibility and a high structural perfection, as it was revealed by electron microscopy techniques. These nanostructures have been immobilized in a satisfactory manner in carbon screen printed platforms with different designs in order to construct new electrochemical detectors for miniaturized flow injection analysis and also in microfluidic-LOC systems. The screen printed electrochemical technology has constituted an added value to the already pertinent symbiosis between microtechnologies and nanotechnologies, allowing the construction of nanoscaled disposable detectors avoiding traditional procedures, as polish, which is required in conventional electrodes. Moreover, the screen printed electrodes, in size terms, are highly compatible with the studied miniaturized flow and microfluidics systems, exhibiting a great signal to noise ratio. Furthermore, the high specific surface and the electrocatalytic effect showed by nickel and copper nanowires towards carbohydrates have allowed an improvement in their electrochemical detection, revealing an excellent selectivity and sensitivity. The other outstanding analytical property has been the good reproducibility obtained due to the extremely

low fouling observed when using these nanoscaled electrodes, avoiding in that way the employment of more complex electrochemical techniques, such as pulsed based ones, commonly used for the electrochemical detection of carbohydrates. In brief, it can be concluded, that the incorporation of nickel and copper nanowires has allowed a much enhanced electrochemical detection of carbohydrates in miniaturized and microfluidic-LOC systems.

On the other hand, the micromotors synthesis process was also optimized using polycarbonate double conical membranes as templates. The synthesis achieved the goals of reproducibility and high structural precision as it was clearly observed through its study using electron microscopy techniques and also when employed under optical detection. These developed micromotors were functionalized with the objective of proteins detection using an immunoassay in microfluidic systems, being constituted as a very powerful analytical tool for the detection of this kind of molecules through the guided movement of highly functionalized micro machines. The studied micromotors have allowed recognize and interact with the target molecule revealing its presence via optical visualization. These characteristics permit not only think in new free flow analytical systems and as a result free of the related instrumentation but also in the possibility of something much more important and imaginative: New ways of exploring the fascinating world of molecular detection.

Due to all the premises stated above, the results presented in this Doctoral Thesis reveal the pertinence and convenience of the coupling between microtechnologies and nanotechnologies for the detection of target molecules in complex analytical systems in agro-food and clinical fields broadening new horizons in current Analytical Chemistry.

Conclusiones generales

Los nanomateriales unidimensionales estudiados –nanohilos de níquel y cobre y los micromotores– han demostrado ser unas herramientas analíticas muy poderosas para mejorar la bio-detección de moléculas objetivo en los ámbitos agroalimentario y clínico empleando sistemas analíticos miniaturizados y microfluídicos basados en la tecnología *lab-on-a-chip* (LOC). Las bondades inherentes de los sistemas microfluídicos tales como rapidez en los análisis y despreciable consumo de muestras y reactivos con aquellas derivadas de la elevada superficie específica y altamente funcionalizada que exhiben los nanomateriales estudiados, han sido creativa y sinérgicamente explotadas.

Por una parte, la electro síntesis de nanohilos de níquel y cobre empleando moldes de membranas de alúmina ha permitido la obtención de nanohilos de forma reproducible y con elevada perfección estructural, tal y como han revelado las técnicas de microscopía electrónica. Estas nanoestructuras se han inmovilizado exitosamente en soportes serigrafiados de carbono de diferente diseño para la construcción de nuevos detectores electroquímicos en sistemas de inyección en flujo miniaturizado y en sistemas microfluídicos-LOC. La tecnología serigrafiada electroquímica ha constituido un valor añadido a la ya pertinente simbiosis entre micro y nanotecnologías, permitiendo la construcción de detectores nanoescalados desechables y exentos de los procedimientos tradicionales de pulido que exigen los electrodos convencionales. Además, los electrodos serigrafiados son, en términos de escala, altamente compatibles con los sistemas de flujo miniaturizado y microfluídicos estudiados; exhibiendo además una excelente S/N. Por su parte, la elevada superficie específica y el efecto electro catalítico que ejercen los nanohilos de níquel y cobre hacia los carbohidratos, han permitido una mejora en la detección electroquímica de los mismos, exhibiendo una elevada selectividad y sensibilidad. La otra

propiedad analítica sobresaliente ha sido la excelente reproducibilidad obtenida debido al bajísimo ensuciamiento que presentan estos electrodos nanoestructurados evitando así el empleo de técnicas electroquímicas más sofisticadas como son las basadas en pulsos y habitualmente empleadas en la detección electroquímica de carbohidratos. Por todo ello, se puede concluir que la incorporación de nanohilos de níquel y cobre ha permitido una detección electroquímica de carbohidratos muy mejorada en sistemas de flujo miniaturizado y microfluídicos-LOC.

Por otra parte, la electrosíntesis de micromotores empleando membranas de policarbonato con forma de doble cono permitió obtener de forma reproducible micromotores con una elevada precisión estructural, tal y como se observó mediante su estudio por técnicas de microscopía electrónica y durante su empleo bajo detección óptica. Dichos micromotores desarrollados se funcionalizaron con el objetivo de detectar proteínas empleando un inmunoensayo en sistemas microfluídicos constituyéndose como una herramienta analítica muy poderosa para la detección de este tipo de moléculas a través del movimiento dirigido de micro-máquinas moleculares altamente funcionalizadas. Los micromotores estudiados han permitido el reconocimiento e interacción con la molécula objetivo revelando su presencia mediante monitorización óptica. Estas bondades permiten no sólo ya pensar en nuevos sistemas analíticos sin flujos y por ello libres de la instrumentación que los generan; sino en algo mucho más importante e imaginativo: en nuevas formas de explorar el fascinante mundo de la detección molecular.

Por todo ello, el conjunto de los resultados presentados en esta Tesis Doctoral revelan la pertinencia y conveniencia del acoplamiento entre las microtecnologías y las nanotecnologías para la detección de moléculas objetivo en sistemas analíticos complejos dentro de los ámbitos agroalimentario y clínico; ampliándose nuevos horizontes en la Química Analítica contemporánea.

V. Publications and conference communications

ARTICLES

M. Garcia, P. Batalla and A. Escarpa "Metallic and polymeric nanowires for electrochemical sensing and biosensing"
Submitted

M. Garcia and A. Escarpa "Disposable electrochemical detectors based on nickel nanowires for carbohydrate sensing"
Biosensors and Bioelectronics 26 (2011) 2527–2533.

M. Garcia and A. Escarpa "A class-selective and reliable electrochemical monosaccharide index in honeys, as determined using nickel and nickel-copper nanowires"
Analytical and Bioanalytical Chemistry 402 (2012) 945–953.

M. Garcia and A. Escarpa "Enzymeless microfluidic electrochemical sensor for inulin detection using catalytic nanowires-based screen-printed electrodes"
Submitted

M. Garcia and A. Escarpa "Microchip electrophoresis-copper nanowires for fast and reliable determination of monossacharides in honey samples"
Electrophoresis: DOI: 10.1002/elps.201300458

M. Garcia, J.R. Alonso-Fernández and A. Escarpa "Copper nanowires immobilized on the boards of microfluidic chips for the rapid and simultaneous diagnosis of galactosemia diseases in newborn urine samples"
Analytical Chemistry 85 (2013) 9116-9125.

M. Garcia, J. Orozco, M. Guix, W. Gao, S. Sattayasamitsathit, A. Escarpa, A. Merkoçi and J. Wang "Micromotor-based lab-on-chip immunoassays" Nanoscale 5 (2013) 1325-1331.

M. Guix, J. Orozco, M. Garcia, W. Gao, S. Sattayasamitsathit, A. Merkoçi, A. Escarpa and J. Wang "Superhydrophobic Alkanethiol-Coated Microsubmarines for Effective Removal of Oil"
ACS Nano 6 (2012) 4445-4451

CONFERENCE COMMUNICATIONS

ORAL PRESENTATIONS

A. Escarpa, M.C. González, M. A. López Gil, A. G. Crevillén, M. Hervás, M. García. "Lab-on-a-chip and nanotechnology approaches in food analysis"
5º Reunión de la Sociedad Española de Seguridad Alimentaria. Palma de Mallorca (Spain, 2008)

A. Escarpa, M.C. González, M. A. Lopez Gil, A. G. Crevillén, M. Hervás, M. García. "Microfluidic devices for food applications".
I Workshop on Analytical Miniaturization ("lab-on-a-chip"). Alcalá de Henares (Spain, 2008)

A. Escarpa, M. García. "Miniaturized flow injection system with disposable magnetic detector based on nickel nanowires: A novel tool for fast detection of total carbohydrates" Euroanalysis 2009. Innsbruck, (Austria, 2009)

A. Escarpa, M.Pumera, M. García and A.G.Crevillén. "Nanomaterials as electrochemical detectors in capillary electrophoresis microchips: Fundamentals, designs, and applications"
LACE 2009. Sevilla (Spain, 2009)

A. Escarpa, M. García. "Analytical performance of electrochemical detectors based on nickel and copper nanowires"
ESEAC 2010. Gijon (Spain, 2010)

A. Escarpa and M.García. "Microchip electrophoresis-copper nanowires platforms for carbohydrate electrochemical sensing"
LACE 2012. Buenos Aires (Argentina 2012)

A. Escarpa, M. Garcia and J.R. Alonso-Fernández. "Copper nanowires immobilized on the boards of microfluidic chips for the rapid and simultaneous diagnosis of galactosemia diseases in newborn urine samples"
V Jornadas y PRemios ACMEIM 2013. Alcázar de San Juan. (Spain 2013)

A. Escarpa and M.García. "Rapid diagnosis of galactosemia diseases in newborn urine samples on microfluidic chips-copper nanowires platforms"
LACE 2013. Lima (Perú 2013)

POSTERS AND FLASH COMMUNICATIONS

A. Escarpa, M. García. "Nickel nanowires for electrochemical detection of total carbohydrates using miniaturized flow injection system"
42nd IUPAC congress. I SECC Glasgow, Scotland, (UK, 2009)

A. Escarpa, M. García. "Nickel nanowires for electrochemical detection of total carbohydrates using miniaturized flow injection system" III Workshop: Nanociencia y nanotecnología analíticas.
Oviedo (Spain, 2009)

M. García, D. Vilela and A. Escarpa. "Nickel nanowires and gold nanoparticles as complementary analytical tools for analysis of honey samples"
IV Workshop: Nanociencia y nanotecnología analíticas. Zaragoza (Spain 2010)

POSTERS

M. Guix, M. García, J. Orozco, W. Gao, S. Campuzano, A. Escarpa, J. Wang and A. Merkoçi. "Synthetic nanomotors towards lab-on-a-chip biosensing applications"
WAM-NANO 2012. Barcelona (Spain, 2012)

M. Guix, M. García, J. Orozco, W. Gao, S.Sattayasamitsathit, A.Escarpa, A.Merkoçi and J.Wang. "Synthetic microsubmarines for environmental purposes" Micro and Nanomotors: Challenges and Perspectives. Dresden (Germany,2012)

M. García, and A. Escarpa. "Copper and nickel nanowires for electrochemical microfluidic sensing of inulin"
VI Workshop: Nanociencia y nanotecnología analíticas. Alcalá de Henares, Madrid (Spain 2013)